A *K*-BAND MICROWAVE POLARIMETER

A Thesis

Submitted to the College of Graduate Studies and Research

in Partial Fulfillment of the Requirements

for the Degree of

Master of Science

in the Department of Electrical Engineering

University of Saskatchewan

by

Martin Paul Poettcker

Saskatoon, Saskatchewan

DECEMBER, 1987

Copyright

Acknowledgements

The author takes pleasure in acknowledging the contributions of those who assisted in the completion of this work. The Electrical Engineering Department provided theoretical expertise, laboratory resources and work space. The advice, guidance and helpful review of Dr. A.G. Wacker is greatly appreciated.

The Canada Center for Remote Sensing both provided the radars, and allowed them to be modified in the midst of a measurement campaign. This is gratefully acknowledged.

The Institute of Space and Atmospheric Studies recognized the need for this research and took steps to encourage it. The many discussions with Dr. G.J Sofko were indispensable to the project, and his enthusiasm made the research much more enjoyable. Assistance and encouragement was provided by all of the graduate students from the Institute involved with the radar project. Special thanks goes to Mr. M. Hinds, who spent many hours developing software for the polarimeter and assisting with the field tests.

The author also wishes to thank his wife Erna and children Renee and Nathan for their support, encouragement, and patience.

Financial assistance was provided by a University of Saskatchewan Graduate scholarship and by an operating grant from the Natural Sciences and Engineering Research Council of Canada (NSERC). Funds for hardware development were made available by both the Electrical Engineering Department and the Institute of Space and Atmospheric Studies. The Institute provided funding for technical and drafting services. All financial assistance is gratefully acknowledged.

UNIVERSITY OF SASKATCHEWAN

Electrical Engineering Abstract 87A287

A *K*-BAND MICROWAVE POLARIMETER

Student: M.P. Poettcker
Supervisor: A.G. Wacker
M.Sc. Thesis presented to the College of Graduate Studies and Research

December 1987

Abstract

Microwave radars are currently being used to examine the backscattering properties of agricultural crops. A multi-band frequency-modulated scatterometer system is in use at the University of Saskatchewan for this purpose. The scatterometer provides only partial information regarding the polarization state of the scattered signals, yet full polarization information would assist in the study of the scattering process. This thesis documents the conversion of one of the scatterometer's transceivers to a polarimeter capable of measuring the complete polarization state.

Some theoretical ramifications of frequency-modulated polarimetry are analyzed, and it is shown that polarization information is available at the intermediate frequency sections of a frequency-modulated scatterometer. Techniques for extracting the polarization information are discussed, and circuitry to provide this information is added to the scatterometer.

The results of testing the polarimeter both in the laboratory and in the field are presented. Several problem areas are identified and discussed including the effects of non-simultaneous channel sampling, channel to channel filter frequency response mismatches, the performance of linear power detection circuitry and the effects of internally generated reflections.

Sample results from the polarimetric characterization of a field of wheat are presented for two different days within the growing season.

List of Acronyms

ARC	Active Radar Calibrator
CCRS	Canada Centre for Remote Sensing
CW	Continuous Wave
D to A	Digital to Analog
FM	Frequency-Modulated
FM-CW	Frequency-Modulated, Continuous Wave
IF	Intermediate Frequency
I/O	Input/Output
JPL	Jet Propulsion Laboratory
RF	Radio Frequency
SAR	Synthetic Aperture Radar
VCO	Voltage-Controlled Oscillator
YIG	Yttrium-Iron-Garnet

Table of Contents

List of Figures

List of Tables

Chapter 1

INTRODUCTION

1.1. Background

The rapid advancement of space technology has heightened interest in the field of remote sensing. The ability to place a satellite in an orbit which covers most of the globe in a matter of days makes it possible for on board sensors to gather enormous amounts of information. This in turn leads to the requirement for efficient methods of interpreting the data as well as for sensors which will provide complementary data. Both of these areas are under investigation by the scientific community.

Most of the sensor systems used to date have been optical in nature. Information is gathered in the visible or near infrared frequency bands. Radiation at these frequencies will not pass through clouds, so the information obtained is not always representative of the underlying terrain. Since electromagnetic energy in the microwave and lower spectral bands passes through clouds with little attenuation, an interest in radio detection and ranging (radar) systems has developed. Radiation at the lower frequencies also interacts with the Earth's surface differently than light, thereby providing information which complements the optical. Radars have been shown to be useful for contour mapping of terrain [1] as well as for measuring wind speed over the sea [2], salinity levels in the ocean [3] and the moisture content of soil [4]. Radar data has also been used both independently and together with optical data to classify forests and agricultural crops [5]. For each of these applications performance can be optimized by choosing the frequency band(s) in which the radar will operate

and the polarization configuration for the radar's transmitter and receiver.

Attempts to classify crops on the basis of radar signatures at various frequencies and polarization states have appeared in the literature for some time[1]. The results show that improved classification accuracies are obtained when using a multiple band radar with at least two and sometimes three or four transmit/receive polarization combinations [7, 5]. More recently measurements taken with the JPL *L*-band synthetic aperture radar (SAR) provided partial phase data along with the amplitudes of the backscattered signals in horizontally and vertically polarized receiver channels. A study of this data by Ulaby et. al. [8] has noted marked changes in the phases of the backscattered signals from corn as opposed to those from bare fields or soybeans. This tends to indicate that the availability of complete polarization information will aid in the classification process and should be sought in future measurement campaigns.

The University of Saskatchewan is currently under contract to the Canada Center for Remote Sensing (CCRS) to carry out measurements on agricultural crops using a microwave radar system. These measurements will strengthen the existing data base and make it easier to interpret data gathered from the RADARSAT satellite in the 1990's. The radar system in use belongs to CCRS and is on loan to the University for the duration of the contract. It consists of three separate frequency- modulated transceivers with a common data acquisition and control unit. The transceivers operate at *L*-band (1.535 GHz.), *C*-band (5.55 GHz.) and *K*-band (13.4 GHz.), respectively. Each can transmit using either vertical or horizontal polarization and can simultaneously receive both of these polarization states. If the relative phase between the two received channels is also measured, the complete polarization state of the backscattered radiation can be determined. The Canada Center for Remote Sensing has allowed the University to pursue

---

[1] A Masters Thesis written by Paul Shepherd in May, 1987 gives a summary of the work from 1970 to date. See reference [6]

this possibility.

The purpose of the research described in this document is to enhance the operation of the existing radar system by adding circuitry to the *K*-band transceiver such that a complete characterization of the polarization state of radiation backscattered from the target can be determined. Modifications to the *C*-band and *L*-band units can be made at a later date if the results from the *K*-band measurements are encouraging.

1.2. Organization of the Thesis

The design of an instrument to measure the polarization state of received radiation requires an understanding of the polarization phenomenon itself. Accordingly, Chapter 2 discusses the theory of polarization. The polarization ellipse for monochromatic radiation will be developed, followed by an extension to the quasi-monochromatic case through the use of the coherency matrix. The coherency matrix is shown to be separable into polarized and unpolarized matrices, from which various parameters describing the polarization state can be easily derived. Methods of determining the coherency matrix elements are given.

The radars in use are continuous-wave (CW), frequency modulated (FM) units. The principles of FM-CW radar are therefore described in Chapter 3. The basic concepts are followed by a description of scatterometry and the monostatic radar equation. The radio frequency (RF) spectrum is discussed, followed by a derivation of the intermediate frequency (IF) spectrum due to a point target. Chapter 3 also describes the operation of the radar system in question, along with a discussion of some of its limitations.

The theory of polarization introduced in Chapter 2 is extended to the FM radar case in Chapter 4. Possible methods for using the existing equipment to measure the polarization state are given and a selected method is developed in detail. The designs used for the modifications are presented and

the resulting system operation is explained.

System calibration and testing is discussed in Chapter 5. Where possible, characterization of the system components is carried out. Since the modifications resulted in a change of gain to the IF subsections, a system calibration was carried out to determine the new gain constants for use in subsequent operation. The calibration process is described in detail.

Performance limitations brought to light during the system testing are discussed in Chapter 6. Their implications on the validity of the field measurements are examined along with a discussion of how the data might be analyzed to recognize system related degradations.

Some preliminary field data resulting from measurements carried out on a field of wheat is given in Chapter 7. A brief discussion of the results is presented in light of the performance degradations brought forth in Chapter 6.

Chapter 8 gives a summary of the research and suggests several methods to improve the operation of the equipment.

Chapter 2

POLARIZATION THEORY

2.1. The Concept Of Polarization

If Maxwell's equations are solved for uniform plane waves travelling in free space, two independent sets of solutions are obtained[2]. When using a rectangular coordinate system, one set pertains to the electric field vector in the x direction (E_x) and the magnetic field vector in the y direction (B_y), while the other pertains to the electric field vector in the y direction (E_y) and the magnetic field vector in the x direction (B_x). The solutions for the electric field are of the form:

$$E_x = A_x \cos(\omega t - kz + \phi_x)$$

and

$$E_y = A_y \cos(\omega t - kz + \phi_y). \tag{2.2}$$

where

- A_x and A_y are the magnitudes of the field components in the x and y axes respectively,
- ω is the angular frequency of the radiation,
- ϕ_x and ϕ_y are constant phase terms,

---

[2]The discussions of polarization given in this chapter essentially follow those of Born and Wolf in [9]

- k is the space phase factor and
- t is time.

By setting $z = 0$, the motion of the tip of the electric field vector can be plotted in the x-y plane as a function of time. From equation (2.2) above, and with $z = 0$,

$$E_x = A_x \cos(\omega t + \phi_x)$$

which can be rewritten in the form

$$\frac{E_x}{A_x} = \cos\omega t \cos\phi_x - \sin\omega t \sin\phi_x \tag{2.3}$$

and similarly,

$$\frac{E_y}{A_y} = \cos\omega t \cos\phi_y - \sin\omega t \sin\phi_y. \tag{2.4}$$

Multiplying equation (2.3) by $\sin\phi_y$ and subtracting from it the product of equation (2.4) and $\sin\phi_x$ gives:

$$\frac{E_x}{A_x}\sin\phi_y - \frac{E_y}{A_y}\sin\phi_x = \cos\omega t \cos\phi_x \sin\phi_y - \sin\omega t \sin\phi_x \sin\phi_y - \cos\omega t \cos\phi_y \sin\phi_x + \sin\omega t \sin\phi_y \sin\phi_x$$

which can be reduced to

$$\frac{E_x}{A_x}\sin\phi_y - \frac{E_y}{A_y}\sin\phi_x = \cos\omega t \sin(\phi_y - \phi_x). \tag{2.5}$$

In the same fashion, multiplying equation (2.3) by $\cos\phi_y$ and subtracting from this the product of equation (2.4) and $\cos\phi_x$ gives:

$$\frac{E_x}{A_x}\cos\phi_y - \frac{E_y}{A_y}\cos\phi_x = \sin\omega t\sin(\phi_y-\phi_x). \tag{2.6}$$

Summing the squares of equation (2.5) and equation (2.6) and reducing results in:

$$\frac{E_x^{\,2}}{A_x^{\,2}} + \frac{E_y^{\,2}}{A_y^{\,2}} - \frac{2E_xE_y}{A_xA_y}\cos(\phi_y-\phi_x) = \sin^2(\phi_y-\phi_x). \tag{2.7}$$

Equation (2.7) describes an ellipse in the x-y plane. It is specifically referred to as the polarization ellipse. A description of its shape is referred to as the polarization of the radiation. The variables describing the polarization ellipse are A_x, A_y, ϕ_x, and ϕ_y. Since ϕ_x and ϕ_y appear only as a difference, the notation can be simplified by defining the difference (ϕ_y -ϕ_x) to be delta (δ). These variables can take on certain values which result in simplification of the polarization equation. If the phase difference (δ) is zero, (i.e, ϕ_x=ϕ_y) equation (2.7) reduces to:

$$E_y = \frac{A_y}{A_x}E_x.$$

This is the equation for a straight line and illustrates the case of linear polarization. Linear polarization states are often described by the magnitude or intensity of the radiation and the angle which the above line makes with the x axis.

Alternately, if A_x=A_y=A and the phase difference δ is either plus or minus $\pi/2$, equation (2.7) becomes:

$$E_x^{\,2} + E_y^{\,2} = A^2.$$

This is the equation of a circle in the x-y plane and shows the case of circular polarization. Substitution of the values $E_x=A\cos(\omega t)$ and $E_y=A\cos(\omega t+\pi/2)$ (i.e. $\delta=\pi/2$) followed by plotting results in a locus which moves counterclockwise as time increases if viewed from the negative z axis. This is termed left-handed polarization. On the other hand, if the phase difference δ is $-\pi/2$, the locus will move in a clockwise direction and will illustrate right-handed polarization. If radiation is known to be circularly polarized, the magnitude of the electric field and the sense of rotation are all that is required to completely specify the polarization.

All other combinations of variables result in elliptical polarization. Specification of the ellipse may then be in terms of A_x, A_y and δ or in terms of the x and y axis intensities (A_x^2 and A_y^2), the axial ratio (the ratio of the major to minor axes), orientation angle (the angle that the major axis makes with the x axis), and the sense of rotation. The ellipticity angle (the tangent of the axial ratio) may be used in place of the axial ratio. In such a case the sense of rotation may be included in the ellipticity angle by including a sign term, with positive values denoting counterclockwise (left-hand) rotation and negative values clockwise (right-hand) rotation [10, 11].

2.2. The Coherency Matrix

The discussion of polarity in the preceding section was based on the analysis of a monochromatic plane wave. In most cases however, an intercepted radiation field will have been generated by the superposition of many individual radiators with many possible polarization states. In addition, the radiation will not be monochromatic, but will have some average frequency with a spread of energy around this average. The coherency matrix was developed to help deal with the analysis of radiation of this sort.

An intercepted radiation field will have electric field vectors in the x and y directions represented by $E_x(t)$ and $E_y(t)$, respectively. These can be formed into a column vector $[E]$ given as:

$$[E] \equiv \begin{bmatrix} E_x(t) \\ \\ E_y(t) \end{bmatrix}$$

The transposed complex conjugate of this column vector is denoted by $[E]^+$ and can be written as:

$$[E]^+ \equiv [E_x^*(t),\ E_y^*(t)].$$

The coherency matrix $[J]$ is formed as the time average of the product of $[E]$ and $[E]^+$:

$$[J] \equiv \langle [E] \times [E]^+ \rangle = \langle \begin{bmatrix} E_x(t) \\ \\ E_y(t) \end{bmatrix} [E_x^*(t),\ E_y^*(t)] \rangle \tag{2.8}$$

$$= \begin{bmatrix} \langle E_x(t)E_x^*(t) \rangle & \langle E_x(t)E_y^*(t) \rangle \\ \\ \langle E_y(t)E_x^*(t) \rangle & \langle E_y(t)E_y^*(t) \rangle \end{bmatrix}$$

$$[J] \equiv \begin{bmatrix} J_{xx} & J_{xy} \\ \\ J_{yx} & J_{yy} \end{bmatrix}$$

The individual elements of the coherency matrix are called coherencies. It should be noted that they are defined using the complex representations for the electric field vectors, so complex notation should always be employed when dealing with them. The definitions show that the diagonal elements in the coherency matrix are real, whereas the off-diagonal elements may be complex quantities. In addition, the two off-diagonal elements are complex

conjugates. From this it can be inferred that a complete description of the coherency matrix requires the determination of four quantities.

The utility of this definition for the coherency matrix lies in the fact that its components can be readily determined by measurement. This will be shown after a discussion relating the coherency matrix to polarization.

2.2.1. Coherency Matrices for Polarized and Unpolarized Radiation

As noted in the previous section, the coherency matrix can describe radiation resulting from the superposition of many wavefronts. Each of these will have a specific magnitude and phase, but the individual magnitudes and phases may vary considerably. The superposition of these wavefronts can result in an electric field vector whose magnitude in the x-y plane is independent of the angle from the x axis. If in addition to this the phase of the resultant field varies randomly with a uniform distribution, the radiation is said to be unpolarized.

In general, the superposition of many wavefronts will result in an electric field which will have both polarized and unpolarized components. Such a field is called partially polarized and can be characterized in part by the polarization ratio (m), defined to be the ratio of the intensity of the polarized portion to the total intensity.

The coherency matrix describing a partially polarized field can be resolved into two components, one which describes the polarized portion of the radiation and the other the unpolarized portion. These two components can then be used to describe the complete polarization state, that being the polarization ratio in addition to the parameters of the polarization ellipse. The methods used to do this are described below.

2.2.1.1. Polarized Radiation

It was shown in section 2.1 that the tip of the electric field vector of a uniform, monochromatic plane wave propagating along the z axis will result in the tracing of an ellipse in the x-y plane. The radiation will therefore be completely polarized and the coherency matrix for polarized radiation can be developed directly from the electric field equation. For the plane waves discussed previously,

$$E_x = A_x \cos(\omega t + \phi_x)$$

and

$$E_y = A_y \cos(\omega t + \phi_y)$$

or, expressed as analytic signals ,

$$E_x = A_x e^{i(\omega t + \phi_x)};$$

and

$$E_y = A_y e^{i(\omega t + \phi_y)}.$$

The definition (2.8) on page 9 then gives for the coherencies:

$$\begin{aligned} J_{xx} &= \langle E_x(t) E_x^{*}(t) \rangle \\ &= \langle A_x^{2} \rangle \end{aligned}$$

$$\begin{aligned} J_{xy} &= \langle E_x(t) E_y^{*}(t) \rangle \\ &= \langle A_x A_y e^{-i\delta} \rangle \end{aligned}$$

$$J_{yx} = \langle E_y(t) E_x^{*}(t) \rangle$$
$$= \langle A_y A_x e^{i\delta} \rangle$$

$$J_{yy} = \langle E_y(t) E_y^{*}(t) \rangle$$
$$= \langle A_y^2 \rangle$$

where δ is defined to be ϕ_y-ϕ_x, and therefore:

$$[J] = \begin{bmatrix} A_x^2 & A_x A_y e^{-i\delta} \\ A_x A_y e^{i\delta} & A_y^2 \end{bmatrix}$$

The parameters of the polarization ellipse can be expressed directly in terms of the coherencies of this matrix. The values of interest are the intensity, the axial ratio and the orientation angle (the angle that the major axis of the ellipse makes with the x axis). Since the total intensity will simply be the sum of the intensities in the x and y axes, it can immediately be expressed as:

$$I_p = J_{xx} + J_{yy}$$

The determination of the axial ratio and orientation angle requires an intermediate development. Starting with the general equation for an ellipse having its major axis lying on the x axis, a rotation of the co-ordinate system is performed to the angle ψ. The coefficients of the rotated equation are equated to the coefficients in equation (2.7) to obtain the relationships between the major axis (a), minor axis (b) and orientation angle (ψ and the parameters A_x, A_y, and δ of equation (2.7). The calculations are quite lengthy and have been documented by Born in [9], so only the results are given here. These are:

$$\tan 2\psi = \frac{2A_x A_y \cos\delta}{A_x^2 - A_y^2}$$

and

$$\sin 2\chi = \frac{2A_x A_y \sin\delta}{A_x^2 + A_y^2}$$

where χ is the ellipticity angle (the tangent of the axial ratio).

The relations between the axial ratio, orientation angle and the coherencies can then be determined as

$$\tan 2\psi = \frac{J_{xy} + J_{yx}}{J_{xx} - J_{yy}} \tag{2.9}$$

and

$$\sin 2\chi = \frac{-i(J_{yx} - J_{xy})}{J_{xx} + J_{yy}}. \tag{2.10}$$

2.2.1.2. Unpolarized Radiation

If the intensity of radiation components in the direction perpendicular to the direction of propagation is independent of orientation, and furthermore if retardation of one of the components with respect to the other has no effect on this intensity at any orientation, the radiation is said to be completely unpolarized. The implications of these statements can be best understood by deriving an expression for the intensity.

With definitions for $E_x(t)$ and $E_y(t)$ as before, the component of the electric field vector in a direction which makes an angle θ with the x axis is:

$$E(\theta) = E_x(t)\cos\theta + E_y(t)\sin\theta, \tag{2.11}$$

where θ is the angle fom the x axis to the electric field vector. If the y axis component is arbitrarily delayed in phase by an amount gamma (γ), equation (2.11) will become:

$$E(\theta,\gamma) = E_x(t)\cos\theta + E_y(t)\sin\theta\, e^{-i\gamma},$$

and the average intensity of the electric field component as a function of θ and γ will be:

$$I(\theta,\gamma) = \langle E \times E^* \rangle$$

$$= \langle \{E_x(t)\cos\theta + E_y(t)\sin\theta\, e^{-i\gamma}\} \times \{E_x^*(t)\cos\theta + E_y^*(t)\sin\theta\, e^{i\gamma}\} \rangle$$

$$= \langle E_x(t)E_x^*(t)\cos\theta\cos\theta + E_x(t)E_y^*(t)\cos\theta\sin\theta e^{i\gamma} + E_y(t)E_x^*(t)\sin\theta\cos\theta e^{-i\gamma} + E_y(t)E_y^*(t)\sin\theta\sin\theta \rangle$$

$$= \langle E_x(t)E_x^*(t)\rangle\cos^2\theta + \langle E_x(t)E_y^*(t)\rangle\cos\theta\sin\theta e^{i\gamma} + \langle E_y(t)E_x^*(t)\rangle\sin\theta\cos\theta e^{-i\gamma} + \langle E_y(t)E_y^*(t)\rangle\sin$$

$$I(\theta,\gamma) = J_{xx}\cos^2\theta + J_{xy}\sin\theta\cos\theta e^{i\gamma} + J_{yx}\sin\theta\cos\theta e^{-i\gamma} + J_{yy}\sin^2\theta \tag{2.12}$$

Examination of this equation reveals that in order to have the intensity independent of gamma, both J_{xy} and J_{yx} must be zero. In addition, for the intensity to be independent of θ requires J_{xx} to be equal to J_{yy}. The statements in the first paragraph of this section therefore imply that the coherency matrix for unpolarized radiation is:

$$[J]_u = \begin{bmatrix} J_u & 0 \\ 0 & J_u \end{bmatrix}$$

where $J_u = J_{xx} = J_{yy}$.

2.2.2. Separation of a Coherency Matrix into Polarized and Unpolarized Components

The determinant of the coherency matrix developed previously for polarized radiation is zero. This fact can be used to advantage when dealing with the coherency matrices of partially polarized radiation. If the determinant of a coherency matrix is non-zero, an unpolarized component must be present. Alternately, since the off-diagonal elements of the unpolarized coherency matrix were zero, a coherency matrix which has J_{xy} and J_{yx} non-zero will imply the presence of a polarized component. The polarized and unpolarized components can be separated by assuming that the coherency matrix is the sum of a polarized and an unpolarized matrix, the individual matrices having the forms derived in sections 2.2.1.1 and 2.2.1.2. In equation form:

$$[J]_t = [J]_p + [J]_u \ .$$

and in full form

$$\begin{bmatrix} J_{xx} & J_{xy} \\ J_{yx} & J_{yy} \end{bmatrix} = \begin{bmatrix} J_{px} & J_{xy} \\ J_{yx} & J_{py} \end{bmatrix} + \begin{bmatrix} J_u & 0 \\ 0 & J_u \end{bmatrix}$$

where J_{px} and J_{py} are the x and y axis components of the intensity of the polarized part of the radiation and J_u is one half of the total intensity of the unpolarized portion of the radiation.

Solving this equation with the constraints that the determinant of the

polarized matrix must be zero, and that the quantities J_{px} and J_{py} must be positive results in the following values:

$$J_u = \frac{1}{2}[(J_{xx} + J_{yy}) - \sqrt{(J_{xx} + J_{yy})^2 - 4(J_{xx}J_{yy} - J_{xy}J_{yx})}\ ]$$

$$J_{px} = J_{xx} - J_u$$
$$J_{py} = J_{yy} - J_u \ .$$

Hence, it is possible to uniquely represent a given coherency matrix as the sum of a completely polarized field and a completely unpolarized field. Having done so, one can assume that the polarized coherency matrix has arisen from a uniform, monochromatic plane wave, and proceed directly to determine the parameters of the polarization ellipse as described in section 2.2.1.1. The polarization ratio m is given directly as the ratio of the polarized intensity to the total intensity. Re-stating this in equation form gives:

$$\tan 2\psi = \frac{J_{xy}+J_{yx}}{J_{xx}-J_{yy}}$$

$$\sin 2\chi = \frac{-i(J_{yx}-J_{xy})}{\sqrt{(J_{xx}-J_{yy})^2 + 4J_{xy}J_{yx}}}$$

$$m = \frac{I_p}{I_t} = \frac{J_{px}+J_{py}}{J_{xx}+J_{yy}} = \frac{\sqrt{(J_{xx}-J_{yy})^2 + 4J_{xy}J_{yx}}}{J_{xx}+J_{yy}}$$

2.2.3. Determination of the Coherency Matrix Elements

Determination of the coherency values through measurement is carried out using a combination of intensity and phase measurements. Since four variables must be determined, at least four measurements must be taken. Two of the measurements must be intensity measurements. The remaining two may be either phase or some combination of intensities. This section will describe two specific sets of measurements which may be used to specify the coherencies. They are illustrative of the many combinations possible[3].

2.2.3.1. Specification with Two Intensities and Two Phase Measurements

Assuming that the intercepted radiation is bandpass in nature, it can be described by the analytic signals

$$E_x(t)=a_x(t)\, e^{i[\omega_c t+\phi_x(t)]}$$

and

$$E_y(t)=a_y(t)\, e^{i[\omega_c t+\phi_y(t)]}$$

where ω_c is the center frequency. The coherencies are then by definition

$$\begin{aligned} J_{xx} &= \langle a_x{}^2(t)\rangle \\ J_{xy} &= \langle a_x(t)a_y(t)\, e^{-i\delta(t)}\rangle \\ J_{yx} &= \langle a_x(t)a_y(t)\, e^{i\delta(t)}\rangle \\ J_{yy} &= \langle a_y{}^2(t)\rangle \ . \end{aligned}$$

Noting that the sum and differences of the off diagonal coherencies are

---

[3]A summary of measurement techniques used by radio astronomers has been compiled by Cohen in [12].

$$J_{xy}+J_{yx} = \langle 2a_x a_y(t)\cos\delta(t)\rangle \quad \text{and}$$
$$-i(J_{yx}-J_{xy}) = \langle 2a_x a_y(t)\sin\delta(t)\rangle = \langle 2a_x a_y(t)\cos(\delta(t)-\frac{\pi}{2})\rangle \ ,$$

the values of the coherencies can be measured using the configuration shown in Figure 2-1. The values of J_{xx} and J_{yy} will then be twice the power measured at points A and D respectively. The signals at points B and C will yield the coherencies according to

$$J_{xx}=2A \qquad J_{yy}=2D$$
$$J_{xy}=2(B+iC) \qquad J_{yx}=2(B-iC).$$

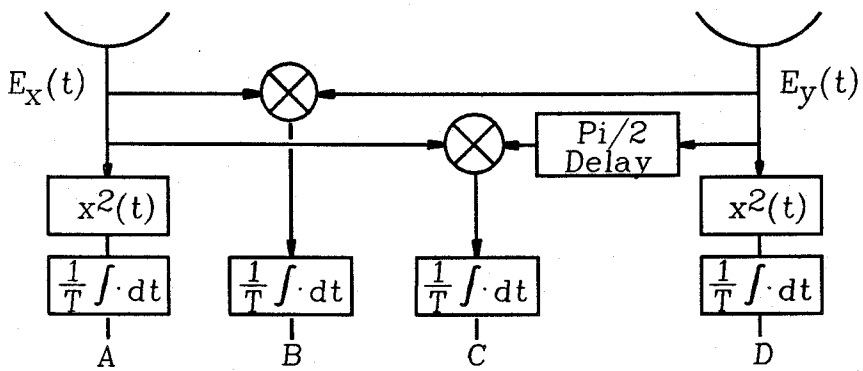

Figure 2-1: Determination of Coherencies using Intensity and Phase Information

2.2.3.2. Specification Using Only Intensity Measurements

Recalling from equation (2.12) that the intensity of the electric field as a function of angle from the x axis (θ) and delay of the y axis component (γ) is given as

$$I(\theta,\gamma) = J_{xx}\cos^2\theta + J_{xy}\sin\theta\cos\theta e^{i\gamma} + J_{yx}\sin\theta\cos\theta e^{-i\gamma} + J_{yy}\sin^2\theta \quad (2.13)$$

simple expressions can be derived for the coherencies by proper selection of θ and γ. This yields

$$J_{xx} = I(0,0)$$

$$J_{xy} = \frac{1}{2}\{I(45,0) - I(135,0) - i[I(45,\frac{\pi}{2}) - I(135,\frac{\pi}{2})]\}$$

$$J_{yx} = \frac{1}{2}\{I(45,0) - I(135,0) + i[I(45,\frac{\pi}{2}) - I(135,\frac{\pi}{2})]\}$$

$$J_{yy} = I(90,0).$$

Thus it is possible to determine the elements of the coherency matrix by measuring the intensity of the electric field vector in the 0, 45, 90 and 135 degree directions with respect to the x axis and by remeasuring the intensity in the 45 and 135 degree directions after the y component of the electric field has been delayed by $\pi/2$ radians with respect to the x component. This corresponds to power measurements with a linearly polarized antenna oriented at angles of 0, 45, 90, and 135 degrees with respect to the x axis, and measurements of the power received by left and right circularly polarized antennas.

Only four of the six intensities mentioned above need be actually measured. This is due to the fact that the total power received by any pair of antennas with orthogonal polarization properties will be identical to the power received by any other orthogonally polarized antenna pair. Once this total power is known (from the measurement of two orthogonal intensities) a single measurement from any other orthogonally polarized pair will suffice.

The polarization parameters may be re-stated in terms of the six intensities discussed above. Doing so results in:

$$\tan 2\psi = \frac{I(45,0) - I(135,0)}{I(0,0) - I(90,0)}$$

$$\sin 2\chi = \frac{I(45,\frac{\pi}{2}) - I(135,\frac{\pi}{2})}{\sqrt{\left(I(0,0) - I(90,0)\right)^2 + \left(I(45,0) - I(135,0)\right)^2 + \left(I(45,\frac{\pi}{2}) - I(135,\frac{\pi}{2})\right)^2}}$$

$$m = \frac{\sqrt{\left(I(0,0) - I(90,0)\right)^2 + \left(I(45,0) - I(135,0)\right)^2 + \left(I(45,\frac{\pi}{2}) - I(135,\frac{\pi}{2})\right)^2}}{I(0,0) + I(90,0)}$$

$$m = \frac{\sqrt{\left(I(0,0) - I(90,0)\right)^2 + \left(I(45,0) - I(135,0)\right)^2 + \left(I(45,\frac{\pi}{2}) - I(135,\frac{\pi}{2})\right)^2}}{I(45,0) + I(135,0)}$$

$$m = \frac{\sqrt{\left(I(0,0) - I(90,0)\right)^2 + \left(I(45,0) - I(135,0)\right)^2 + \left(I(45,\frac{\pi}{2}) - I(135,\frac{\pi}{2})\right)^2}}{I(45,\frac{\pi}{2}) + I(135,\frac{\pi}{2})}$$

Chapter 3

FM-CW RADAR

3.1. General

This chapter will discuss the operation of frequency-modulated, continuous wave (FM-CW) radar. The basic operating priciples are described first, followed by an extension of the concepts to include scatterometry. An approximate expression for the spectrum of the transmitted waveform is then obtained, and the IF spectrum resulting from backscatter due to a point target is developed. A detailed description of the radar being used to fulfill the obligations under the CCRS contract is given to provide the background necessary for the polarimeter implementations discussed in Chapter 4.

3.2. Basic Operation Of FM Radar

In an FM radar, the carrier sent from the radar transmitter is frequency modulated. If the carrier is turned on periodically for only a short time , the radar is called a pulsed-FM or chirp radar. On the other hand, if the carrier is continuously transmitted, the radar will be called a CW radar, hence the term FM-CW.

A generalized block diagram for an FM-CW radar system is shown in Figure 3-1. The transmitting and receiving antennas are shown as separate units for simplicity. The transmitter consists of a frequency variable source driving the transmitting antenna. Modulation of the carrier is provided by a waveform generator connected to the source. The radio frequency (RF) signals sent by the transmitting antenna are scattered by the target and

return to be intercepted by the receiving antenna. Inside the receiver, they are multiplied by a sample of the transmitted RF. The signal resulting from this multiplication is passed through a bandpass filter to become the intermediate-frequency (IF) output signal.

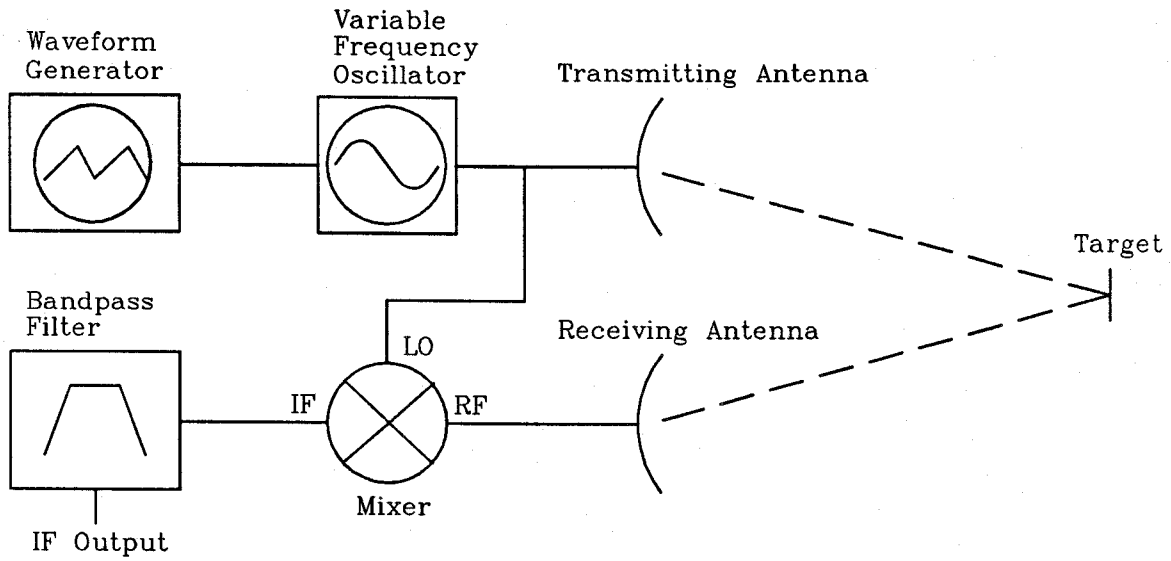

Figure 3-1: A Basic FM-CW Radar System

A plot of the carrier frequency vs. time is shown in Figure 3-2 where the modulation waveform is assumed to be triangular, centered about the frequency f_c, and ranging from a lower frequency f_l to an upper frequency f_u. Also shown on this plot is the frequency of the signal intercepted by the receiving antenna. The received signal has been delayed by a time τ, which corresponds to the time of travel from the transmitting antenna to the target and thence to the receiver. Since the multiplication process in the receiver will result in the sum and difference frequencies of the transmitted and received signals, and the sum frequency will be rejected by the bandpass filter, the instantaneous IF frequency can be taken from the graph as the difference between the two lines at any given point in time.

This instantaneous IF frequency can be quite simply related to the range

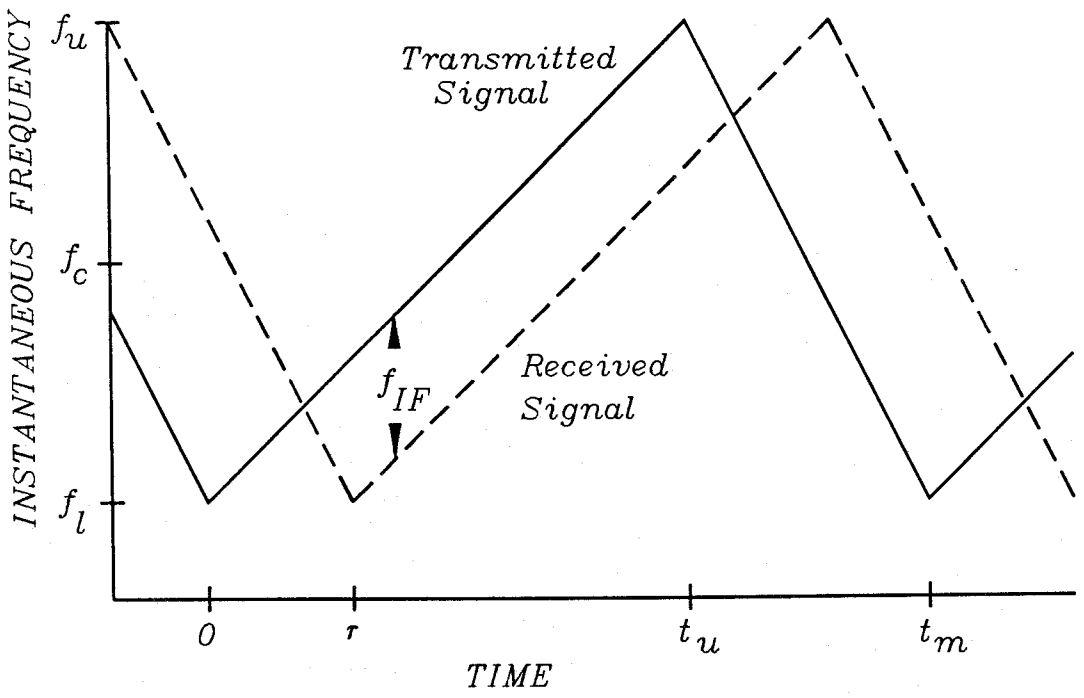

Figure 3-2: T_x and R_x Frequencies vs. Time for Basic FM-CW Radar

to the target. For the upsweep period, the magnitude of the change in frequency over a time interval t will be given by:

$$\Delta f = \frac{Bt}{t_u}$$

where

- Δf is the change in frequency,
- B is the bandwidth of the sweep(i.e. the peak to peak frequency deviation) and
- t_u is the total time taken for the positive going frequency ramp.

If it is assumed that the radar signals are travelling through a low dielectric medium (such as air or space) the speed of the signals will be

approximately equal to the speed of light. Thus the time of travel between the transmitting and receiving antennas will be given by:

$$\tau = \frac{R_1 + R_2}{c} \tag{3.2}$$

where

- R_1 is the range from the transmitting antenna to the target,
- R_2 is the range from the target to the receiving antenna and
- c is the speed of light.

Then, since the difference frequency at the IF output (f_{IF}) is simply the change in frequency over the time τ, it will be given by

$$\Delta f = f_{IF} = \frac{B(R_1 + R_2)}{ct_u} \ . \tag{3.3}$$

If the two antennas are co-located (the monostatic case) R_1 will equal R_2 and equation (3.3) can be rewritten as

$$R = \frac{ct_u f_{IF}}{2B} \ . \tag{3.4}$$

The range to the target can thus be determined from a measurement of the instantaneous IF frequency, all other values being known.

The above explanation has overlooked several factors. First, it has only dealt with the positive going portion of the sweep. A second IF frequency will be generated by the negative going portion, which can cause ambiguity in the frequency measurement. This problem can be overcome by ensuring that the upsweep time is long in comparison to the downsweep interval. The

difference frequency generated during the downsweep interval can then be made high enough to be rejected by the bandpass filter.

A second factor results from the use of a periodic modulating signal. The true spectrum at the IF is not simply a delta function, but consists of a line spectrum with many components. This complicates the measurement of the IF frequency. If the IF frequency is taken to be that corresponding to the largest spectral line, discrete IF frequencies will result, which in turn implies discrete range indications through use of equation (3.4). The range resolution of the system will therefore depend on the modulation frequency, which controls the spacing of the spectral lines.

3.3. Scatterometry And The Radar Equation

The above section gave details on how the FM-CW radar operates and determines the range to target. It said nothing, however regarding the amplitude of the reflected signal. If the device is calibrated such that it provides a measure of the signal attenuation between the transmitted and returned signals, it is said to be a scatterometer. Such a device measures the scattering cross section due to a target or targets located within a certain range extent. To fully understand what this means, an explanation of the radar equation is required.

3.3.1. The Radar Equation

Considering again the situation depicted in Figure 3-1, energy from the transmitting antenna propagates toward the target. At a given distance R from the antenna aperture, the power incident on an area A is given by [13]

$$P_i = \frac{P_t G_{ts} A}{4\pi R^2_{ts}}$$

where

- P_i is the power incident on the area A,
- P_t is the power as measured at the transmit antenna terminals,
- G_{ts} is the gain of the transmitting antenna in the direction of the area A,
- R_{ts} is the distance from the antenna aperture to the area A and
- A is the area under consideration.

If the area A contains a target (scatterer) to be measured, the power intercepted by the target will be

$$P_{is} = \frac{P_t G_{ts} A_s}{4\pi R^2_{ts}} .$$

Here P_{is} is the power intercepted by the scatterer and A_s is the effective area of the target. This distinction between the actual area illuminated and the effective area of the target is necessary because some of the energy in the physical area may not be intercepted by the target (for example if the target contains some large holes).

In general, the target will absorb some of the incident radiation while re-radiating the remainder. The portion re-radiated may be sent in any direction, depending on the physical configuration of the target and its orientation with respect to the incident radiation. The power radiated from the target in the direction of the receiving antenna will be

$$P_{sr} = P_{is} \, (1-f_a) \, G_{sr} \, ,$$

with

- P_{sr} being the power radiated from the scatterer in the direction of the receiver,

- f_a as the fraction of the power absorbed by the target and
- G_{sr} as the gain of the target in the direction of the receiver.

The power available at the terminals of the receiving antenna will then be

$$P_r = \frac{\lambda^2 P_{sr} G_{rs}}{(4\pi)^2 R^2_{sr}}$$

where

- P_r is the received power,
- λ is the wavelength of the radiation,
- G_{rs} is the gain of the receiving antenna in the direction of the target and
- R_{sr} is the distance from the target to the receiver.

A combination of these equations results in the radar equation

$$P_r = \frac{\lambda^2 \ P_t G_{ts} G_{rs}}{(4\pi)^3 R^2_{ts} R^2_{sr}} \ [A_s (1-f_a) G_{sr}] \ .$$

The term in square brackets represents a special quantity. It consists of an effective area multiplied by a fraction and a dimensionless gain, and thus has units of area. Since the individual components are difficult to estimate, they are left lumped together and called the scattering cross section of the target, denoted by the Greek letter σ. The radar equation then becomes the familiar form of

$$P_r = \frac{\lambda^2}{(4\pi)^3} \ \frac{P_t G_{ts} G_{rs}}{R^2_{ts} R^2_{sr}} \ \sigma$$

for the bistatic case (when the receving and transmitting antennas are at different locations) and reduces to

$$P_r = \frac{\lambda^2}{(4\pi)^3} \frac{P_t G^2}{R^4} \sigma \tag{3.5}$$

in the monostatic case (ie. $G_{ts}=G_{rs}=G$ and $R_{ts}=R_{sr}=R$).

The development above assumed that all points in the target area were at a range R from the radar transmitter, and in addition that the angular extent of the target as viewed from the radar was small. If this is not the case, then both the varying range to target and the antenna pattern of the radar must be accounted for. When the target contains a multiplicity of small scatterers spread throughout the target area, the return from each scatterer must be considered. The total received power will then be the summation of the individual powers as given in equation (3.5) (for the monostatic case). Thus,

$$P_r = \frac{\lambda^2 P_t}{(4\pi)^3} \sum_{scat.} \frac{G^2_i}{R^4_i} \sigma_i$$

where

- P_r is the total received power,
- G_i is the antenna gain in the direction of the i^{th} scatterer,
- σ_i is the scattering cross section of the i^{th} scatterer and
- R_i is the range to the i^{th} scatterer.

If in addition, the magnitudes of the individual scattering cross sections are similar in magnitude, the σ_i's can be replaced by the differential scattering coefficient, defined as the average value of the scattering cross section per

unit area. Then for large numbers of scatterers, the summation may be replaced with an integral to yield the area extensive form of the radar equation

$$P_r = \frac{\lambda^2 P_t}{(4\pi)^3} \int \frac{G_A^2 \sigma^0}{R^4} \, dA \; .$$

where

- G_A is the gain in the direction of the elemental area dA,
- σ^0 is the differential scattering cross section,
- and the integral is evaluated over the entire illuminated area.

For radars with narrow beam width antennas, the radiation's angle of incidence upon the scatterers will be essentially constant over the illuminated area. This allows the differential scattering cross section to be brought outside the integral to yield

$$P_r = \frac{\lambda^2 P_t}{(4\pi)^3} \sigma^0(\theta) \int \frac{G_A^2}{R^4} \, dA \; . \tag{3.6}$$

As was the case in equation (3.5) above, all quantities in equation (3.6) are known or can be measured except for the differential scattering coefficient σ^0 at the angle of incidence θ, which can then be calculated.

A volume extensive form for the scattering cross section can also be defined and related to a form of the radar equation. It will not be presented here since it does not bear on the problem at hand. It is mentioned only for completeness. The interested reader is referred to the work of Ulaby, Moore and Fung [13].

3.4. Spectra Associated With FM-CW Radar

An FM-CW radar will illuminate the target with radiation that is not monochromatic. The target will scatter this radiation and return some portion of it, which will then be processed by the radar's receiving circuitry. To understand the details of what is actually being measured, a description of both the radiated and the intermediate-frequency spectrums is necessary. This section provides those details as they pertain to the measuring system in use.

3.4.1. Spectrum of the Radiated Signal

The determination of the spectrum for an FM signal is in general quite complex. Even for the case of a sinusoidal modulating signal, the exact solution contains an infinite number of sidebands, the magnitude of each being determined by a Bessel function. Closed form solutions for the Bessel functions do not exist, but values for them have been tabulated. The calculation of an FM spectrum is then possible, but quite tedious [14].

The radar system described in this document uses a triangular modulating waveform. In addition, the ratio of the RF frequency deviation to the highest modulating frequency (i.e. the deviation ratio) is on the order of several million. Either of these facts is sufficient grounds to rule out the calculation of the exact spectral components of the radiated signal, allowing only general observations to be made.

Since the modulating waveform is periodic, the spectrum at the RF will be a line spectrum. The spectral lines will have a frequency separation corresponding to the modulation frequency.

The application of Carson's rule [14] results in an estimate of the RF bandwidth essentially equal to the peak to peak frequency deviation.

The magnitude of the spectral lines can be estimated by an application of

Woodward's theorem [15] which states that the magnitude of the power spectrum for an FM waveform with large modulation index is proportional to the amount of time the carrier spends at the corresponding instantaneous frequency. Since the modulation is triangular, the carrier will spend the same time at every frequency within the RF sweepwidth, implying that the magnitudes of all spectral lines are equal.

Summarizing the above, the expected power spectrum for the radiated signal is a rectangular line spectrum having a bandwidth equal to the peak to peak frequency deviation. No information has been determined regarding the phases of the spectral lines in the amplitude spectrum.

3.4.2. The Spectrum of a Signal Scattered from a Point Target

This section will present the derivation of the spectrum resulting at the IF port of an FM radar due to backscattering from a point target. The configuration of the radar is assumed to be as shown in Figure 3-1.

It is assumed that the instantaneous frequency of the source waveform at the radar is similar to that shown in Figure 3-2. The parameters of interest are:

- ω_c, the center frequency of the modulated carrier,
- t_u, the time interval occupied by the positive going sweep,
- t_d, the time interval occupied by the negative going sweep and
- t_m, the period of the composite modulating waveform.

Recalling that the voltage of an FM waveform is described by

$$v(t) = A \cos [\omega_c t + \int_0^t m(t)dt],$$

where $m(t)$ is the modulating waveform, and that the instantaneous

frequency is given by

$$\frac{d}{dt}\left[\omega_c t+\int_0^t m(t)dt\right]=\omega_c+m(t),$$

the modulating waveform can be described as

$$\begin{aligned} m(t) &= \frac{2\Delta\omega t}{t_u} && ;-\frac{t_u}{2}\le t\le\frac{t_u}{2} \\ &= \Delta\omega-\frac{2\Delta\omega}{t_d}\left(t-\frac{t_u}{2}\right) && ;\frac{t_u}{2}\le t\le\frac{t_u}{2}+t_d, \end{aligned}$$

where Δw is the peak frequency deviation of the carrier. The complete phase expression for the modulated carrier can then be obtained by integrating. Due to the nature of the source (a modulated VCO), the modulated carrier will be continuous in phase, therefore the phase function itself must be continuous. To ensure this, a constant of integration is added to the phase expression during the downsweep portion of the period. The resulting phase function is:

$$\begin{aligned} \theta(t) &= \omega_c t+\int_0^t m(t)dt \\ &= \omega_c t+\frac{\Delta\omega t^2}{t_u} && ;-\frac{t_u}{2}\le t\le\frac{t_u}{2} \\ &= \omega_c t+\Delta\omega\left(t+\frac{tt_u}{t_d}-\frac{t^2}{t_d}-\frac{t_u^2}{4t_d}-\frac{t_u}{4}\right) && ;\frac{t_u}{2}\le t\le\frac{t_u}{2}+t_d. \end{aligned} \quad (3.7)$$

The transmitted signal propagates to the point target, is scattered by that target, and propagates back to the receiving antenna. The time taken for the round trip travel will be given by

$$\tau = \frac{2R}{c},$$

where τ is the round trip time delay, R is the range to the target, and c is the speed of light. In addition to the time delay, the signal will experience an attenuation due to the free space path loss, over both the outgoing and incoming paths. The voltage sensed at the receiving antenna can then be described as:

$$v_r(t) = A_p \cos\{\theta_r(t)\},$$

where

- θ_r denotes the received phase, and
- A_p is a gain term incorporating both the attenuation over the outgoing and incoming paths and the antenna gain.

The voltage at the IF port of the mixer will be

$$v_{IF}(t) = A_p \cos\{\theta_t(t)\} \cos\{\theta_r(t)\}, \tag{3.8}$$

using $\theta_t(t)$ to denote the transmitted phase, and can be rewritten as

$$v_{IF}(t) = \frac{A_p}{2}\{\cos[\theta_t(t) - \theta_r(t)] + \cos[\theta_t(t) + \theta_r(t)]\}. \tag{3.9}$$

Noting that the second term of equation (3.9) will be removed by filtering leaves the IF voltage as

$$v_{IF}(t) = \frac{A_p}{2}\cos[\theta_t(t) - \theta_r(t)]. \tag{3.10}$$

Since the received phase term differs from the transmitted phase only by a

time delay τ, an expression for it can be obtained by substitution of values into equation (3.7). Subsequent mathematics is simplified if the time origin is chosen to give θ_t and θ_r as

$$\theta_t=\theta(t+\frac{\tau}{2}) \quad \text{and} \quad \theta_r=\theta(t-\frac{\tau}{2}).$$

The use of equation (3.7) then results in the phase difference expression given below.

$$\begin{aligned}
\theta_t-\theta_r &= \omega_c\tau+\Delta\omega\,(at^2+bt+c) && ; -\frac{t_u}{2}-\frac{\tau}{2} \le t \le -\frac{t_u}{2}+\frac{\tau}{2} \\
&= \omega_c\tau+\frac{2\Delta\omega\tau t}{t_u} && ; -\frac{t_u}{2}+\frac{\tau}{2} \le t \le \frac{t_u}{2}-\frac{\tau}{2} \\
&= \omega_c\tau+\Delta\omega\,(-at^2+bt-c) && ; \frac{t_u}{2}-\frac{\tau}{2} \le t \le \frac{t_u}{2}+\frac{\tau}{2} \\
&= \omega_c\tau-\frac{2\Delta\omega\tau t}{t_d}+\Delta\omega\tau\,(1+\frac{t_u}{t_d}) && ; \frac{t_u}{2}+\frac{\tau}{2} \le t \le \frac{t_u}{2}+t_d-\frac{\tau}{2}
\end{aligned} \qquad (3.11)$$

with the constants a, b and c defined as

$$\begin{aligned}
a &= \frac{1}{t_u}+\frac{1}{t_d} \\
b &= 1+\frac{t_u}{t_d}+\tau(\frac{1}{t_u}-\frac{1}{t_d}) \\
c &= \frac{t_u^2}{4t_d}+\frac{t_u}{4}-\frac{t_u\tau}{2t_d}+\frac{\tau^2}{4t_u}+\frac{\tau^2}{4t_d}-\frac{\tau}{2}.
\end{aligned}$$

The spectrum is obtained by finding the Fourier series associated with the IF voltage.

$$v_{IF}(t)=\sum_{n=-\infty}^{\infty} X_n e^{jn\omega_0 t}$$

$$X_n = \frac{1}{t_m} \int_{-t_u/2}^{t_u/2 + t_d} v_{IF}(t) e^{-jn\omega_0 t}\, dt \tag{3.12}$$

This integral can be broken into four using the time intervals over which the phase functions of equation (3.11) are defined. Note that the integrals for the first and third time intervals span a duration of only τ. For short range systems, this will be an extremely small fraction of the modulation period, and the integration over this interval will not significantly affect the overall result. The integral can thus be simplified by using only the second and fourth phase expressions and assuming that these apply to the entire integration interval. Equation (3.12) can then be evaluated as

$$X_n \approx \frac{A_p}{t_m} \int_{-t_u/2}^{t_u/2} \cos\left(\omega_c t + \frac{2\Delta\omega\tau t}{t_u}\right) e^{-jn\omega_0 t}\, dt + \frac{A_p}{t_m} \int_{t_u/2}^{t_u/2 + t_d} \cos\left[\omega_c t - \frac{2\Delta\omega\tau t}{t_d} + \Delta\omega\tau\left(1 + \frac{t_u}{t_d}\right)\right] e^{-jn\omega_0 t}\, dt$$

Denoting the first term of this expression by FT and the second term by ST, the evaluation of these integrals yields:

$$FT = \frac{A_p}{t_m} \int_{-t_u/2}^{t_u/2} \cos\left(\omega_c t + \frac{2\Delta\omega\tau t}{t_u}\right) e^{-jn\omega_0 t}\, dt$$

$$FT = \frac{A_p}{t_m} \left[\frac{e^{j\omega_c \tau} \sin\left(\Delta\omega\tau - n\omega_0 t_u/2\right)}{2\Delta\omega\tau/t_u - n\omega_0} + \frac{e^{-j\omega_c \tau} \sin\left(\Delta\omega\tau + n\omega_0 t_u/2\right)}{2\Delta\omega\tau/t_u + n\omega_0} \right] \tag{3.13}$$

$$ST = \frac{A_p}{t_m} \int_{t_u/2}^{t_u/2 + t_d} \cos\left[\omega_c t - 2\Delta\omega\tau t/t_u + \Delta\omega\tau(1 + t_u/t_d)\right] e^{-jn\omega_0 t}\, dt$$

$$ST = \frac{A_p}{t_m}\left(e^{-jn\omega_0 t_m/2 - j\omega_c\tau}\right)\frac{\sin\left(-\Delta\omega\tau - n\omega_0 t_d/2\right)}{-2\Delta\omega\tau/t_d - n\omega_0} + \frac{A_p}{t_m}\left(e^{jn\omega_0 t_m/2 + j\omega_c\tau}\right)\frac{\sin\left(-\Delta\omega\tau + n\omega_0 t_d/2\right)}{-2\Delta\omega\tau/t_d + n\omega_0} \qquad (3.14)$$

If the Fourier series is rewritten in the form

$$v_{IF}(t) = X_0 + \sum_{n=1}^{\infty}\left(X_n e^{jn\omega_0 t} + X_{-n} e^{-jn\omega_0 t}\right)$$

the terms in equations (3.13) and (3.14) can be used to obtain the series

$$\begin{aligned} v_{IF}(t) = {} & \frac{A_p t_u}{t_m}\frac{\sin(\Delta\omega\tau)}{\Delta\omega\tau}\cos(\omega_c\tau) + \frac{A_p t_d}{t_m}\frac{\sin(\Delta\omega\tau)}{\Delta\omega\tau}\cos(\omega_c\tau) \\ & + \sum_{n=1}^{\infty}\left[\frac{A_p t_u}{t_m}\frac{\sin(\Delta\omega\tau - n\pi t_u/t_m)}{\Delta\omega\tau - n\pi t_u/t_m}\cos(n\omega_0 t + \omega_c\tau)\right. \\ & + \frac{A_p t_u}{t_m}\frac{\sin(\Delta\omega\tau + n\pi t_u/t_m)}{\Delta\omega\tau + n\pi t_u/t_m}\cos(n\omega_0 t - \omega_c\tau) \\ & + \frac{A_p t_d}{t_m}\frac{\sin(\Delta\omega\tau - n\pi t_d/t_m)}{\Delta\omega\tau - n\pi t_d/t_m}\cos(n\omega_0 t + n\pi - \omega_c\tau) \\ & \left. + \frac{A_p t_d}{t_m}\frac{\sin(\Delta\omega\tau + n\pi t_d/t_m)}{\Delta\omega\tau + n\pi t_d/t_m}\cos(n\omega_0 t - n\pi - \omega_c\tau)\right] \end{aligned} \qquad (3.15)$$

An examination of this equation results in the observation that it can be considered to be the sum of two waveforms, one arising from the upsweep time interval and the other from the downsweep interval. As will be discussed later, the scatterometer under scrutiny in this document blanks the IF signal during the downsweep time interval. The IF spectrum will then be due only to those terms in equation (3.15) containing the factor t_u.

An example of a spectrum calculated by using equation (3.15) is shown in

Figure 3-3. The figure shows the relative power (i.e. the square of the amplitude) for each spectral line as a function of the harmonic number (n). The overall magnitude of the spectral lines have been normalized for ease of viewing. It was assumed for the purposes of the plot that the range to target was 17.1m, corresponding to a time delay (τ) of .114 μs, that the RF center frequency was 12.81 GHz. , that the total swept bandwidth of the RF was 700 MHz. , and that the ratio of upsweep to downsweep times (t_u/t_d) was .6552. These values closely match what can be expected in practice.

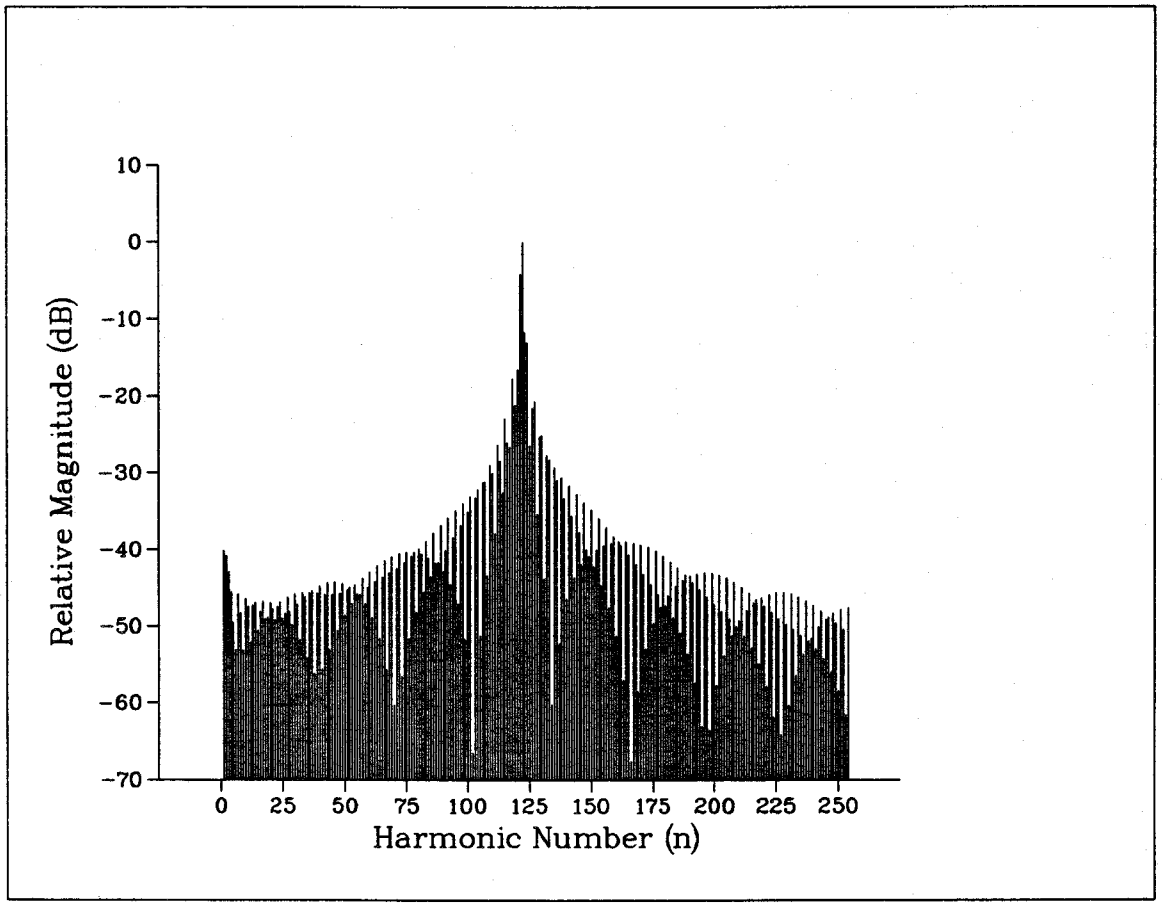

Figure 3-3: Normalized Spectrum of Point Target Backscatter

3.5. Description Of The Measuring System

3.5.1. General

This section provides a description of the measuring system in use. The equipment is the property of the Canada Center for Remote Sensing, and has been loaned to the University of Saskatchewan for a scatterometry campaign. It was manufactured by Applied Microwave Corp. of Lawrence, Kansas.

The system consists of three separate radar transceivers and a system control unit. It has been mounted on a flatbed truck with the control unit placed in the cab and the transceivers at the end of a fifty foot rotatable boom. A positioner allows adjustment of the radar look angle. A television camera has been mounted with the radars on the boom and connected to a monitor, also in the cab. A diesel generator on the truck bed powers the system.

This system was specifically designed for agricultural measurements. In use, the transceivers are pointed at a crop with the aid of the television camera. The look angle (i.e. the elevation angle of the antennas) is set to the desired value and the boom height is adjusted to illuminate a representative crop area. Since a large number of independent measurements is desirable, the truck is slowly driven along the perimeter of the crop so that different areas are illuminated as the measurements are being taken.

The parameters of interest in the measurement campaign are the scattering, differential scattering and volume scattering cross sections for various crops as functions of the radar frequency, look angle, furrow direction, soil moisture content, plant moisture content, plant biomass and crop development. Details of the measurement campaign will not be discussed in this document, but can be found in the work of Morton [16] and Shepherd [6].

3.5.2. Block Diagram Description

The system functions as a multiband FM-CW scatterometer. A block diagram of the components has been reproduced from the system documentation supplied by Applied Microwave Corp. as Figure 3-4. The dashed line on the diagram signifies the physical separation of the equipment mounted on the boom (above line) and that in the cab (below line).

The three radar transceivers operate at *L*-band, *C*-band and *K*-band. All simultaneously illuminate the target. Each transceiver is equipped with a dual polarization antenna (horizontal and vertical) and can be configured electronically to transmit with either of these electric field polarizations. Both polarizations are continuously received. The scattered waveform from a target within a specific range extent is amplified, full wave rectified and averaged before being passed to the data acquisition unit via the control cable. Six separate channels are available (horizontal and vertical for each transceiver). A table of pertinent system specifications is given as Table 3-1.

The control electronics consist of a Hewlett-Packard 3497A data acquisition unit, a controller for the radar positioner and camera, and an Olivetti IBM compatible personal computer. The data acquisition unit is equipped with a twenty channel analog relay card, a digital I/O card, a dual channel D to A card and a digital voltmeter. Communication with the personal computer is handled by the Hewlett-Packard interface bus.

The signals passed between the transceivers and the control electronics include selection signals to place different bandwidth filters in line, a gain select signal to change the IF gain, a delta frequency select signal to allow two different RF frequency deviations to be used, a polarization selection signal for switching between horizontal and vertical transmit polarizations, tuning voltage signals to allow adjustment of the modulation frequencies, sensed signals from measurement of RF center frequency, transceiver temperature and transmit power, and the transceiver output signals. A

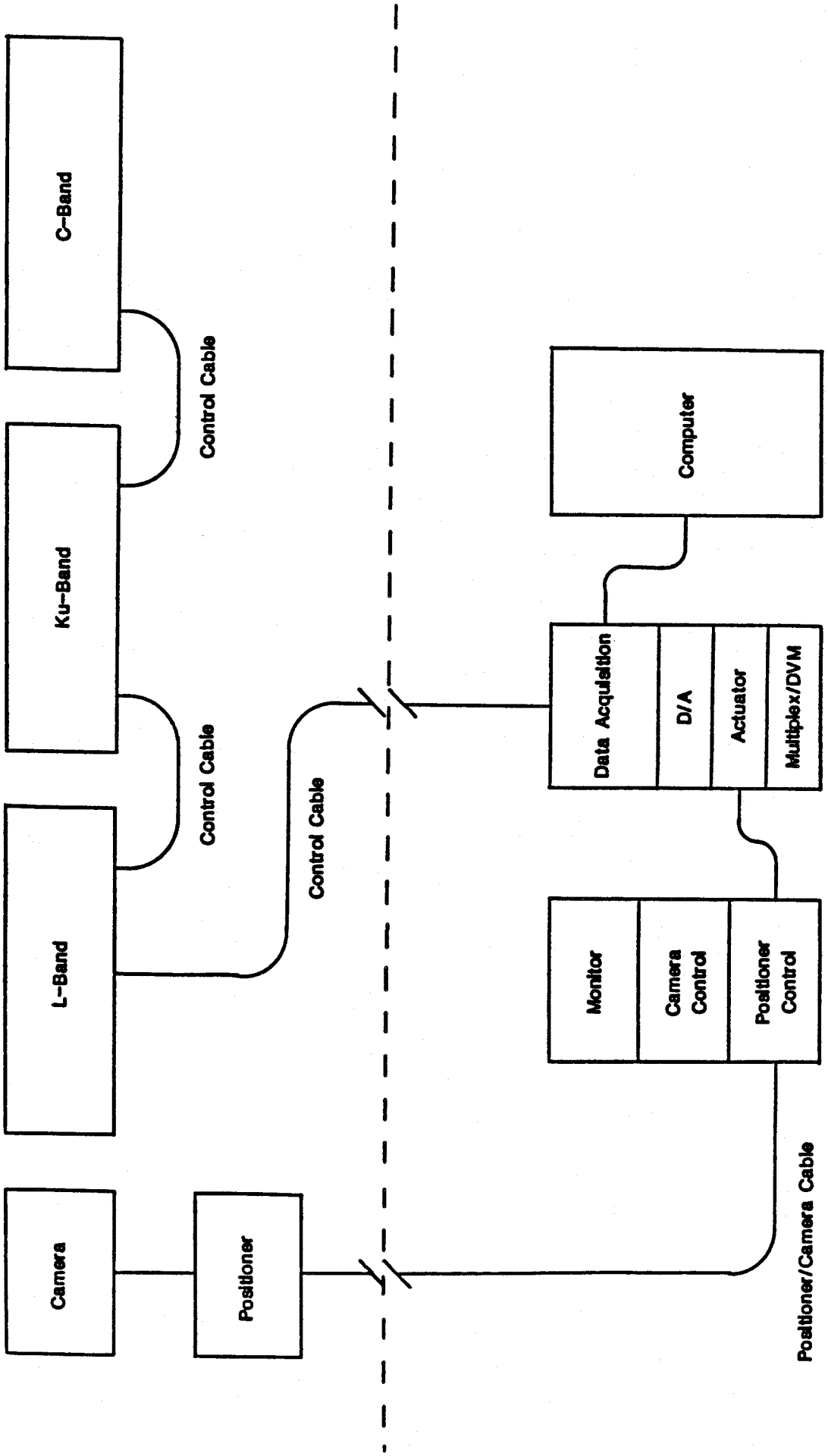

Figure 3-4: Scatterometer Overall Block Diagram

description of the control lines connecting the control electronics and the radar transceivers is given in Table 3-2.

An operational description of the scatterometry system will be given with reference to the *K*-band transceiver in the next section.

Table 3-1: Scatterometer System Specifications

Transceiver	*L*-Band	*C*-Band	*K*-Band
RF Center Frequency	1.5 Ghz	5.3 Ghz	13.4 Ghz
RF Frequency Deviation	500 Mhz	500 Mhz	500 Mhz
Modulation type	----------Linear Sawtooth----------		
Upsweep/downsweep time ratio	----------Approximately 2/1----------		
Transmit Polarization	---------Horizontal or Vertical---------		
Receive Polarization	--------Horizontal and Vertical---------		
Antenna Type	--Parabolic Reflector with custom feed--		
Antenna Diameter	1.37m	.61m	.305m
Antenna Far Field Distance	9.7m	6.7m	4.2m
Antenna Beamwidth(3 dB)	7.7 deg.	5.1 deg.	4.6 deg.
Antenna Sidelobe level	-14 dB	-16 dB	-17 dB
Antenna Gain(boresight)	26 dB	29 dB	31 dB
Intended Target Range	---------- 9m to 40m ----------		
Transmit Power(nominal)	12 dBm	10 dBm	10 dBm
Temperature Stability	-- +/-.2 dB, -10 to +40 degrees Celsius-		

3.5.3. Transceiver Description

A functional block diagram of the electronics for a transceiver is given in Figure 3-5. The operation of each transceiver is identical, the only differences between the three being due to the use of different frequency range components in the microwave section and the corresponding adjustments of the YIG driver/data selection circuitry. The unit is organized into the main functional operating units of the microwave section, the YIG driver/Data select section, and the IF processing sections, which consist of both vertical and horizontal IF processors and a filter bank for each.

Table 3-2: Scatterometer Control and Signal Lines

Connector Pin	Signal Type	Signal Name	Signal Description
A	Dig.	Filter Select 5%	Open selects 5% filter
B	Dig.	Filter Select 4%	Open selects 4% filter
C	Dig.	Filter Select 3%	Open selects 3% filter
D	Dig.	Filter Select 2%	Open selects 2% filter
E	Dig.	Filter Select 1%	Open selects 1% filter
F	Dig.	Gain Select	Open selects high IF gain
G	Dig.	Pol. Select	Open selects Horiz. Tx Polarity
H	Dig.	Delta Freq. Sel.	Open selects wide RF deviation
J	Dig.	Test Data DS0	DS0 DS1 h,j and m
K	Dig.	Test Data DS1	open open no connection open closed RF center freq. closed open unit temperature closed closed transmit power
L	Dig.	Digital Gnd.	Ground for digital lines
M	An.	L H Out	*L*-Band Horizontal Output
N	An.	L H Com	*L*-Band Horizontal return line
P	An.	C H Out	*C*-Band Horizontal output
R	An.	C H Com	*C*-Band Horizontal return line
S	An.	Ku H Out	*K*-Band Horizontal output
T	An.	Ku H Com	*K*-Band Horizontal return line
U	An.	L V Out	*L*-BL Band Vertical Output
V	An.	L V Com	*L*-Band Vertical return line
W	An.	C V Out	*C*-Band Vertical Output
X	An.	C V Com	*C*-Band Vertical return line
Y	An.	Ku V Out	*K*-Band Vertical Output
Z	An.	Ku V Com	*K*-Band Vertical return line
a	An.	Guard	Guard line for analog signals
b		Chassis	Chassis connection
c	An.	Angle	Angle potentiometer connection
d	An.	C/Ku FM Tune	V-tune for C/K modulation VCOs
e	An.	C/Ku FM Tune Com	return line for d
f	An.	L FM Tune	V-tune for L modulation VCO
g	An.	L FM Tune Com	return line for f
h	An.	L Test Data	see J,K
i	An.	L Data Com	return line for h
j	An.	C Test Data	see J,K
k	An.	C Data Com	return line for j
m	An.	Ku Test Data	see J,K
n	An.	Ku Data Com	return line for m
p	An.	spare	
q	An.	spare	
r		120 Vac	system power
s		120 Vac	system power
t	An.	Pol. Sel. Com	return line for G

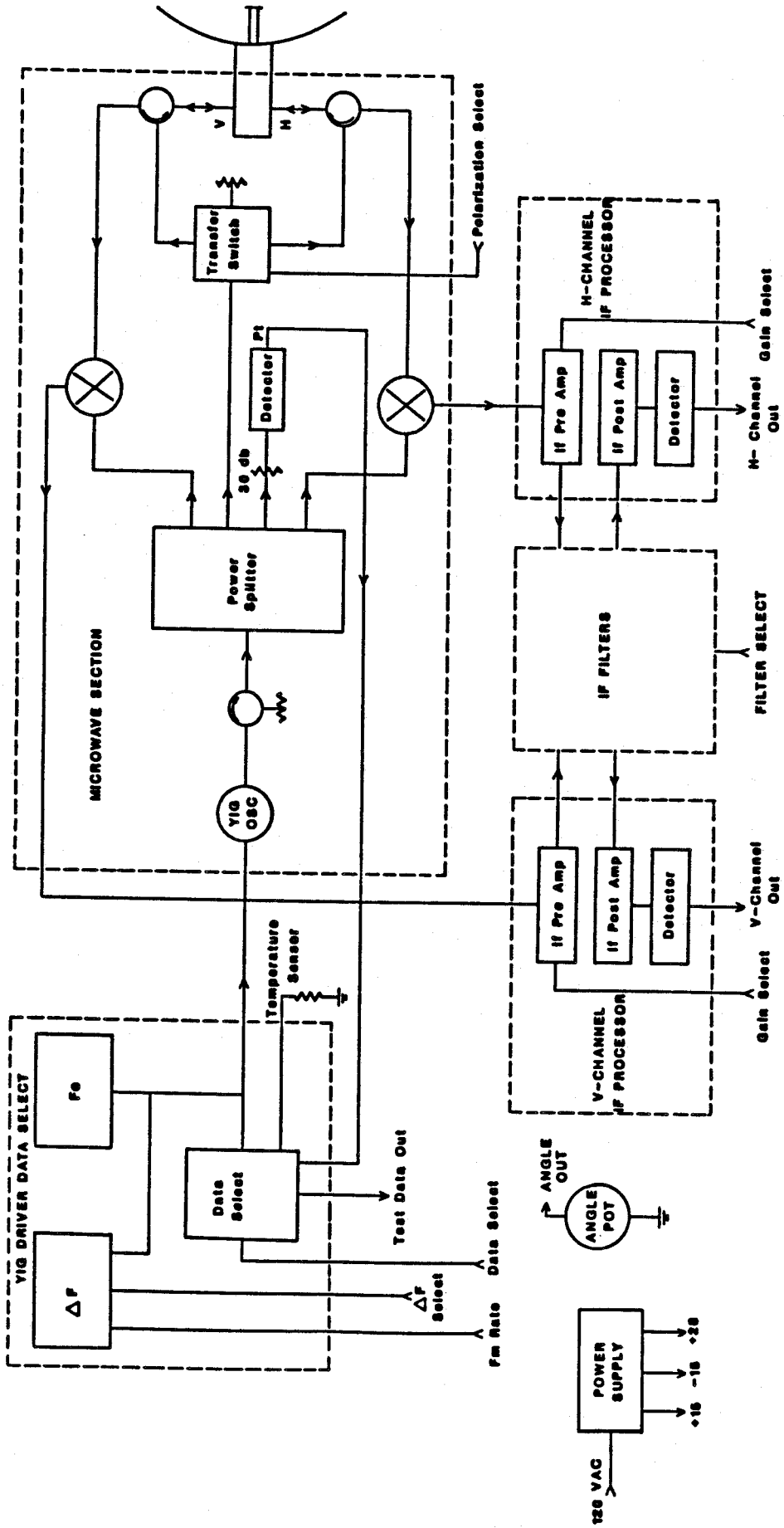

Figure 3-5: Transceiver Block Diagram

3.5.3.1. The Microwave Section

The microwave section is driven by an oscillator using an yttrium-iron-garnet (YIG) resonator. The frequency of the oscillator is controlled by providing a current bias to the coils surrounding the resonator. The oscillator is terminated with a circulator[4] to improve its frequency stability. Signals generated are passed to a four way power splitter for distribution to the rest of the microwave circuitry.

One of the splitter outputs is passed through a transmit switch which allows the polarization select signal to direct it to either the vertical or horizontal port of an ortho-mode junction connected to the antenna feed, thereby controlling the transmitted polarization. The power to be transmitted is prevented from travelling down the receiving path by circulators placed at both of the ortho-mode junction ports.

A power detector terminates another of the splitter outputs and provides an indication of the power being transmitted. The remaining two power splitter outputs provide the local oscillator signals for the H and V channel mixers.

The ortho-mode junction will allow both transmission to and reception from the antenna. The power received is separated into orthogonal components (in this case H and V) and is passed through the circulators to the RF ports of the mixers. The IF ports of the mixers thus provide the product of the transmitted signal and the received signal, as was the case in Figure 3-1. Further conditioning of these IF signals is provided by the IF processors.

---

[4]A circulator is a multi-port device which allows signals to pass only from their port of entry to the next port in the direction of circulation.

3.5.3.2. YIG Driver/Data Select Circuitry

This circuitry provides the control waveform for the YIG oscillator as well as providing an analog multiplexer for selection of pertinent measurement information.

The YIG driver consists of a current waveform generator and an adjustable current source. The waveform generator is voltage controlled. It generates a periodic current consisting of a linear up ramp and a linear down ramp. The ratio of the time durations of the upramp to downramp is fixed at approximately 2/1. The frequency of the waveform is adjustable from approximately 50 to 300 Hz on the basis of the analog level of the FM Rate line. The magnitude of the current swings is switchable electronically between two values, which are themselves adjustable through the use of trimming potentiometers in the circuitry. The ΔF Select line controls which of the two values will be used. The output of the waveform generator is summed with the output of the adjustable current source to provide the control for the YIG oscillator. This allows for separate adjustment of the oscillator center frequency (from the adjustable current source), the RF deviation (magnitude of the current swings from the waveform generator) and the FM modulation rate (frequency of the current swings from the waveform generator).

The multiplexing circuitry allows any of the YIG oscillator control line, the power detector output from the microwave section, the temperature sensor or a spare line to be switched through to the data acquisition unit via a single pair of wires in the control cable. The control signals for the multiplexor circuitry are provided by the Test Data DS0 and DS1 lines (see Table 3-2).

3.5.3.3. IF Processors

Each of the vertical and horizontal receiving channels has its own IF processor. The processors highpass filter the incoming signals to reduce the power present due to internal system reflections and amplify the signals before routing them through one of a bank of bandpass filters. A blanking circuit allows only the signals received during the positive going portion of the RF sweep to pass through to the filters. During the downsweep interval the filter inputs are grounded. Signals passing through these filters are then amplified again before being detected. The detection circuitry consists of a precision full wave rectifier followed by a lowpass filter.

Control lines allow for one of two IF gains to be used and for the selection of any one of the filters in the filter bank. The filters all have center frequencies of 22 KHz and have bandwidths of 1, 2, 3, 4 or 5 percent of the center frequency.

3.5.4. Transceiver Operation

Under operation, after positioning the antenna to illuminate the desired target area, the polarization of the transmitted signal is set. Control of the frequency of the modulation waveform will then allow the scattering cross section of the target within a specific range extent to be measured. Since the center frequencies for the bandpass filters in the IF processors are fixed and the equation relating the IF backscattered frequency to the range was given previously as

$$R = \frac{ct_u f_{IF}}{2B} \quad . \tag{3.16}$$

it can be seen that varying the modulation rate will have the effect of centering the spectrum due to the target at only one range. By choosing the bandwidth of the filter used, the range resolution of the system can be tailored to best suit the target parameters. Caution must be exercised in this

procedure if an accurate scattering cross section is of importance. The spectrum of the IF return will consist of harmonics of the modulation frequency, and at short ranges these spectral lines will be spaced fairly far apart (i.e. 250Hz at a 10m range). Use of the 1% filter when measuring these short ranges implies that only one or two spectral lines will be included in the measurememnt bandwidth (1% of 22 KHz is 220 Hz). Small variations in the range to the target can then result in significant changes to the measured scattering cross section as the spectral lines move about on the skirts of the filter response.

For a given modulation rate, the equipment will provide indications for the transmitted power, the average of the rectified received voltage within the chosen filter bandwidth and with the selected transmit and receive polarities, the current look angle of the transceiver antenna, and the center frequency of the RF radiation. Knowledge of the boom height will allow determination of the range to target. These values, together with a knowledge of the system gain constants[5] allow equation (3.5) and equation (3.6) to be solved for the scattering cross section and the differential scattering cross section associated with the target.

The integrity of the measurements will be based on the accuracy of the determined calibration constants, variations due to instabilities in the equipment, and the signal to interference ratio in effect at the time of measurement. Wheras the error due to calibration and the variation due to equipment instabilities are relatively fixed parameters, the signal to interference ratio is not, and must be examined further.

The major contributor to the system noise is interference generated by reflections generated internal to the equipment. Referring again to Figure 3-5 and looking specifically at the microwave section, it can be seen that

---

[5]A discussion of the system gain constant (also called system calibration constant) and its determination will be given in Chapter 5.

interfering signals can be generated by leakage from the transmit signal through the circulator(s), transmit signals that are reflected by impedance mismatches at the orthomode junction and the antenna feed, and to a lesser extent by local oscillator signals passing from LO to RF ports in the mixers and subsequently being reflected by mismatches at the circulators, orthomode junction and antenna feed.[6] All of these mechanisms are equivalent to point targets at extremely short range. The spectral lines generated by them can and do extend upwards in frequency to enter the passband of the IF filters. They are then detected and result in a residual detected power which effectively forms the noise floor of the equipment. It is possible to reduce the magnitude of the spectral lines somewhat by choosing the major component and lengthening the cable connecting the power divider and the mixers to reduce the effective range to this target to zero. This will minimize but not eliminate their contribution to the total interference.

---

[6]An additional interference signal was discovered during the system testing which is not included in the mechanisms mentioned, and which proved to be the major contributor. The antenna feed consists of a ring loaded dipole with a disk reflector. The dipole is illuminated by open ended waveguide and radiates toward the disk, which then reflects the signal to the parabolic reflector. Energy reflecting from the disk can be directed to the central portion of the parabolic dish and be reflected directly back to the disk, from where it is redirected back into the waveguide to become a received signal.

Chapter 4

DESIGN AND IMPLEMENTATION

4.1. General

Previous chapters have dealt with the basic theory of polarization and the operating principles of FM-CW radar. This chapter shows how the polarization theory can be applied in the radar environment. It then continues to discuss possible methods of implementing polarization measurement circuitry and selects a specific method as the most applicable. Circuit designs which implement the method are then presented and described, after which the relationships between the measured quantities and the polarization parameters are summarized.

4.2. The Application Of Polarization Theory To FM-CW Radar

To illustrate how polarization theory can be applied in the FM-CW radar case the results of section 3.4.2 are extended to yield spectral descriptions of the voltage waveforms at both the horizontal and vertical antenna outputs when a known target is illuminated with horizontally polarized radiation. These descriptions are then related to the formulas presented in Chapter 2.

In general, radiation incident on the target will be scattered over a range of angles, with some of the scattered signals being intercepted by the receiving antenna. A scatterer may have a scattering cross section which varies as a function of the azimuth or elevation angle of the incoming radiation. In addition, it may have a cross section which varies with the

polarization state of the incident radiation, and may cause a phase shift to occur between the incident and scattered radiation. The radiation received will then have a polarization state different from the state transmitted. A description of the scattered radiation may be obtained by making use of the target scattering matrix, described by Graves in 1956 [17]. It relates the transmitted signals to the received signals (while neglecting any range dependence) as is shown by equation (4.2).

$$\begin{bmatrix} E_{rh}(t) \\ E_{rv}(t) \end{bmatrix} = \begin{bmatrix} a_{hh} & a_{vh} \\ a_{hv} & a_{vv} \end{bmatrix} \begin{bmatrix} E_h(t) \\ E_v(t) \end{bmatrix} \tag{4.2}$$

In this case

- $E_{rh}(t)$ and $E_{rv}(t)$ are horizontal and vertical components of the scattered electric field vector at the receiving antenna,
- the a_{ii}'s are the scattering matrix elements and
- $E_h(t)$ and $E_v(t)$ are the horizontal and vertical components of the transmitted electric field.

The elements of the scattering matrix (a_{ii}'s) are complex quantities which can be represented as

$$a_{hh} = \sqrt{\sigma_{hh}}\, e^{j\phi_{hh}} \quad \text{and} \quad a_{hv} = \sqrt{\sigma_{hv}}\, e^{j\phi_{hv}}.$$

where

- σ_{hv} is the scattering cross section resulting from reception by a vertically polarized receiver when a horizontally polarized signal was transmitted and
- ϕ_{hv} is the phase of the signal received by a vertically polarized receiving channel after a horizontally polarized signal has been transmitted and

- σ_{hh}, σ_{vh}, σ_{vv}, ϕ_{hh}, ϕ_{vh} and ϕ_{vv} are defined similarly.

Their use will therefore take into account any magnitude or phase variations which the scatterer may introduce.

Use of the scattering matrix to describe a scattered field at the receiving antenna due to illumination of a target by a horizontally polarized source gives the following equation[7].

$$E_r(t) = \hat{h}\, a_{hh} E_h(t) + \hat{v}\, a_{hv} E_h(t) = \hat{h}\, E_{rh}(t) + \hat{v}\, E_{rv}(t) \qquad (4.3)$$

The symbols $\hat{h}$ and $\hat{v}$ used in equation (4.3) denote unit vectors in the horizontal and vertical directions.

Since the voltage at the antenna terminals will be proportional to the magnitude of the electric field components given in equation (4.3), descriptions of the received horizontal and vertical voltage waveforms will be known. Both of these waveforms will be magnitude scaled, phase shifted replicas of the transmitted voltage. The voltage waveforms at the IF outputs of the radar can then be obtained by using the methods of section 3.4.2, with the inclusion of the magnitude scaling and phase shifts.

This results in the following expressions describing the magnitude and phase of the n^{th} harmonic line in the Fourier series:

$$v_h(n,t) = \frac{A_p \sqrt{\sigma_{hh}}\, t_u}{t_m} \left[\frac{\sin(\Delta\omega\tau - n\pi t_u/t_m)}{\Delta\omega\tau - n\pi t_u/t_m} \cos(n\omega_0 t + \omega_c \tau + \phi_{hh}) + \frac{\sin(\Delta\omega\tau + n\pi t_u/t_m)}{\Delta\omega\tau + n\pi t_u/t_m} \cos(n\omega_0 t - \omega_c \tau - \phi_{hh}) \right]$$

---

[7] A similar equation will result from the use of a vertically polarized source. The resulting equations will be identical in form to those given in the text for the horizontal case.

$$v_v(n,t)=\frac{A_p\sqrt{\sigma_{hv}}\,t_u}{t_m}\left[\frac{\sin(\Delta\omega\tau-n\pi t_u/t_m)}{(\Delta\omega\tau-n\pi t_u/t_m)}\cos(n\omega_0 t+\omega_c\tau+\phi_{hv})\right.$$
$$\left.+\frac{\sin(\Delta\omega\tau+n\pi t_u/t_m)}{(\Delta\omega\tau+n\pi t_u/t_m)}\cos(n\omega_0 t-\omega_c\tau-\phi_{hv})\right]$$

The region of interest in the radar case is the region of maximum spectral response. Around this region, the first term in the brackets of these equations will dominate (the denominator is close to zero). The second term will have a much smaller response and can be ignored. This allows the formulas to be rewritten as

$$v_h(n,t)=K_n\sqrt{\sigma_{hh}}\cos(n\omega_0 t+\omega_c\tau+\phi_{hh})$$

and

$$v_v(n,t)=K_n\sqrt{\sigma_{hv}}\cos(n\omega_0 t+\omega_c\tau+\phi_{hv}). \tag{4.4}$$

where the term K_n represents the constant term

$$K_n=\frac{A_p t_u}{t_m}\,\frac{\sin(\Delta\omega\tau-n\pi t_u/t_m)}{(\Delta\omega\tau-n\pi t_u/t_m)}.$$

Examination of these equations reveals that they are of the same form as the equations used to introduce the theory of polarization in Chapter 2 (equation (2.2)). As in section 2.1, the common phase term $\omega_c t$ and the frequency term $n\omega_0$ will drop out in the polarization equations, leaving only the magnitude terms and the phase difference ϕ_{hh}-ϕ_{hv} to describe the polarization ellipse.

Two important conclusions can be drawn from this. First, that polarization information is available at the IF frequency in an FM radar, and second that this polarization information is available in each spectral line.

As was the case in Chapter 2, the electric field present at the receiving antenna is expected to consist of the superposition of many individual fields, due to the many individual scatterers in the area being illuminated. The components of the resultant field can however be described as the sum of individual returns in the horizontal and vertical axes, with each return being dictated by the scattering matrix of the target which caused it. The resultant voltage at the IF output of the radar will then also consist of the sum of many terms, each having the form of equation (3.10). The use of the Fourier transform on this sum will then imply that the resultant IF spectrum consists of the superposition of the many individual spectrums, since it is a linear operator.

The examination of a spectral line at the IF of the radar is therefore directly analogous to the examination of a quasimonochromatic field at the antenna terminals, and the theory developed in Chapter 2 can be applied directly to determine the polarization ratio and the parameters of the polarization ellipse. This conclusion states that the polarization state can be measured, but not necessarily that the state of polarization can be related to target parameters, since many scatterers at different ranges may have contributed to the phase terms. A relation between the state of polarization and the target parameters can be determined using the following argument if several assumptions are made.

The terms in equation (4.4) above are all of the same frequency, and can be regarded as phasors (Figure 4-1-a). Two phasors are shown here, one having magnitude h_1 and phase $\omega_c\tau_1+\phi_{h1}$ and representing the horizontal component, the other having magnitude v_1 and phase $\omega_c\tau_1+\phi_{v1}$ and representing the vertical component. These two phasors are assumed to have arisen from a point scatterer. A second point scatterer will give rise to an additional two phasors as shown in Figure 4-1(b). The two scatterers are assumed to be located at different ranges, so the phase terms $\omega_c\tau_1$ and $\omega_c\tau_2$ will be different. The resultant phasors in the horizontal and vertical channels can then be formed using phasor addition as shown in Figure 4-2.

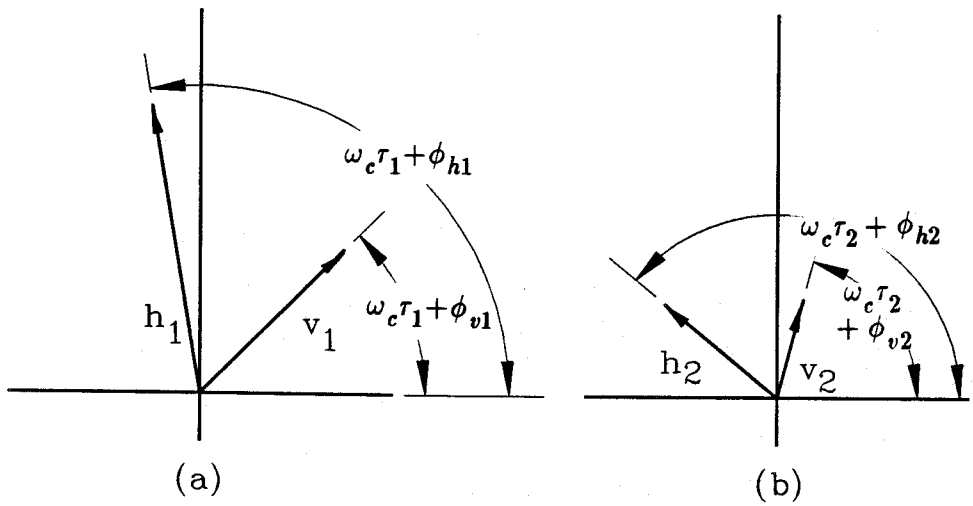

Figure 4-1: Phasor Representation of Spectra Due to Point Scatterers

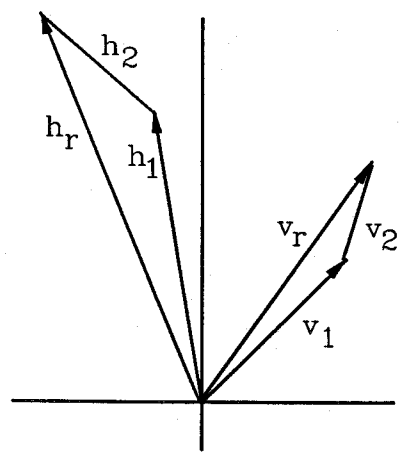

Figure 4-2: Representation of Resultant Spectra Due to Point Scatterers

If it is now assumed that the two point scatterers have similar characteristics so that the phase terms ϕ_{h1} and ϕ_{v1} are the same as ϕ_{h2} and ϕ_{v2} respectively, and that the ratio of the magnitudes of h_1 to h_2 is the same as the ratio of v_1 to v_1, the two triangles in Figure 4-2 will be similar in the geometrical sense. The resultant phasors h_r and v_r will thus have the same phase difference as that between h_1 and v_1 or between h_2 and v_2. In

addition, the ratio of the magnitudes of h_r to v_r will be the same as the ratio of the magnitudes for the component phasors.

By extension of the above argument, it can be concluded that the polarization state arising from the sum of any number of point scatterers can be related to the target scattering parameters in the same way that the polarization state arising from a single point scatterer could.

In review, the polarization state of the radar return from a collection of point scatterers can be determined by applying the methods of Chapter 2 to any single spectral line in the IF spectrum. Furthermore, the polarization state so measured can be related to the scattering parameters of the individual point targets if the scattering matrices for the individual scatterers differ only by numerical constants.

It should be noted however that several assumptions have been made in arriving at these conclusions. They are:

- that the spectral response of each scatterer is flat (this assumption was made in the development of the IF spectrum due to a point target),
- that the phase shifts introduced by the scatterers are constant values, and that each scatterer introduces the same differential phase shift between the horizontal and vertical scattered signals,
- that the ratio of the power scattered in the vertical direction to that scattered in the horizontal direction is the same for each scatterer
- that no additional phase shifts are introduced by the radar's receiving equipment, and
- that the scatterer is motionless with respect to the observation point.

4.3. Methods Of Measuring The Polarization State

The previous section has shown that the methods of measuring the polarization state discussed in Chapter 2 can be applied at the IF output of an FM scatterometer. These methods will now be discussed in the context of the scatterometer under consideration.

It was determined in Chapter 2 that any method for measuring the polarization state must include the measurement of at least two intensities (to determine the diagonal elements of the coherency matrix), and that the remaining parameters can be determined through either a crossmultiplication method or by additional intensity measurements (to determine the off-diagonal elements). Selection of an implementation method therefore requires a discussion of the relative merits of the methods used to determine the off diagonal elements of the coherency matrix.

4.3.1. The Crossmultiplication Method

The application of the method shown in Figure 2-1 at the IF output of the scatterometer must take into account the nature of the IF spectrum. If, as suggested by the development in section 4.2 only one spectral line is used in the multiplication process, the result would be difficult to relate to the measured intensities, which typically measure the power in a five percent bandwidth and therefore include many spectral lines. This problem can be avoided by allowing the inputs to the multiplier to consist of the same portion of the spectrum as is applied to the detectors in the IF processors. It can be shown[8] that the results of this will yield polarization parameters consistent with the single spectral line case.

Such a solution would also ensure that the spectral contributions due to internal reflections within the microwave circuitry would be excluded as

---

[8]The derivation is carried out in section 4.3.2.

much as possible from the measured values. If the signals used are taken directly from the outputs of the filters in the IF processors, the blanking circuitry within those processors will also reject the spectral contributions arising during the downsweep.

The use of filters before the multipliers in this arrangement implies that phase shifts will be introduced. Since phase is one of the parameters to be measured, any phase shifts introduced must be matched between the two channels. This implementation method was originally rejected on the basis that it would be difficult to achieve this matching over the operating temperature range of the equipment. Subsequent work indicated that phase matching is also required for the intensity method of the next section however, so in retrospect this is not a disadvantage when comparing the two methods.

4.3.2. The Intensity Method

As noted in Chapter 2, the elements of the coherency matrix can be completely specified by measuring the intensity of the electric field vector in the 0, 45, 90 and 135 degree directions with respect to the x axis, and by remeasuring the intensity in the 45 and 135 degree directions after the y component of the electric field has been delayed by $\pi/2$ radians with respect to the x component. Reference to equation (2.11) reveals that the 45 and 135 degree measurements correspond to the intensities of the sum and difference of the x and y field components, multiplied by the numerical constant $1/\sqrt{2}$.

These results can be applied directly to the scatterometer in use at the University of Saskatchewan. Measurements with the linearly polarized horizontal and vertical antennas will correspond to the 0 and 90 degree directions. The sum and difference of the voltage waveforms present at the horizontal and vertical antennas will correspond to the 45 and 135 degree directions. A phase delay of ninety degrees applied to the voltage waveform

at the vertical antenna terminals will allow the measurement of the remaining two quantities.

The same statements can be made with respect to the voltage waveform due to a single spectral line in the IF spectrum as was shown in section 4.2. This allows polarization information to be determined by using a system illustrated by Figure 4-3. Each of the six IF processors provides an output corresponding to the power (half the intensity) present in one of the waveforms mentioned above. The filters within the IF processors ensure that the power in only one spectral line is measured.

Unfortunately, the measurement of a single spectral line is complicated by two factors. The first of these is that the spacing of the spectral lines can be as small as 70 Hz. Since the IF center frequency is 22 KHz., a bandpass filter to select one spectral line would have a percentage bandwidth of about .3%. The second factor is that the precise location of the spectral lines is dictated by the frequency of the modulating waveform, which is adjusted as needed to examine a particular range. The proper measurement of a single spectral line would therefore require the use of a tracking filter to ensure that the line in question would fall within the filter bandwidth. This filter would be required to scan a frequency range of at least 250 Hz., the upper range of the modulating frequency. Since more than one spectral line could be present within this frequency range, some method of selecting the correct line would be required. These factors represent severe constraints.

The scatterometer as constructed measures the power in a collection of spectral lines, typically representing the power in a five percent IF bandwidth. If it could be shown that polarization information could be determined from a collection of spectral lines, rather than just one, the original equipment could provide two of the required intensities and the implementation of additional circuitry could be greatly simplified, while avoiding the problems described in the previous paragraph. An analysis of the multiline case is accordingly carried out below.

It is assumed that the radiation under consideration is completely polarized, and has a spectrum consisting of spectral lines of the form:

$$v_h(n,t) = K_n \sqrt{\sigma_{hh}} \cos(n\omega_0 t + \omega_c \tau + \phi_{hh})$$

$$v_v(n,t) = K_n \sqrt{\sigma_{hv}} \cos(n\omega_0 t + \omega_c \tau + \phi_{hv}).$$

The horizontal and vertical waveforms are then taken to be a collection of these spectra, as given by

$$V_h(t) = \sum_{n=p}^{q} K_n \sqrt{\sigma_{hh}} \cos(n\omega_0 t + \omega_c \tau + \phi_{hh}) \tag{4.5}$$

$$V_v(t) = \sum_{m=p}^{q} K_m \sqrt{\sigma_{hv}} \cos(m\omega_0 t + \omega_c \tau + \phi_{hv}). \tag{4.6}$$

The intensities discussed in section 2.2.3.2 can then be calculated by finding the power in the waveforms. The results of the calculations are shown below, with T indicating the averaging time[9] .

$$I(0,0) = \frac{2}{T}\int_0^T \left[\sum_{n=p}^{q} K_n \sqrt{\sigma_{hh}} \cos(n\omega_0 t + \omega_c \tau + \phi_h) \right]^2 dt$$

$$I(0,0) = \sigma_{hh} \left[\sum_{n=p}^{q} K_n^2 + \frac{2}{T}\int_0^T \sum_{\{mn\}} K_n K_m \cos([n-m]\omega_0 t)\, dt \right]$$

---

[9]The calculations are shown in full in Appendix A

where $\{mn\}$ is taken to be the set of all values of m and n between p and q such that the value of $m-n$ ranges from one to $q-p$.

$$I(90,0) = \sigma_{vv} \left[\sum_{n=p}^{q} K_n^2 + \frac{2}{T}\int_0^T \sum_{\{mn\}} K_n K_m \cos([n-m]\omega_0 t)\, dt \right]$$

$$I(45,0) = \langle [V_h(t) + V_v(t)]^2 \rangle$$

$$I(45,0) = J_{xx} + J_{yy} + \sqrt{\sigma_{hh}\sigma_{hv}} \cos(\delta) \left[\sum_{n=p}^{q} K_n^2 + \frac{2}{T}\int_0^T \sum_{\{mn\}} K_m K_n \cos([n-m]\omega_0 t) dt \right]$$

$$I(135,0) = J_{xx} + J_{yy} - \sqrt{\sigma_{hh}\sigma_{hv}} \cos\delta \left[\sum_{n=p}^{q} K_n^2 + \frac{2}{T}\int_0^T \sum_{\{mn\}} K_m K_n \cos([n-m]\omega_0 t) dt \right]$$

$$I(45,\tfrac{\pi}{2}) = \langle [V_h(t) + V_v(t,\tfrac{\pi}{2})]^2 \rangle$$

$$I(45,\tfrac{\pi}{2}) = J_{xx} + J_{yy} + \sqrt{\sigma_{hh}\sigma_{hv}} \sin(\delta) \left[\sum_{n=p}^{q} K_n^2 + \frac{2}{T}\int_0^T \sum_{\{mn\}} K_m K_n \cos([n-m]\omega_0 t) dt \right]$$

$$I(135,\tfrac{\pi}{2}) = J_{xx} + J_{yy} - \sqrt{\sigma_{hh}\sigma_{hv}} \sin\delta \left[\sum_{n=p}^{q} K_n^2 + \frac{2}{T}\int_0^T \sum_{\{mn\}} K_m K_n \cos([n-m]\omega_0 t) dt \right]$$

Use of these intensities to determine the coherencies and subsequent substitution into equations (2.9) and (2.10) results in

$$\tan(2\psi) = \frac{2\sqrt{\sigma_{hh}\sigma_{hv}}\cos\delta\left[\sum_{n=p}^{q} K_n^2 + \frac{2}{T}\int_0^T \sum_{\{mn\}} K_m K_n \cos([n-m]\omega_0 t)dt\right]}{(\sigma_{hh}-\sigma_{vv})\left[\sum_{n=p}^{q} K_n^2 + \frac{2}{T}\int_0^T \sum_{\{mn\}} K_m K_n \cos([n-m]\omega_0 t)dt\right]}$$

$$\sin(2\chi) = \frac{2\sqrt{\sigma_{hh}\sigma_{hv}}\sin\delta\left[\sum_{n=p}^{q} K_n^2 + \frac{2}{T}\int_0^T \sum_{\{mn\}} K_m K_n \cos([n-m]\omega_0 t)dt\right]}{(\sigma_{hh}+\sigma_{vv})\left[\sum_{n=p}^{q} K_n^2 + \frac{2}{T}\int_0^T \sum_{\{mn\}} K_m K_n \cos([n-m]\omega_0 t)dt\right]}$$

Note that the bracketed term appears in both the numerator and the denominator and so will cancel out when ratios are used to determine the orientation angle and the ellipticity of the polarization ellipse. From this it can be concluded that the polarization information can be obtained from the spectrum by measuring the intensities due to a number of spectral lines, rather than just one. Also shown by this development is the fact that the integration time over which the power is measured is immaterial, as long as it is the same for each intensity being measured.

The derivation above made use of the calculated IF spectrum. If the spectrum at the inputs to the IF processors is modified by filtering to select some subset of spectral lines, both the amplitudes and phases of the spectral components may be changed. The effects of this may be analysed by including the amplitude and phase variations before calculating the intensities. Each of the six channels will have its own filter (Figure 4-3) and will thus operate on its own specific set of spectral lines, but all of these sets may be obtained from the original spectrum by applying a magnitude weighting (M) and a phase offset (β) to each spectral line. Both of the

additional terms will depend upon the filter characteristics and the particular spectral line in question. Equations (4.5) and (4.6) can then be rewritten as

$$V_{h*}(t)=\sum_{n=p}^{q} M_*(n)K_n\sqrt{\sigma_{hh}}\cos\{n\omega_0 t+\omega_c\tau+\phi_{hh}+\beta_*(n)\}$$

$$V_{v*}(t)=\sum_{m=p}^{q} M_*(m)K_m\sqrt{\sigma_{hv}}\cos\{m\omega_0 t+\omega_c\tau+\phi_{hv}+\beta_*(m)\}.$$

where

- V_{h*} and V_{v*} are the horizontal and vertical waveforms at the output of the * th filter, and the asterisk is one of H, V, A, B, C or D,
- $M_*(n)$ is the magnitude weighting factor for the nth spectral line passing through the * th filter, and
- $\beta_*(n)$ is the additional phase shift caused in the nth spectral line by the * th filter.

Recalculation of the intensities using these definitions and subsequent determination of the polarization parameters leads to

$$\tan(2\psi)=\frac{2K_H\sqrt{\sigma_{hh}\sigma_{hv}}\cos\delta}{(K_H\sigma_{hh}-K_V\sigma_{vv})}$$

$$\sin(2\chi) = \frac{2K_A\sqrt{\sigma_{hh}\sigma_{hv}}\sin\delta}{\sqrt{\langle K_H\sigma_{hh} - K_V\sigma_{vv}\rangle^2 + \langle 2K_C\sqrt{\sigma_{hh}\sigma_{hv}}\cos\delta - 2K_D\sqrt{\sigma_{hh}\sigma_{hv}}\cos\delta\rangle^2 + \langle 2K_A\sqrt{\sigma_{hh}\sigma_{hv}}\sin\delta - 2K_B\sqrt{\sigma_{hh}\sigma_{hv}}\sin\delta\rangle^2}}$$

$$m = \frac{\sqrt{\langle K_H\sigma_{hh} - K_V\sigma_{vv}\rangle^2 + \langle 2K_C\sqrt{\sigma_{hh}\sigma_{hv}}\cos\delta - 2K_D\sqrt{\sigma_{hh}\sigma_{hv}}\cos\delta\rangle^2 + \langle 2K_A\sqrt{\sigma_{hh}\sigma_{hv}}\sin\delta - 2K_B\sqrt{\sigma_{hh}\sigma_{hv}}\sin\delta\rangle^2}}{(K_H\sigma_{hh} + K_V\sigma_{vv})}$$

where

$$K_* = \sum_{n=p}^{q} K_n{}^2 M_*{}^2(n) + \frac{2}{T}\int_0^T \sum_{\{mn\}} K_m K_n M_*(n) M_*(m)\cos\left([n-m]\omega_0 t + \beta_*[n] - \beta_*[m]\right)dt.$$

If the values of the K_*'s are equal, these equations will reduce to the simple forms given in section 2.2.1.1. For this to happen however, requires that the terms in the expressions for the K_*'s equate on a term by term basis. This is equivalent to requiring the individual filters to be matched both in amplitude response and in phase across the passband.

Having shown that a collection of spectral lines may be used in the determination of the polarization parameters, it is possible to make use of the intensity information which the scatterometer already provides, and to arrange matters such that any additional intensity measurements will be carried out using the same bandwidth and hence utilize the same set of spectral lines. An added benefit would be that the circuitry to measure the intensity in the existing channels could be duplicated directly, thereby saving considerable design effort and construction time.

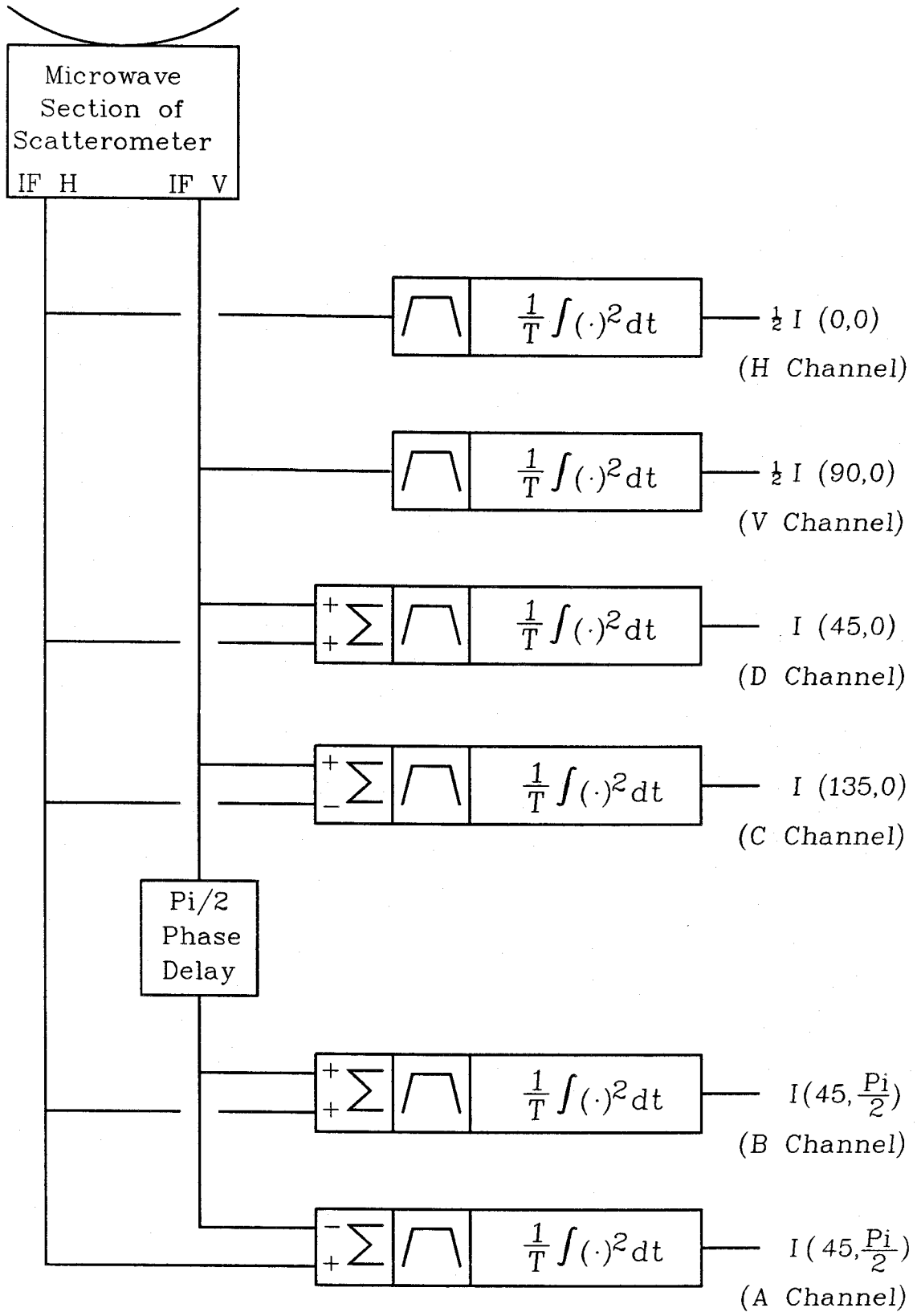

Figure 4-3: Implementation of Polarimeter using Intensity Measurements

4.3.3. Selection of Implementation Method

The discussions in the previous two sections have indicated that both the phase method and the intensity method are applicable to the situation at hand. Implementation of the phase method would require matching of the IF filters and the design and construction of a phase delay unit, a multiplication circuit, and an averaging circuit.

Implementation of the intensity method would again require matching of the IF filters, but at least four filters would need to be used instead of the two required in the phase method. Design of a phase delay unit and a network to provide the sum and difference signals would also be required. The circuitry already used in the scatterometer could be duplicated to provide the intensity measuring circuitry.

The design effort required to implement a multiplier is considerably greater than that needed for a summing network, especially when an accurate DC response is needed, as is the case here. On the other hand, the intensity method of implementation requires considerably more circuitry and would therefore be more expensive.

The intensity method of implementation was chosen. This minimized the design time required and maximized the likelihood that the additional circuitry would be operational in time for the summer measurement campaign. It also allowed the inclusion of additional channels which could be used to check that the individual channels were operating as they should.

4.4. Design Details

Sections 4.2 and 4.3 of this document have explained how an FM-CW scatterometer can be modified to incorporate the measurement of the polarization state, and have selected the method deemed to be the most suitable. This section provides the details pertaining to both the overall modifications and the individual circuit designs.

In addition to the phase shifting circuitry, summing circuitry and the IF processors mentioned in sections 4.3.1 and 4.3.2 the inclusion of phase matching circuits, power supplies, cabling and additional multiplexing circuits was required. The first three of these topics will be discussed individually, and the remaining topics discussed together in relation to the overall measuring unit.

4.4.1. Phase Matching Circuits

It was noted in section 4.3.2 that phase shifts between the horizontal and vertical channels of the radar were to be avoided. This is true not only with respect to the IF filtering, but also throughout the downconversion circuitry. An examination of the microwave circuitry shown in Figure 3-5 shows that phase shifts can occur at the antenna feed, in the orthomode coupler, in the mixers and along the paths connecting these components. If the differential phase shifts between the horizontal and vertical channels are linear with frequency, they can be compensated for by placing a compensating delay in one of the paths between the power divider and the local oscillator ports of the mixers. If they are not linear with frequency, they can still be reduced by using phase equalizing circuits, placed either in the RF lines or at the IF ports of the mixers.

The center frequency of the RF for the *K*-band transceiver is approximately 13 Ghz. and has a corresponding wavelength of about 2.3 cm. This implies that a 1 mm change in the RF path length would result in a phase change of over 15 degrees. Such a high sensitivity to length means that even a slight difference in the torque used to tighten the connectors could unbalance the system after it had been matched. It was therefore decided to place an adjustable microwave connector called a line stretcher in one of the local oscillator lines. This would allow the phase shifts between the vertical and horizontal channels to be matched after all the connectors had been tightened. New cables were constructed to connect the local oscillator ports of the mixers to the power dividers. Care was taken to ensure that the

lengths of these cables would make the signal paths between the two channels of equal distance. The overall length of the cables was increased by approximately 60 cm. as compared to the original cables. This reduced the magnitudes of the in band spectral components arising from internal reflections.

After installation of the new cabling and the line stretcher a test was performed to compare the phase response of the two channels. Although it was found that up to a 10 or 15 degree differential remained, the line stretcher allowed the phase to be adjusted such that the differential was centered about zero as the RF frequency was swept from its minimum to maximum value. Phase equalization to remove this residual phase imbalance was not attempted.

4.4.2. Phase Shifting Circuits

Previous discussions have assumed that the phase shifting circuit would provide an output signal having the same spectral content as its input, and with the magnitude of each spectral line unchanged, but with the phase of each spectral line at the output shifted (ie. delayed) by $\pi/2$ radians with respect to its counterpart in the input spectrum.

Such a device may be approximated by a time delay in the narrowband case, or by a differential phase shifter over both narrow and wide bandwidths. Use of a time delay corresponding to $\pi/2$ radians at the IF center frequency of 22 Khz would result in a phase shift which varied from approximately 88 to 92 degrees over the 5% bandwidth of the filters. A differential phase shifter can do much better than this while using a fairly simple circuit. The differential phase shifter was thus selected to implement the phase delay.

A differential phase shifter is composed of first order all-pass networks, each having a transfer function of the form

$$T(s) = \frac{-(s-\alpha)}{s+\alpha}$$

The magnitude of the all-pass transfer function is always one, but the phase response varies from 0 to -180 degrees as the applied frequency is swept from a low to a high frequency. This is shown in Figure 4-4. The portion of the curve close to the region where the normalized frequency (i.e. ω/α) is equal to one is quite linear. If two such networks are constructed with slightly different time constants (α's) and a common input signal is applied, the differential phase between the two outputs will remain relatively constant in the region where both normalized frequencies are close to one. The magnitude of the phase difference can be adjusted to any desired value by choosing the corresponding ratio of time constants, thereby moving the two phase responses closer or farther apart in Figure 4-4.

The phase difference between the two outputs will diverge from the desired value as the applied frequency moves away from the near linear portion of the curves. This restricts the useable bandwidth of a two network system quite markedly, especially if the required phase difference is large. Cascading networks will overcome this problem. Two all-pass networks in series will range in phase from 0 to -360 degrees, and if the corresponding time constants are chosen properly, the near linear portion can be extended significantly. Using two cascaded all-pass networks to replace the original two networks can thereby increase the bandwidth over which a given phase difference can be obtained.

All-pass networks arranged in this manner to implement wideband phaseshifters have been documented by Bedrosian [18]. He has generated tables relating the required phase accuracy and bandwidth to the order of the network required, and has also tabulated the corresponding pole-zero locations. Use of his tables and design guidelines resulted in the fourth order network shown in Figure 4-5, where the all-pass networks have been

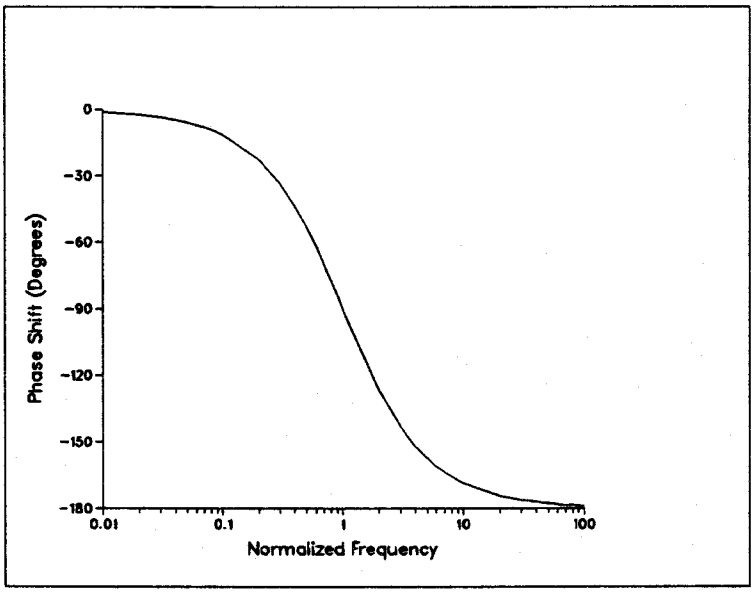

Figure 4-4: Phase Response of All-Pass Network

implemented in the active form [19].

This type of network is normally employed where the required output signals are identical except for the required phase difference. The requirement for the polarimeter is rather that the phase of the vertical signal be delayed by ninety degrees with respect to the horizontal signal. This can be acheived by decoupling the inputs to the two networks and applying the vertical signal to one and the horizontal signal to the other. This will result in the horizontal signal being delayed in phase by some amount $\phi_{ph}(\omega)$, and the vertical signal being delayed by an amount which can be approximated by $\phi_{ph}(\omega)$-$\pi/2$ over the bandwidth of interest.

Verification that this modification will result in the required measurement parameters can be acheived by replacing the phase terms ϕ_{hh} and ϕ_{hv} in equations (4.5) and (4.6) with ϕ_{hh}-$\phi_{ph}(\omega)$ and ϕ_{hv}-$\phi_{ph}(\omega)$-$\pi/2$ respectively. Working through the developments given then shows that the end results are identical to those acheived with the strict $\pi/2$ phase delay used originally.

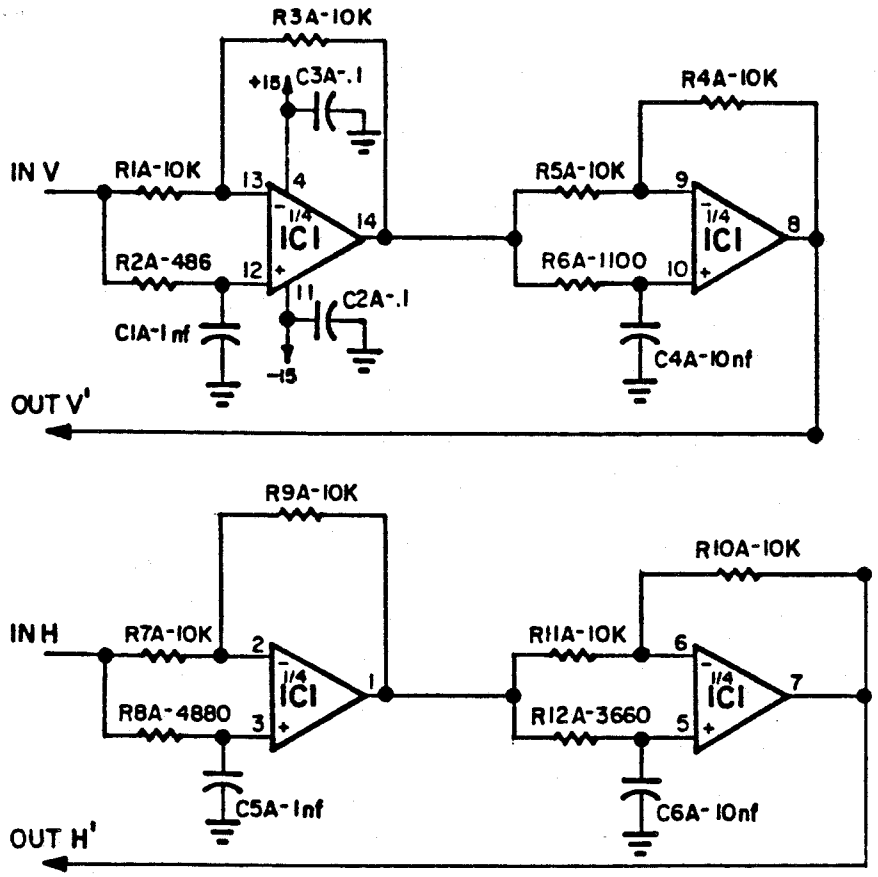

Figure 4-5: Phase Shifter Schematic

4.4.3. Sum and Difference Networks

Determination of the intensities in the 45 and 135 degree angles requires the design of circuitry to provide the sum and difference of the horizontal and vertical IF responses. Since the signals generated in this manner are passed through bandpass filters after combination, the DC response is not of concern and the networks can be constructed using simple configurations.

The designs used for the networks are shown in Figure 4-6. These circuits

were implemented by modifying the existent circuitry on the IF processor boards and used the operational amplifiers already on board. Since these amplifiers were not compensated, the inclusion of the capacitors in the feedback paths was necessary to prevent oscillation of the circuitry.

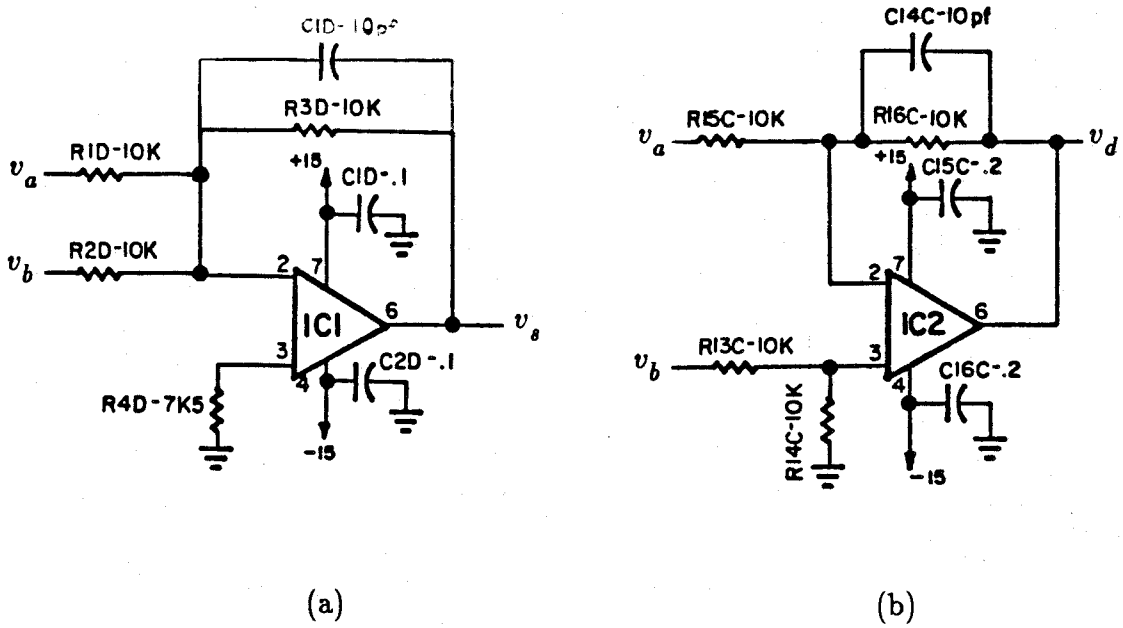

(a) (b)

Figure 4-6: Sum and Difference Amplifiers

Analysis of the configurations leads to the following equations relating the output voltages to the inputs

$$v_s = -\frac{v_a R_3}{R_1(R_3 C_1 s + 1)} - \frac{v_b R_3}{R_2(R_3 C_1 s + 1)}$$

for the summing network(a), and

$$v_d = v_b \left(\frac{R_{14}}{R_{13} + R_{14}}\right)\left(1 + \frac{R_{16}}{R_{15}(R_{16} C_{14} s + 1)}\right) - \frac{v_a R_{16}}{R_{15}(R_{16} C_{14} s + 1)}$$

for the difference network(b). If the constraints that $R_3C_1s \ll 1$, $R_{16}C_{14}s \ll 1$ and that the ratios R_3/R_1, R_3/R_2, R_{16}/R_{15} and R_{14}/R_{13} are all equal to one are applied, the transfer functions reduce to the desired forms

$$v_s = -(v_a + v_b) \quad \text{and} \quad v_d = v_b - v_a.$$

4.4.4. Test Filters

Comparison of the phase between the vertical and horizontal channels of the scatterometer was necessary to complete the phase matching described in section 4.4.1. This comparison was complicated by internal reflections, which caused large low frequency components to occur at the IF ports of the mixers. Measurement of the phase between the two higher frequency signals due to the target reflection was then almost impossible. To reduce the magnitude of the low frequency components bandpass filters were designed and placed on one of the IF processor boards (Board C). The IF outputs of the mixers were then applied to these filters and the outputs of the filters used to provide the signals used for adjusting the phase.

Each bandpass filter consists of a third order highpass network followed by a third order lowpass network. Both sections have a Butterworth response. The lowpass network has a cut-off frequency of 10 KHz., while the highpass network has its break point at 45 KHz. Schematic diagrams for these filters are shown in Figure 4-7.

4.4.5. Incorporating the Modifications

The phase shifting and summing circuitry described in the previous sections was combined with additional IF processor boards supplied by Applied Microwave Corp. Since the IF processors contain filtering, rectification and averaging circuitry, this combination was sufficient to complete the implementation of the signal processing circuits.

Four IF processors were added. Each processor was preceded by either a

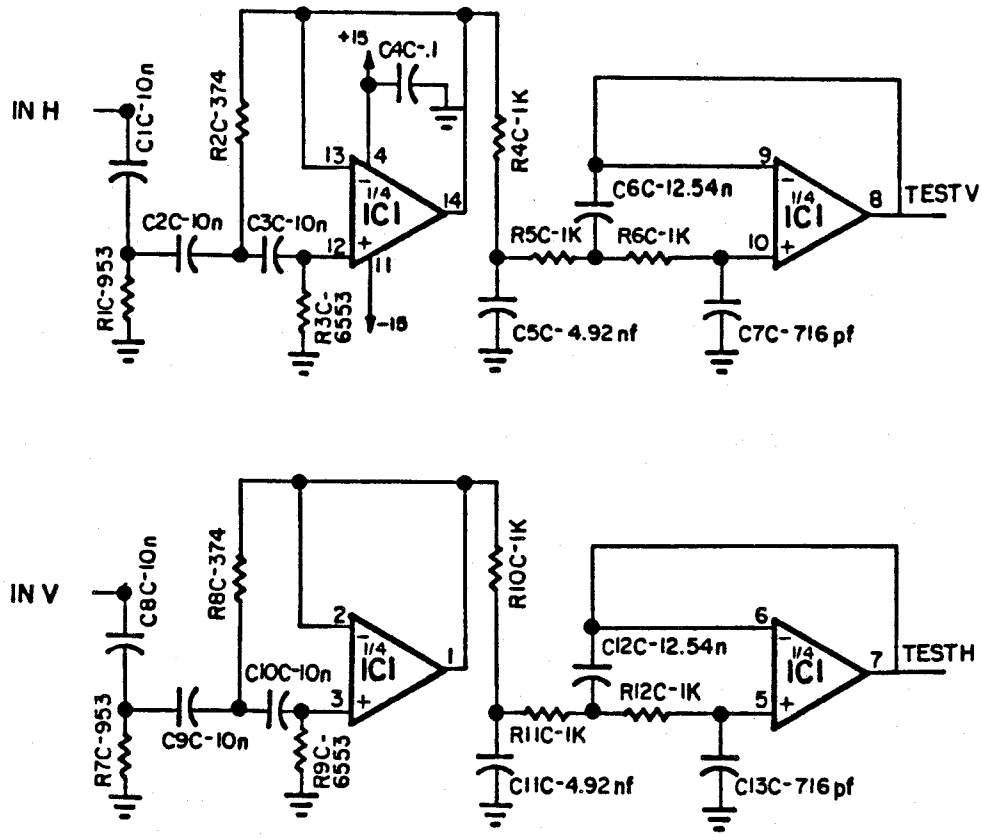

Figure 4-7: Bandpass Filters used for Testing

summing or a difference amplifier. The inputs to these amplifiers were connected such that the four additional channels measured the sum of the horizontal and vertical IF signals, the difference of these, the sum of the phase shifted versions of the horizontal and vertical IF signals, and the difference of the phase shifted versions. Schematics showing the complete circuitry for each of the boards in addition to a schematic of the original horizontal (or vertical) channel circuitry are included as Figures 4-8, 4-9, 4-10, 4-11, and 4-12 to show how this was acheived. The phase shifting circuitry was mounted piggy-back on board A. The portions of the

schematics which differ from the original design are enclosed in dashed boxes.

Each IF processing board as designed by Applied Microwave Corp. contains front end circuitry which interfaces to the mixers in the Microwave sections of the scatterometer and high pass filters the incoming signals to reduce the magnitude of the low frequency components. The IF signals are also gated at this point to allow only those contributions resulting from the positive going portion of the RF sweep to pass through to the filters and detectors. After buffering, the input signals are passed to the IF filters via the signal lines labelled as P1-5 on the schematics. This provides a convenient access point for the additional circuitry to tap in to the horizontal and vertical signals. An overall transceiver wiring diagram showing the results of this is given in Figure 4-13.

The horizontal and vertical IF processors in the scatterometer are enclosed in aluminum boxes so they can be mounted easily within the transceiver enclosure. Although a box is provided for each, it was found that two IF processor boards could be contained by a single box. Accordingly, the four additional processors were mounted using only two boxes. The two processors using the signals directly from the horizontal and vertical IF processors (boards C and D) were mounted together and called the IF In Phase Combination Unit. The two boards combining the phase shifted signals (boards A and B) were placed in a separate box and called the IF Quadrature Combination Unit.

The outputs of the horizontal and vertical IF processors are led to a connector in the transceiver enclosure where they are passed through to a cable which connects them to the data acquisition unit. Only two spare wires were available in this cable. The transfer of the output signals from the In Phase and Quadrature combination units thus required the addition of a separate connector and cable. The connector pin out is shown in the wiring diagram, along with the color coding of the wires used.

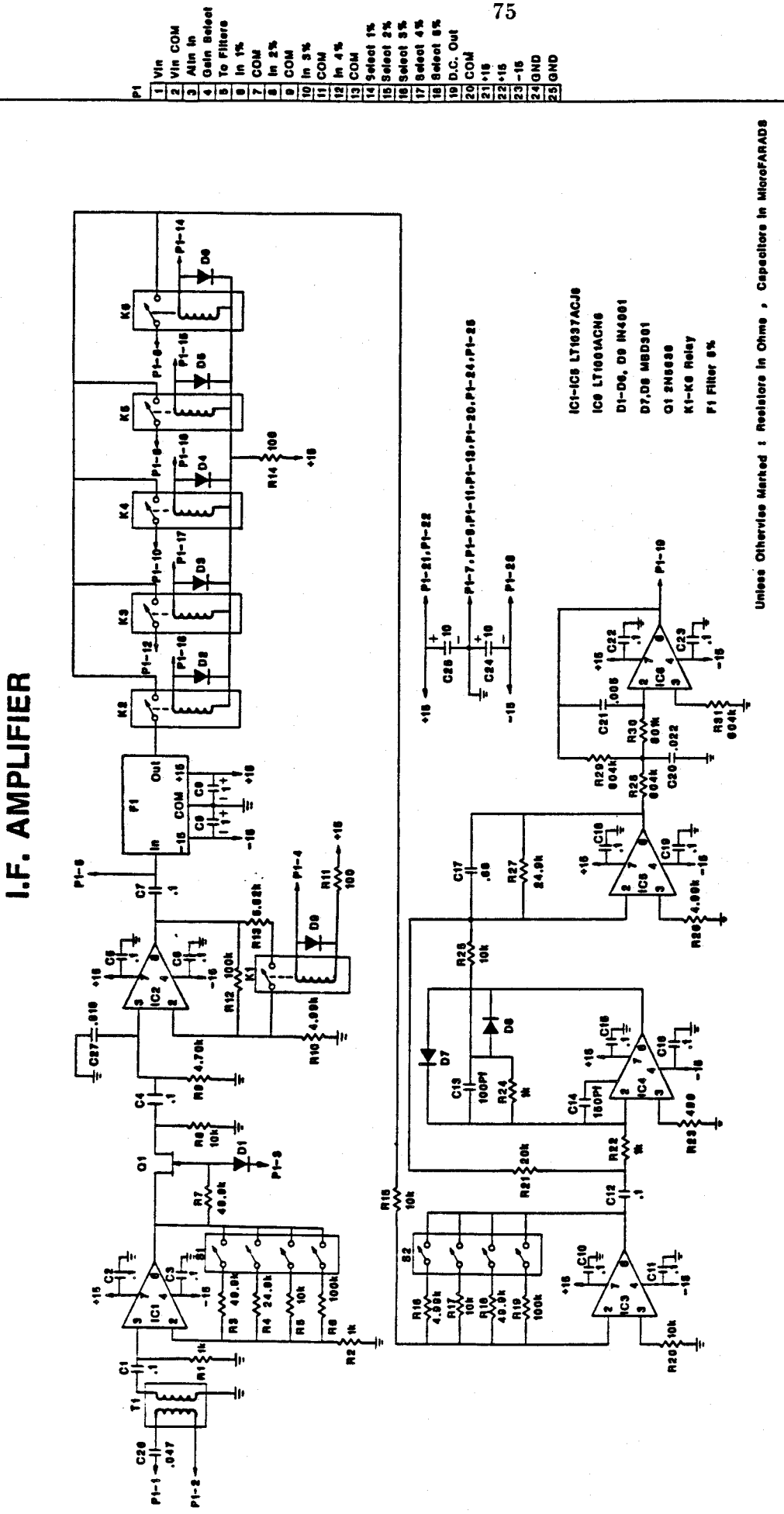

Figure 4-8: Horizontal or Vertical IF Processing Section

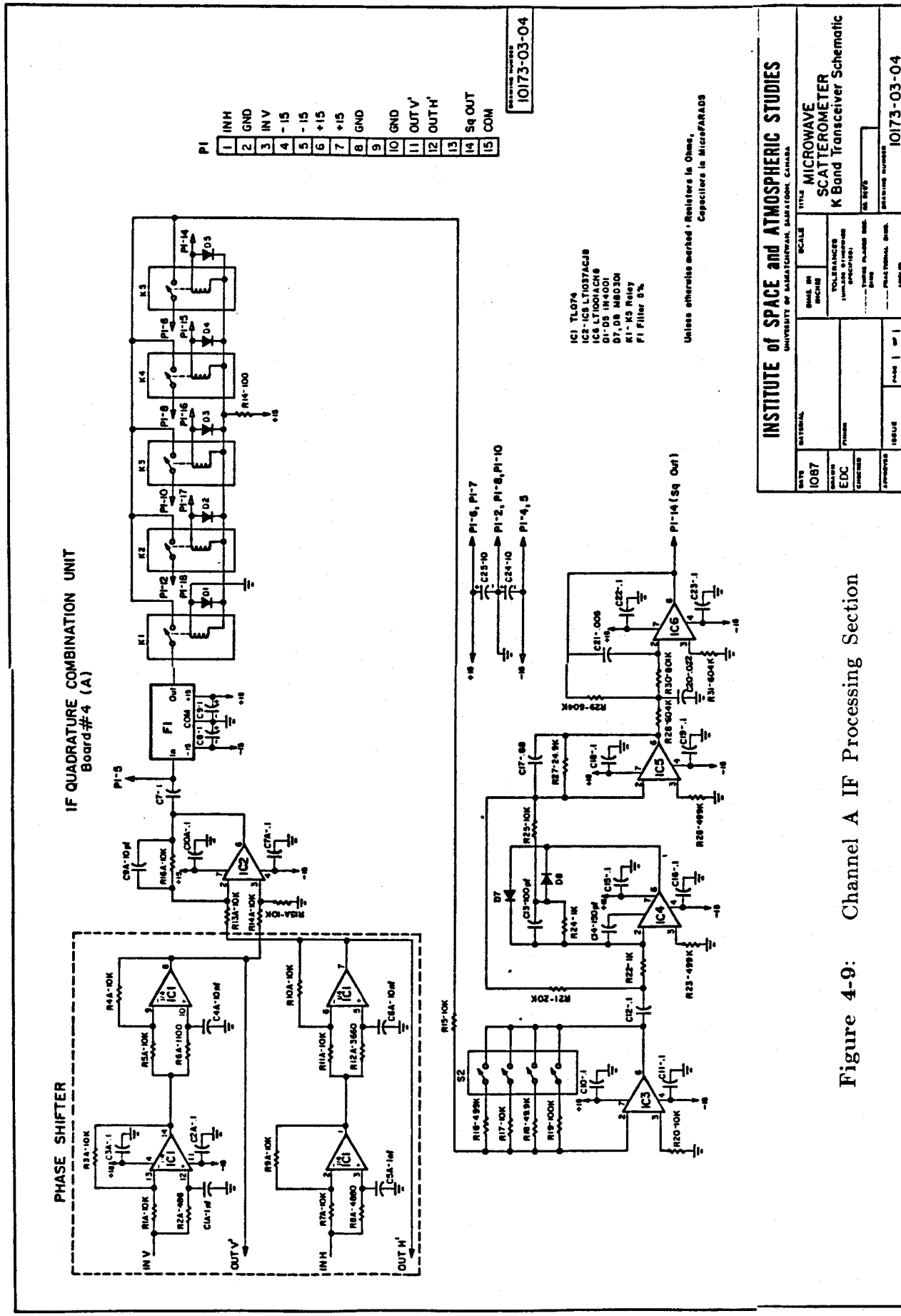

Figure 4-9: Channel A IF Processing Section

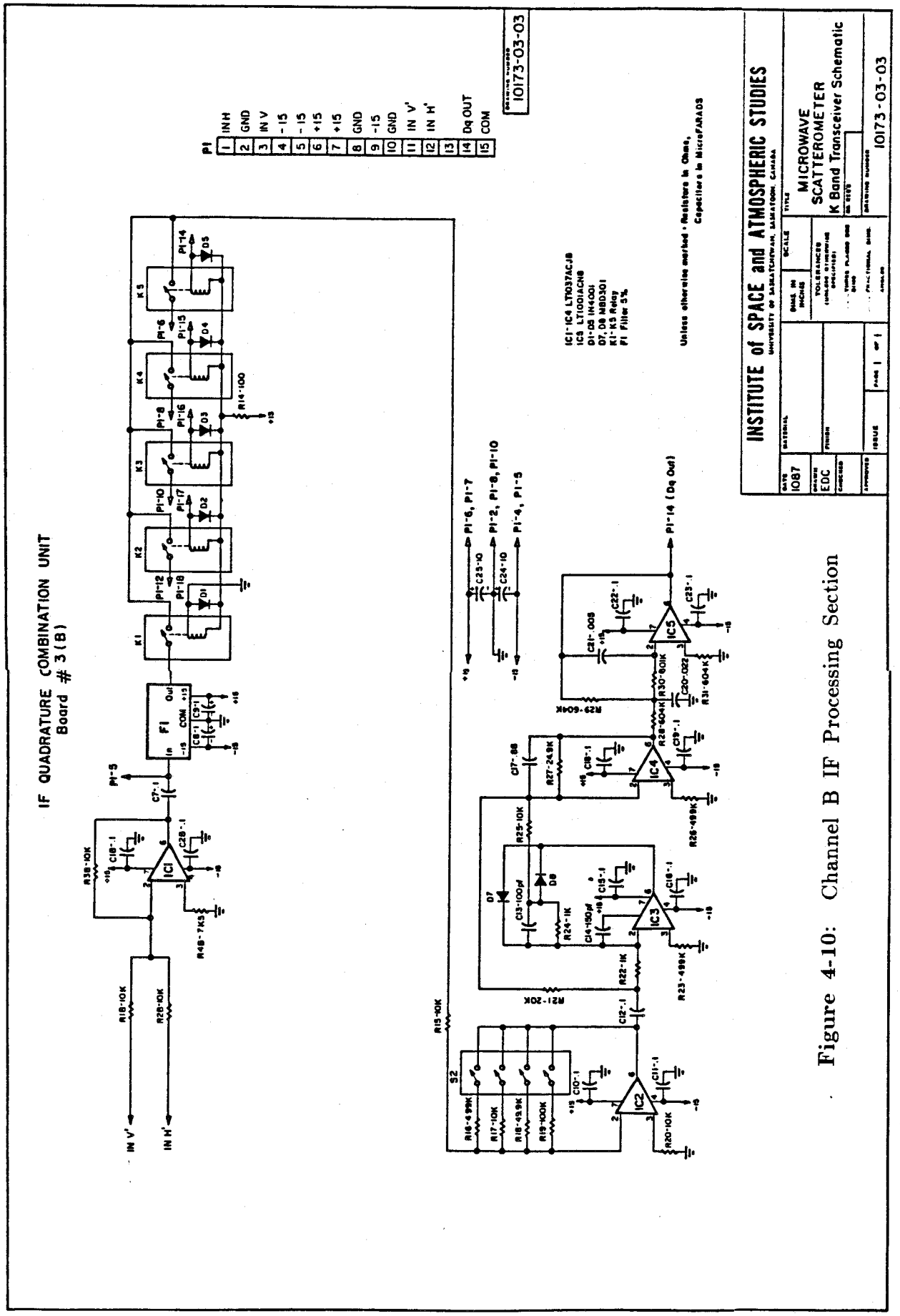

Figure 4-10: Channel B IF Processing Section

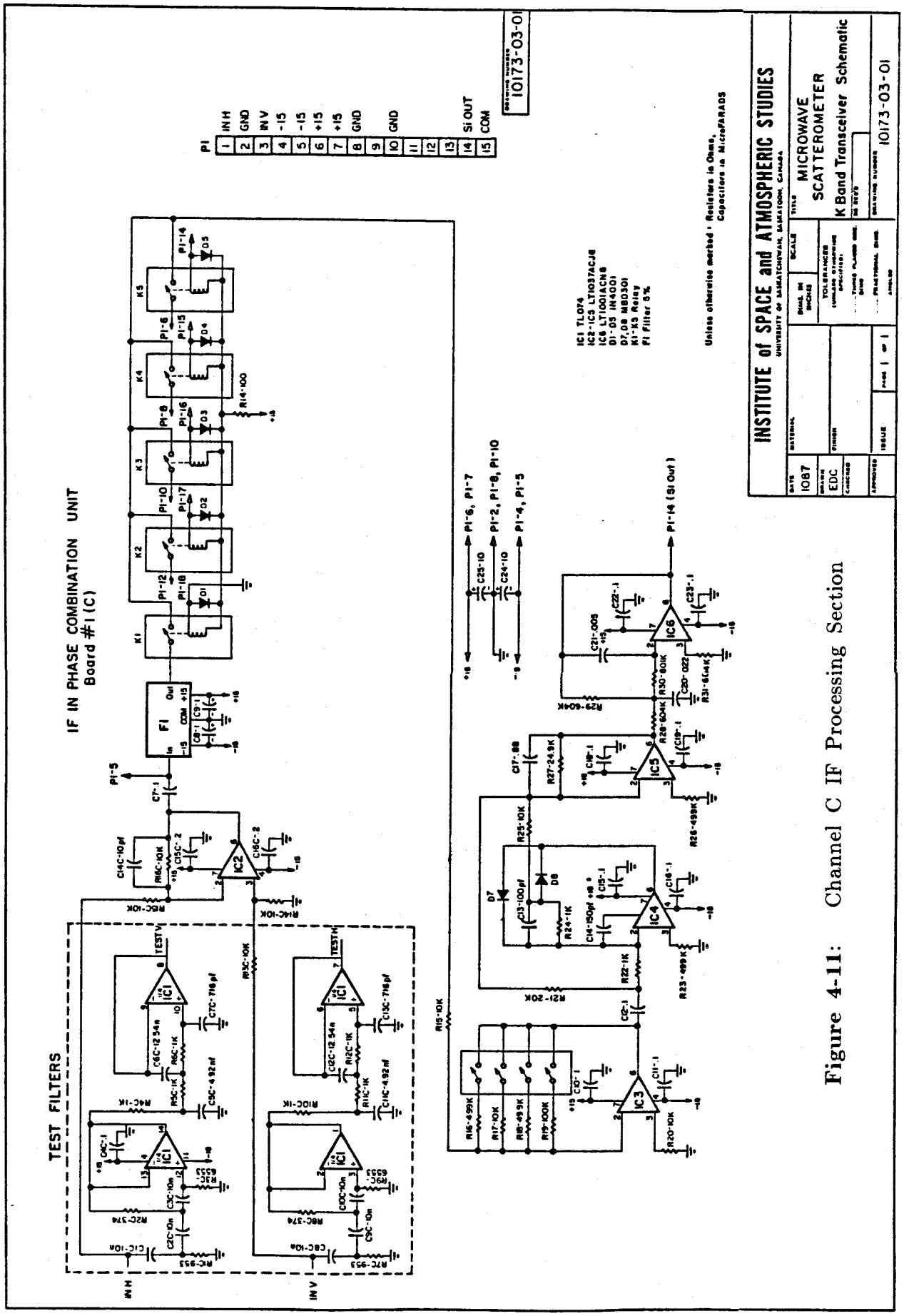

Figure 4-11: Channel C IF Processing Section

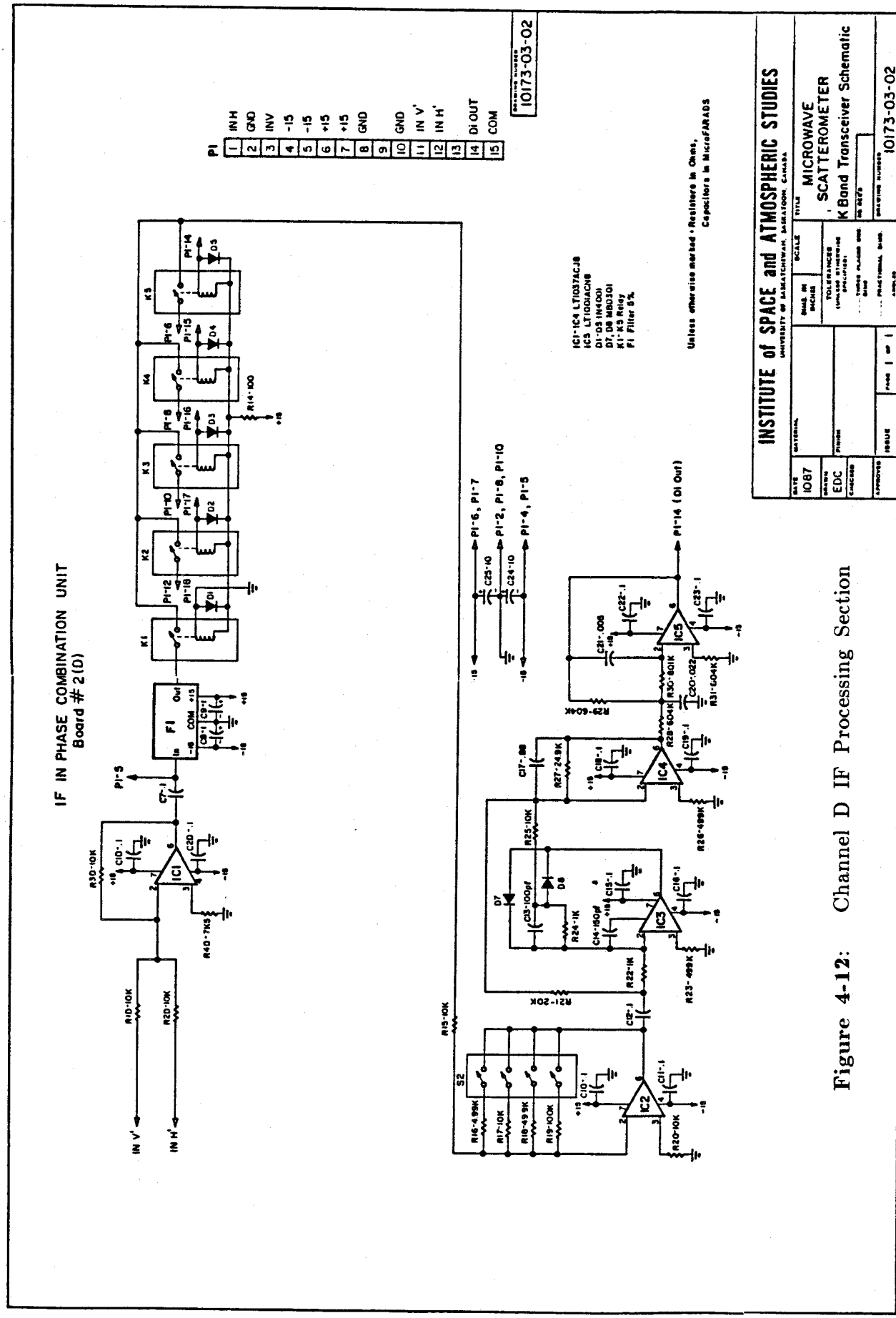

Figure 4-12: Channel D IF Processing Section

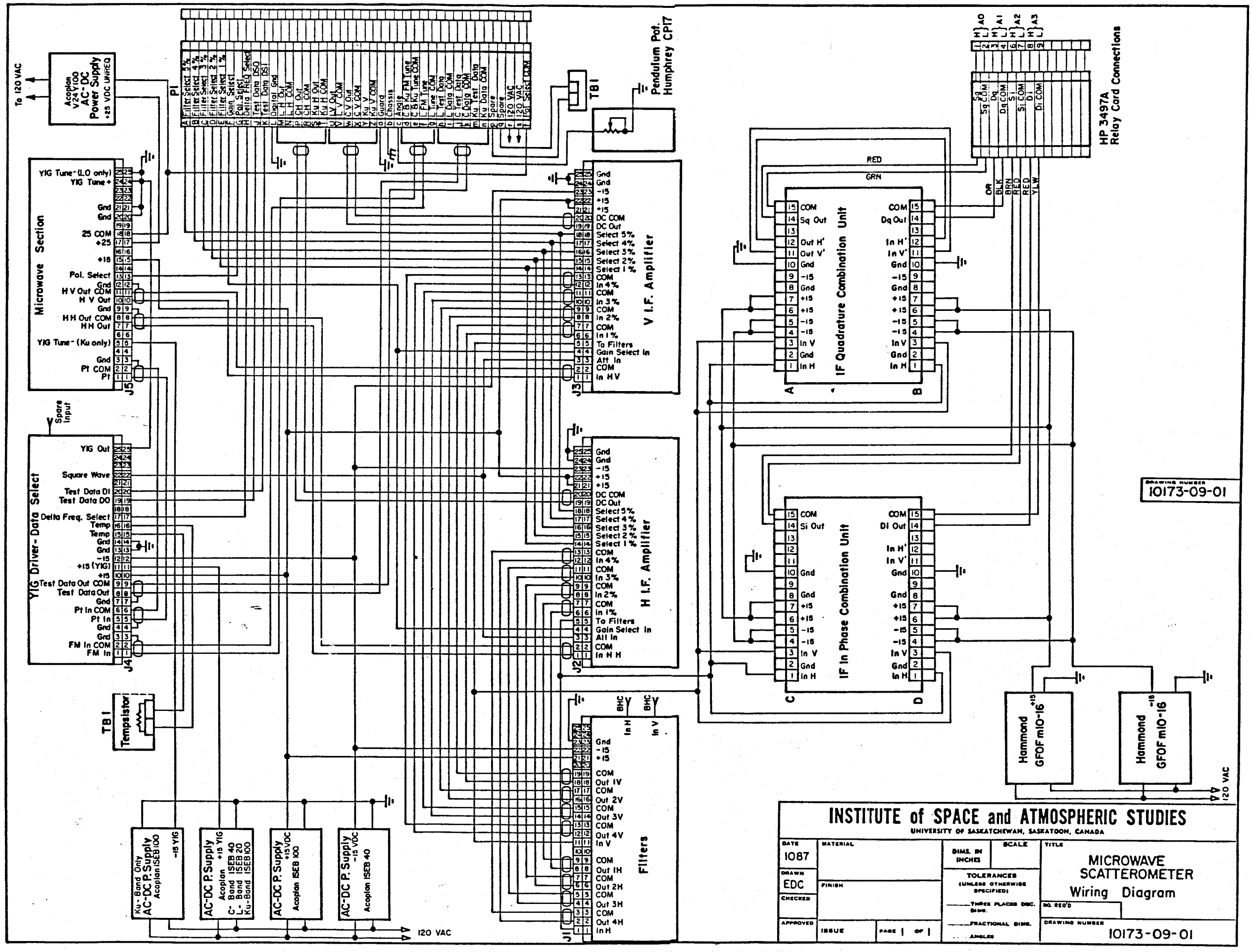

Figure 4-13: Overall Wiring Diagram for Modified Transceiver

The data acquisition unit uses multiplexing circuitry to connect the analog signals produced by the IF processors to a digital voltmeter. This allows a single voltmeter to be used to measure all of the processor outputs. The addition of extra processor outputs necessitated the expansion of this multiplexing circuitry. Accordingly, an extra analog relay card (Hewlett-Packard option 010) was added to the acquisition unit in slot 3. A table showing the connection details is given as Table 4-1. The table also shows the acquisition unit channel numbers which correspond to the various processor outputs.

Table 4-1: Analog Relay Card Connections and Corresponding Channel Allocations

Signal Line	Description (As per H,V)	Connector Pin No.	Wire Color	Relay Card Connection	Dacu Channel Assignment
Output A	Quadrature Diff	1	Red	A0-High	AC-60
Return A	Return for A	2	Green	A0-Low	
Output B	Quadrature Sum	3	Orange	A1-High	AC-61
Return B	Return for B	4	Black	A1-Low	
	Guard	5		None	
Output C	Difference	6	Brown	A2-High	AC-62
Return C	Return for C	7	Red	A2-Low	
Output D	Sum	8	Red	A3-High	AC-63
Return D	Return for D	9	Yellow	A3-Low	
	Spare	10	Yellow	None	None
	Spare	11	Black	None	
	Spare Guard	12			

An option on the scatterometer allows the choice of different bandwidth IF filters. The selection process is carried out by switching the desired filter in line with a relay. Each IF processor carries five relays for this purpose. Although the implementation of the polarization measuring circuitry uses only one filter per processor, it was not known at the time of construction whether or not the additional filters would be desired. If so, the power

supplies in the transceiver would have been inadequate to drive the extra relays. It was also noted that the power supplies were operating near their rated capacity even without the additional circuitry. Separate power supplies were thus used to drive the in phase and quadrature combination units. They are indicated on the wiring diagram.

4.5. Relation Of Signal Lines To Polarization Parameters

As a conclusion to this chapter on design and implementation, this section will relate the measured values of the IF processor outputs to the desired polarization parameters in a convenient form.

The explanations given in section 4.3.2 showed that the measured power in the sum and differences of the horizontal and vertical IF signals corresponded to the intensity in the 45 and 135 degree directions respectively. The power in the sum and difference of the phase shifted horizontal and vertical signals corresponded to the intensity in 45 and 135 degree directions after the vertical signals had been delayed by $\pi/2$ radians. The detection circuitry within the scatterometer does not measure power, however. It measures the average value of the full wave rectified signal, and is therefore proportional to the square root of the power[10]. The combination of this fact with the relations between the intensities and the polarization parameters given in Chapter 2, section 2.2.3.2 results in

$$\tan 2\psi = \frac{S_i^2 - D_i^2}{2(H^2 - V^2)} \tag{4.7}$$

$$\sin 2\chi = \frac{S_q^2 - D_q^2}{2\sqrt{(H^2 - V^2)^2 + .25\,(S_i^2 - D_i^2)^2 + .25\,(S_q^2 - D_q^2)^2}} \tag{4.8}$$

---

[10]The performance of the detection method used in relation to the measured parameters is discussed in Chapter 6

$$m = \frac{\sqrt{(H^2 - V^2)^2 + .25\,(S_i^{\,2} - D_i^{\,2})^2 + .25\,(S_q^{\,2} - D_q^{\,2})^2}}{H^2 + V^2}. \tag{4.9}$$

where

- H is the output of the horizontal channel IF processor board,
- V is the output of the vertical channel IF processor board,
- S_i is the output of the D channel IF processor board (the in-phase sum),
- D_i is the output of the C channel IF processor board (the in-phase difference),
- S_q is the output of the B channel IF processor board (the quadrature sum), and
- D_q is the output of the A channel IF processor board (the quadrature difference).

Chapter 5

CALIBRATION AND TESTING

5.1. General

Chapter 4 of this document has shown that the polarization state of the radiation received by the scatterometer may be determined through the measurement of six intensities (powers). Ideally, these six intensities correspond to the intensities of various components of the electric field vector of the radiation incident on the antenna. In the practical case however, the measured values will not correspond exactly to those electric field intensities but will differ by some gain constant determined by the receiving equipment. The constant is not necessarily the same for all six of the measured channels and can in fact be different for each.

If the gain constants for the six channels are made to be equal, the relations given in equations (4.7), (4.8) and (4.9) will apply directly, since any multiplicative constant will cancel out in the ratios. The true value of the constant need not be known. The determination of the scattering cross section however does require a knowledge of the gain constants, as will be shown in section 5.3.1, so the constants must be determined.

This chapter deals both with the testing of the modifications made to the scatterometer to allow its use as a polarimeter and with the tests of the completed unit to determine the proper calibration (i.e. gain) constants.

The determination of the system gain constants is referred to as calibration. Two methods of calibrating a radar system are common. The first is to fully

characterize each part of the system and use the information derived to calculate the overall system gain. This method is termed internal calibration. It is used mostly just after the system has been constructed so that the builder can be certain that all portions of the radar are functioning as they should. It is however very complex and time consuming to carry out.

If it is known that the system is operating as it should, but there is some doubt regarding the validity of the calibration constants, a much simpler external calibration method can be used. It involves taking measurements of a target which has a known scattering cross section. The indicated cross section can then be equated to the known cross section of the target through the determination and use of a calibration constant.

Since the modifications carried out on the scatterometer required some examination of internal components as well as the determination of the calibration constants, a combination of the above two methods was used. The IF processing sections were fully characterized and tuned to match their gains as closely as possible. An external calibration was then carried out to include the effects of the microwave sections and determine the overall system constants. The following sections describe the tests carried out and the results obtained.

5.2. Internal Calibration

The internal calibrations carried out on the radar system were intended to ensure that the modifications made to the system were functioning as they should, as well as to verify that they did not interfere with the original radar circuitry. To fulfill these objectives many tests of a characterization nature were carried out in addition to several calibration (in this case gain matching) procedures.

The calibration and testing proceeded from small circuit blocks to larger. First the phase shifter as designed in Chapter 4 was characterized. It was

found that calibration here was unnecessary. After this, the IF sections were examined individually. The gain through each of the six IF blocks was measured, and adjustments were made such that the steady state AC gains were matched to within several percent of each other. The overall gain from IF input (AC) to IF output (DC) was then measured and adjustments made such that these gains were matched as well. Following this, the IF sections were characterized in frequency using a spectrum analyzer. The IF sections were then connected to the microwave receiving section and tests carried out with the transmit signal from the radar fed through a cable to a transmitting antenna which beamed it back to the radar. This allowed the operation of the radar to be examined without the complications associated with reflections from a target and without interference from internal reflections. Initially, a linear antenna oriented at 45 degrees from the horizontal axis was used and the line lengths in the microwave sections adjusted for minimum phase difference between the horizontal and vertical IF signals. More complete tests were then performed with both linear and elliptically polarized transmitting antennas at various orientation angles.

The sections which follow describe each of the tests in more detail.

5.2.1. Phase Shifter Tests

To verify the correct operation of the phase shifter, tests were carried out to determine its phase vs frequency response. These tests were done by measuring the time difference between the two output signals when a common sinusoidal signal was applied to the two inputs labelled IN-H and IN-V in Figure 4-9. The measured time difference was converted to phase by dividing by the period of the input sinusiod. The input sinusoid was generated by a Hewlett-Packard (HP) 3300A signal generator, and the period of the output and time difference between output waveforms were measured using HP 5315 counters.

The test results from this series of measurements are given graphically in

Figure 5-1. The tabular data from the tests along with a discussion on the effects of counter offsets and signal distortions are given in Appendix B. The graph shows an absolute error in phase which varies from the ideal value of 90 degrees by .67 to .78 degrees over the 20 to 24Khz frequency range. The estimated accuracy of the measurements is .05 degrees.

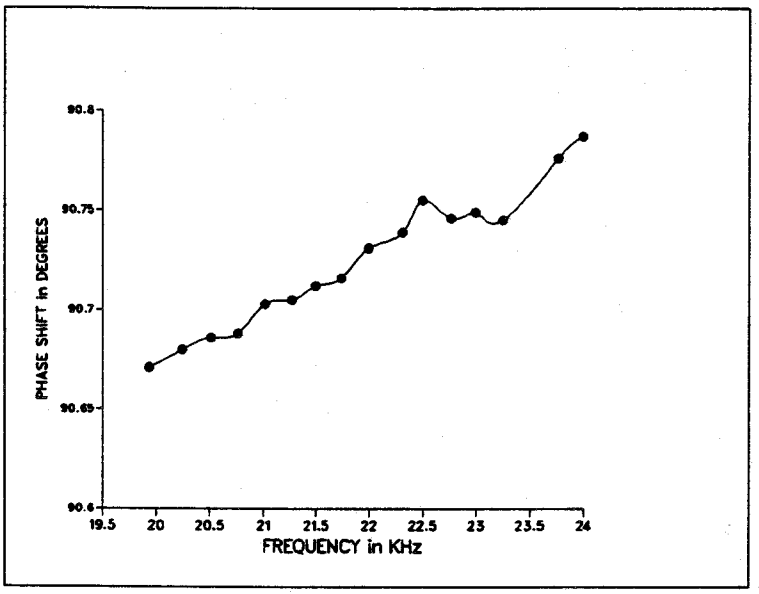

Figure 5-1: Differential Phase Shift vs. Frequency for Phase Shifter

5.2.2. Gain and Frequency Response Calibrations

Section 5.1 noted that if the gain constants for the six intensity channels were equal, the constants would drop out when calculating the polarization parameters. It is therefore desirable to ensure that the six gain constants are equal. This section describes the method used to match the IF gains and includes the data from the subsequent IF characterization.

The measurement set up used for the gain matching process is shown in Figure 5-2. The first step was to ensure that the AC gain from the IF input (P1-1, P1-2)[11] to the intermediate IF output (P1-5) was the same on the

---

[11]The connector pin number and part number designations given in this section refer to the schematics detailed on pages 75 to 79.

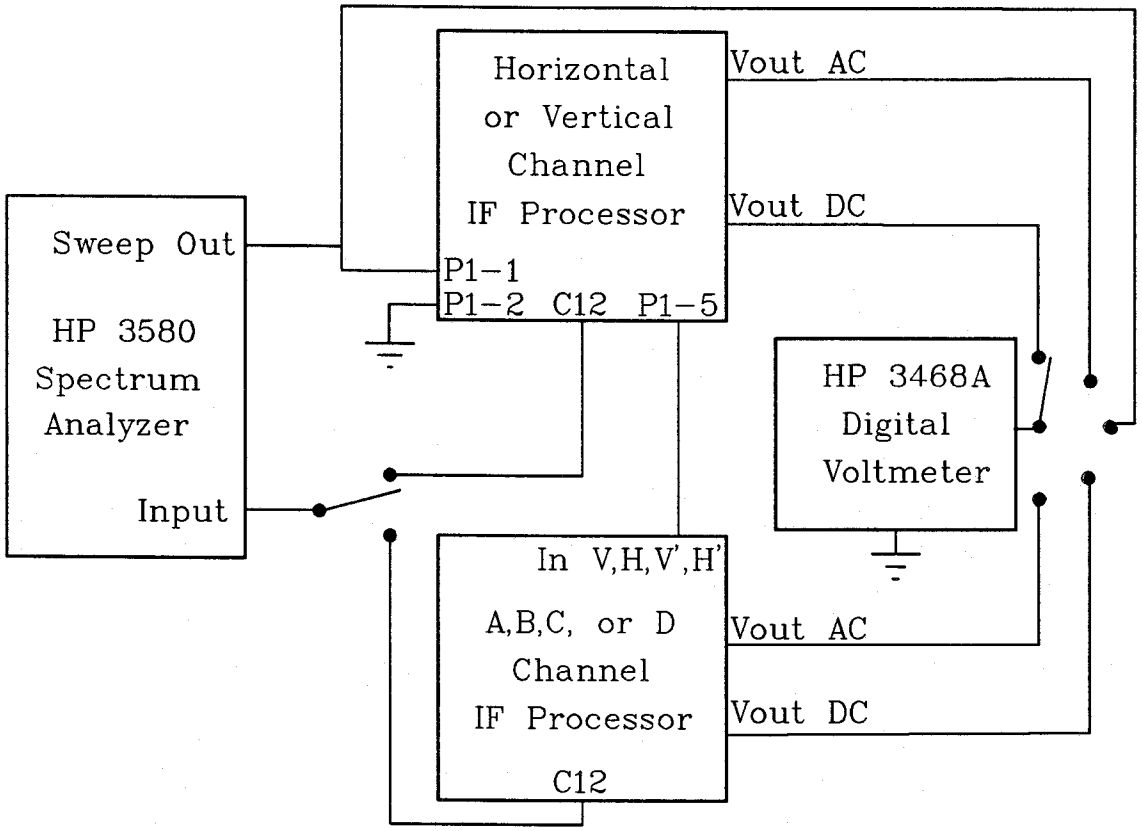

Figure 5-2: Test Setup for Gain Measurements

horizontal and vertical IF boards. A fixed frequency sinusoid at 22 Khz. was used as the input. It was discovered that the capacitors C26 (on page 75) caused a gain mismatch between the horizontal and vertical processing boards, so these capacitors were replaced with a matched pair. Capacitors C7 were replaced with a larger value to prevent the additional load caused by the four extra boards from affecting the output level. Any residual gain mismatch was then removed by placing appropriate resistors in parallel with R2.

Relay K2 was then closed to place the five percent filters in the signal path and the value of R15 adjusted by way of parallel resistors such that the AC gain (Vout AC in table 5-1) from P1-5 to C12 was the same for all six of the IF boards. The gains from P1-5 to the DC output (P1-19) were

then measured. It was found that adjusting the value of R15 was sufficient to match the AC gains to C12 as well as the DC gains through to P1-19.

Table 5-1 shows the resulting AC and DC gains. The maximum variation in DC gain between boards is 2.6 percent.

Table 5-1: IF Steady State Gain Measurements at 22KHz

Measurements taken on July 8, 1987

Board	Vin AC (mVrms)	Vac P1-5 (Vrms)	Vout AC (Vrms)	Vout DC (Vdc)	AC Gain on board	DC Gain on board
H-Pin 1	4.280	0.6850	3.3985	-3.8525	4.9613	-5.6241
V-Pin 1	4.280	0.6819	3.4270	-3.8400	5.0257	-5.6313
A-Pin 1	4.270	0.6787	3.3260	-3.7240	4.9005	-5.4870
A-Pin 3	4.270	0.6790	3.3440	-3.7400	4.9249	-5.5081
B-Pin 11	4.265	0.6792	3.4190	-3.8180	5.0339	-5.6213
B-Pin 12	4.267	0.6795	3.4280	-3.8270	5.0449	-5.6321
C-Pin 1	4.270	0.6792	3.3800	-3.7550	4.9764	-5.5286
C-Pin 3	4.268	0.6792	3.3745	-3.7495	4.9683	-5.5205
D-Pin 1	4.278	0.6803	3.4370	-3.8080	5.0522	-5.5975
D-Pin 3	4.280	0.6805	3.4290	-3.7980	5.0389	-5.5812

Measurements taken on May 7, 1987

Input Pin	Outputs at P1-19 of board V	H	A	B	C	D
H-1	0.0000	-3.749	-3.738	-3.731	-3.733	-3.737
V-1	-3.782	-0.005	-3.789	-3.769	-3.767	-3.769

The IF sections were then characterized in frequency with the aid of a spectrum analyzer. The frequency responses obtained are shown in Figures 5-3 and 5-4. The input signal for boards A through D was taken from P1-5 on the IF V board. The analyzer was not calibrated for absolute level, so the spectra should be compared only as to shape.

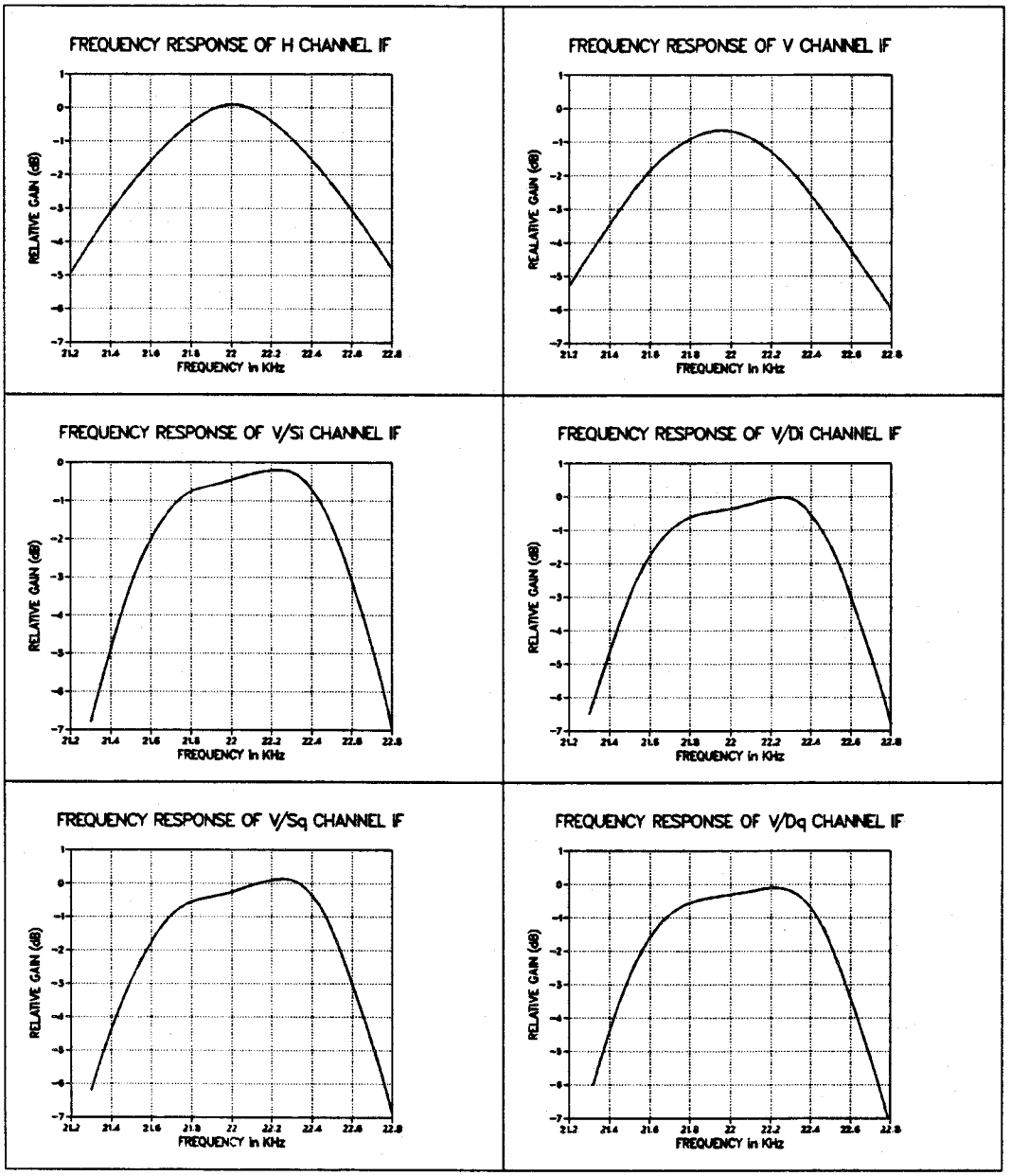

Figure 5-3: IF Spectra at 1dB per Division

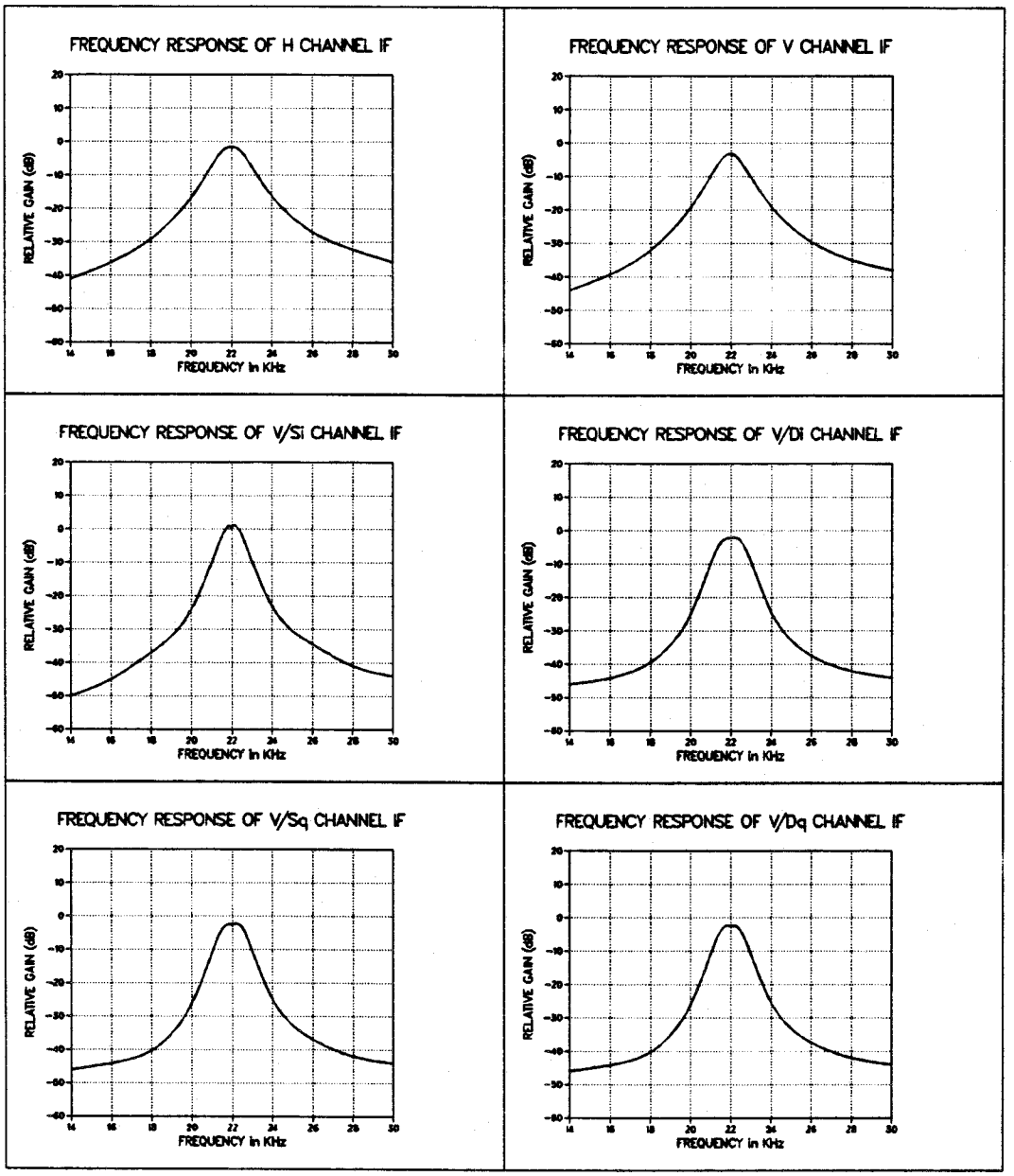

Figure 5-4: IF Spectra at 10dB per Division

5.2.3. Initial System Testing and Tuning

This section describes the tests carried out in the lab on the *K*-band radar to verify the overall system operation. The configuration of the equipment for these tests is shown in Figure 5-5. While this testing was carried out, the cable connecting the power splitter to the transfer switch (see Figure 3-5 on page 43) was disconnected. The transfer switch was then terminated with a fifty ohm termination and the disconnected port on the power divider used to drive the test antenna of Figure 5-5 via a fifteen foot length of semirigid coaxial cable and a microwave line stretcher. The test antenna was placed in a rotatable mount to allow rotation about the axis of transmission. Care was taken to ensure that the antenna on the *K*-band radar transceiver and the test antenna were aligned for maximum power transfer.

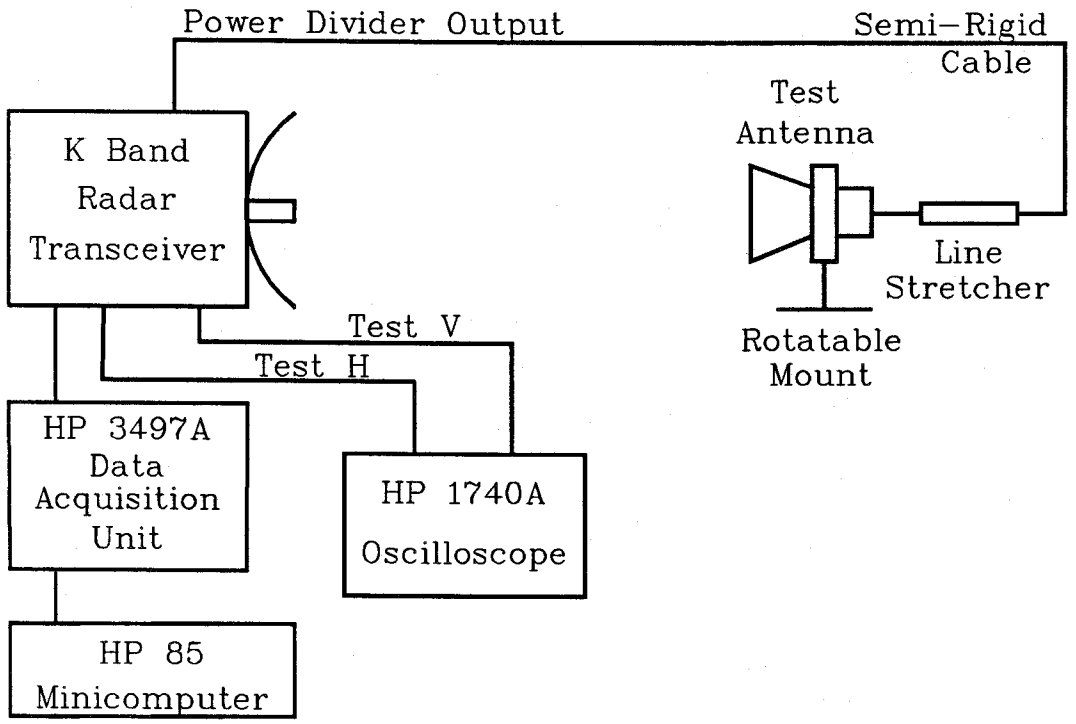

Figure 5-5: Equipment Configuration for System Testing

5.2.3.1. Path Length Adjustments

As noted in previous chapters, the line lengths in the microwave section must be matched if the polarimeter is to provide reliable information. A line stretcher was installed in the local oscillator path to one of the mixers to allow this. Matching of the line lengths was carried out by monitoring the signals at the Test-H and Test-V outputs of the horizontal and vertical IF sections (see page 78). If a linearly polarized signal oriented at 45 degrees to the horizontal is received, these IF signals will be in phase when the horizontal and vertical signal paths are of equal length. Consequently, the transmitting horn was oriented at 45 degrees and the line stretcher adjusted to minimize the phase variations. It was found that the monitored signals could not be perfectly synchronized over the length of the RF upsweep. The phase difference between the two signals varied between plus and minus 12 degrees (in time, 1.5μs out of a total upsweep time of 45.45μs).

5.2.3.2. Tests Using a Linear Transmitting Antenna

Following the adjustments to the line stretcher, measurements of the six IF output voltages were taken at various orientations (ψ) of the linear transmitting horn. The data from these measurements was used to calculate the polarization ratio, orientation angle and ellipticity angle corresponding to each antenna orientation. The indicated orientation angle from each calculation was compared to the measured (with protractor and spirit level) angle at the transmitting horn.

The results of these tests are presented graphically in Figures 5-6 and 5-7. The tabular data including the measured voltages at the IF processor outputs are given in Appendix C.

Tests were carried out with both mixers terminated with 6 dB pads in addition to the testing with the mixers driving the IF sections directly. Comparison of the data from the measurements with and without the pads reveals that the impedance mismatch between the mixers and the IF

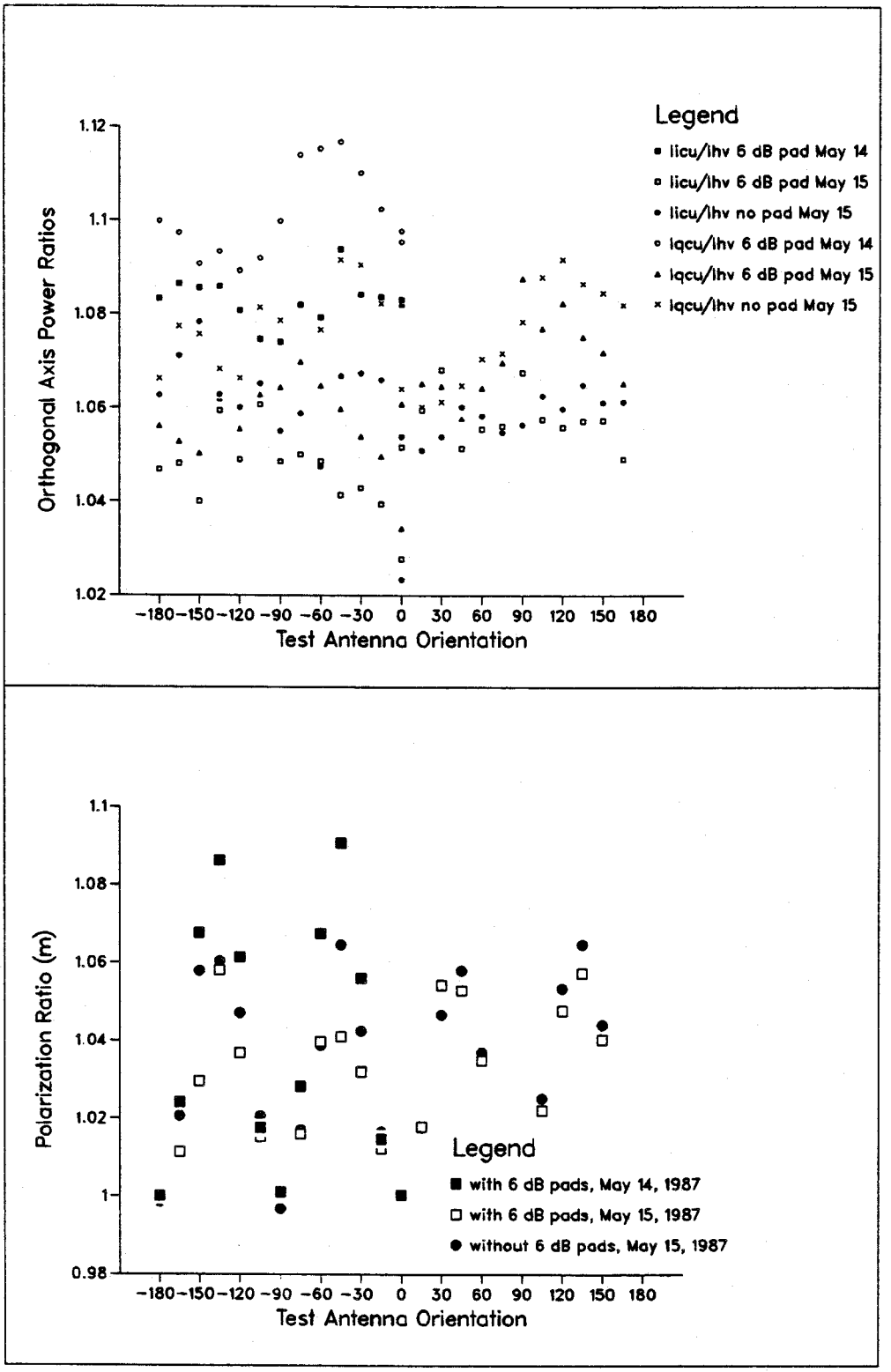

Figure 5-6: Results of Tests Using Horn Antenna

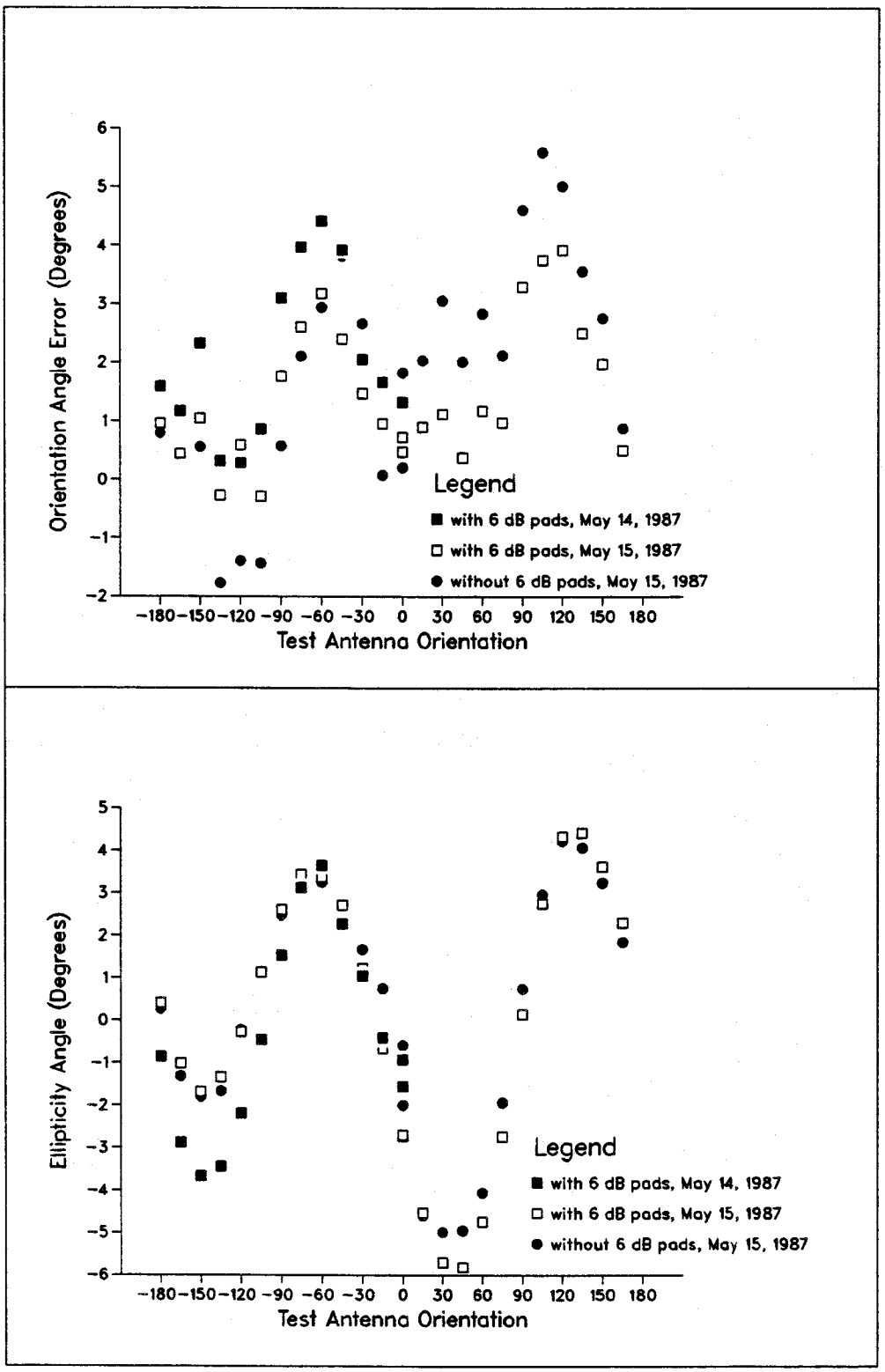

Figure 5-7: Results of Tests Using Horn Antenna

processor input circuitry does not adversely affect the results.

The top plot in Figure 5-6 shows the ratio of the total power measured at the outputs of the in phase combination unit (I_{icu}) to the total power measured in the horizontal and vertical channels (I_{hv}). Also shown is the ratio of the total power from the quadrature combination unit to the total power in the horizontal and vertical channels (I_{qcu}/I_{hv}). Each of the three sets of powers consists of the sum of powers measured in orthogonal axes (H and V, 45 degrees and 135 degrees, and left circular and right circular). Each should therefore indicate the total received power, and the ratios mentioned above should both equal one.

The plot shows ratios varying from 1.02 to 1.12, indicating an error in the measuring system, even though the individual channel gains were matched to within 3 percent during the gain calibrations. The explanation for this effect was found to be due to the different frequency responses of the IF bandpass filters (shown in Figures 5-3 and 5-4 on pages 90 and 91). If the spectrum of the IF signal is not correctly centered in the passband of the filters, but rather is offset to the higher frequency side, the in phase and quadrature combination unit filters will have a larger gain than the horizontal and vertical channel filters, thereby causing ratios larger than one.

The results shown for the polarization ratio range in value from .99 to 1.09. Since the polarization ratio is a measure of the power in the polarized portion of the received signal to the total power of that signal it should never be greater than one, and the results again point to a calibration error. The cause is again the differences between the IF filters.

These differences between the IF filters have consequences for field measurements, and are discussed again in Chapter 6.

The results shown in Figure 5-7 for the orientation angle and the ellipticity angle show that the equipment measures the parameters of the polarization

ellipse fairly well. The largest error in the measured orientation angle is about 5.5 degrees. The ellipticity varies from the expected value of 0 degrees for linearly polarized radiation by at most 6 degrees. The plots show a rather striking variation with the orientation angle of the test antenna, both plots showing peaks at approximately -60 and 120 degrees, and valleys at -150 and 30 degrees. During the testing process it was noted that movement of the semi-rigid coaxial cable connecting the test antenna to the power divider in the transceiver caused marked changes in the oscilloscope traces of the TEST H and TEST V signals. It was therefore assumed that a reflection from this cable was causing multipath interference and creating the cyclical patterns in the plots of orientation angle and ellipticity angle.

Pictures of the TEST V and TEST H signals were taken at several orientations of the test antenna to illustrate the operation of the system. They are shown in Figures 5-8 and 5-9. They show that when the test antenna is oriented at right angles to either the horizontally or vertically polarized receiving antenna, the received signal is minimized for that receiving channel while being maximized for the other. When the test antenna is oriented at 45 degrees to the receiving antennas, the signals in the two channels are approximately equal in magnitude and have either equal or opposite phases. The sum or difference of the two signals then indicates how well the phases between the two receiving channels match (if the phase responses tracked perfectly and the antennas had infinite cross polarization isolation the value would be zero). Figure 5-9 shows examples of several of these sums and differences.

In addition, X-Y oscilloscope traces for several test antenna orientations are given in Figure 5-10. They show that the polarization ellipses for the linearly polarized signals are quite close to the expected straight line. The picture shown for the test antenna orientation angle of 215 (-145) degrees shows a somewhat larger ellipticity as is corroborated by the plot in Figure C-1.

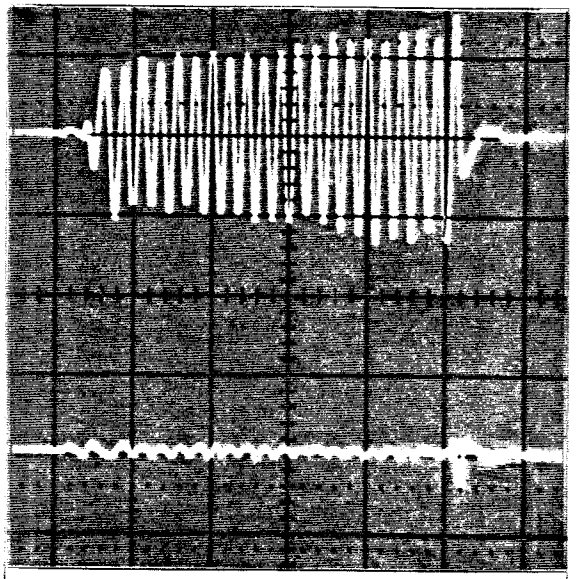

Test Antenna Orientation: 0 deg.
Top: TEST H at .2 v/div.
Bottom: TEST V at .2 v/div.
Time Scale: .2 mS/div.
Mixers terminated with 6 dB pads

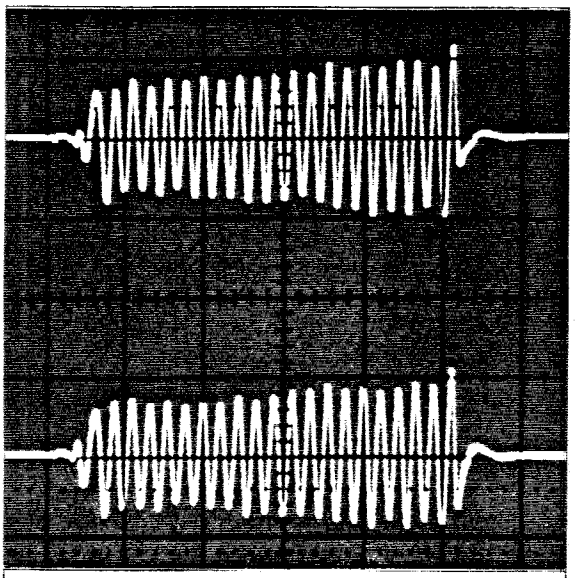

Test Antenna Orientation: 45 deg.
Top: TEST H at .2 v/div.
Bottom: TEST V at .2 v/div.
Time Scale: .2 mS/div.
Mixers terminated with 6 dB pads

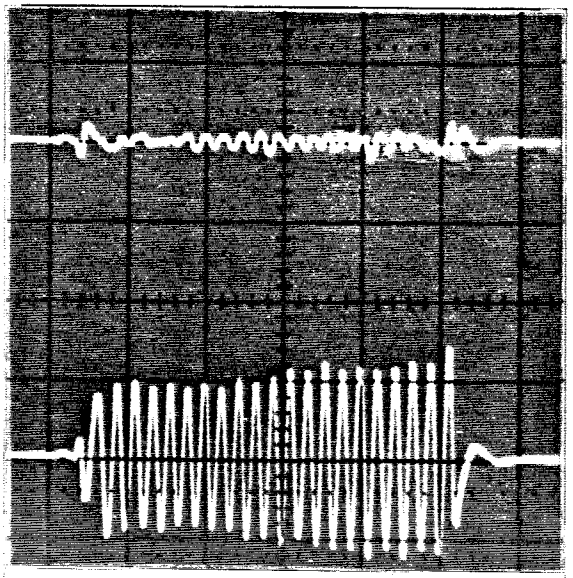

Test Antenna Orientation: 90 deg.
Top: TEST H at .2 v/div.
Bottom: TEST V at .2 v/div.
Time Scale: .2 mS/div.
Mixers terminated with 6 dB pads

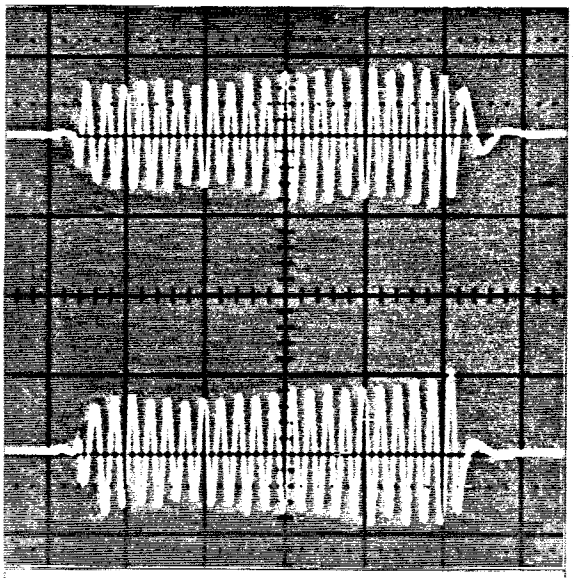

Test Antenna Orientation:135 deg.
Top: TEST H at .2 v/div.
Bottom: TEST V at .2 v/div.
Time Scale: .2 mS/div.
Mixers terminated with 6 dB pads

Figure 5-8: TEST H and TEST V Traces for Linearly Polarized Signals

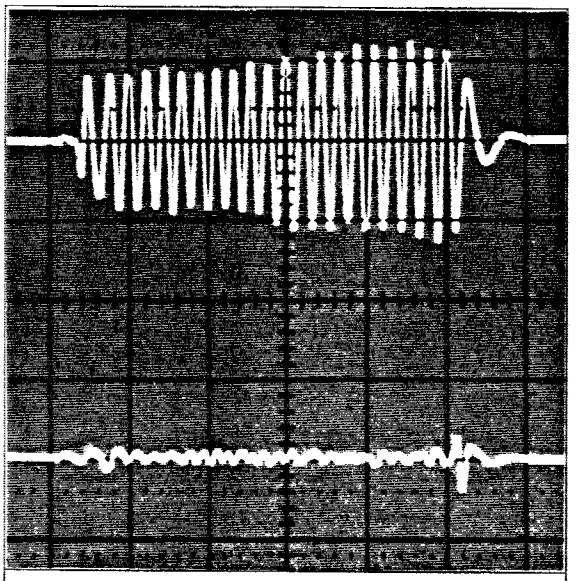

Test Antenna Orientation:180 deg.
Top: TEST H at .2 v/div.
Bottom: TEST V at .2 v/div.
Time Scale: .2 mS/div.
Mixers terminated with 6 dB pads

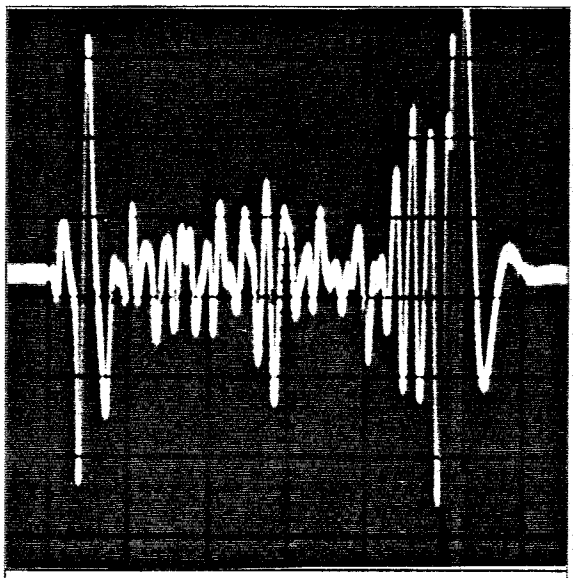

Test Antenna Orientation:135 deg.
Trace: TEST H + TEST V
Scale: .02 v/div.
Time Scale: .2 mS/div.
Mixers terminated with 6 dB pads

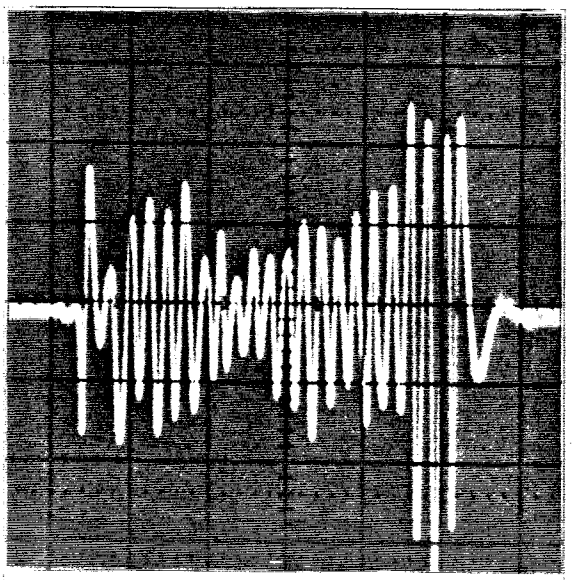

Test Antenna Orientation:225 deg.
Trace: TEST H - TEST V
Scale: .02 v/div.
Time Scale: .2 mS/div.
Mixers terminated with 6 dB pads

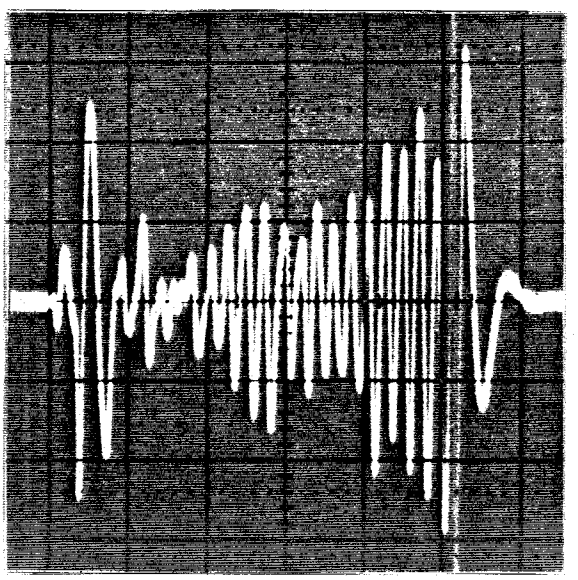

Test Antenna Orientation:315 deg.
Trace: TEST H + TEST V
Scale: .02 v/div.
Time Scale: .2 mS/div.
Mixers terminated with 6 dB pads

Figure 5-9: TEST H and TEST V Traces for Linearly Polarized Signals

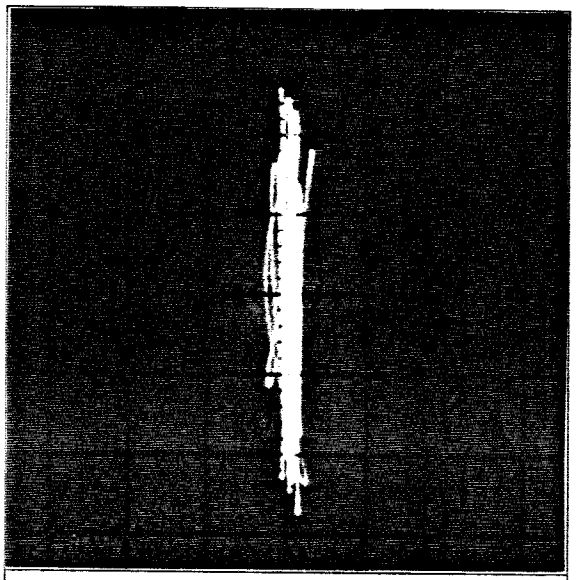

Test Antenna Orientation: 0 deg.
X-Y Plot
H: TEST V at .1 v/div.
V: TEST H at .1 v/div.

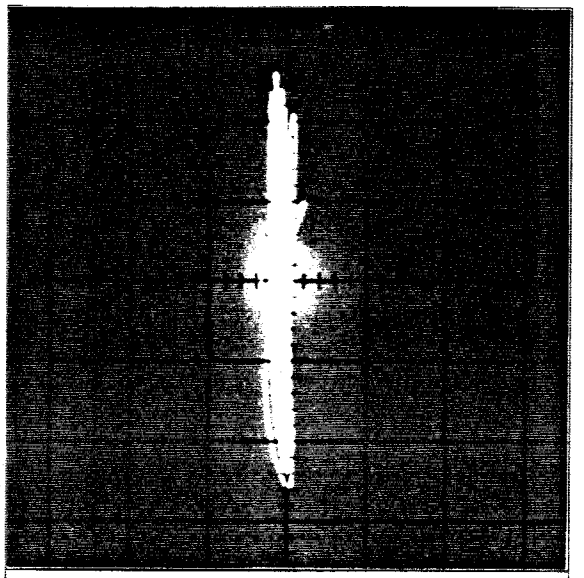

Test Antenna Orientation: 180 deg.
X-Y Plot
H: TEST V at .1 v/div.
V: TEST H at .1 v/div.

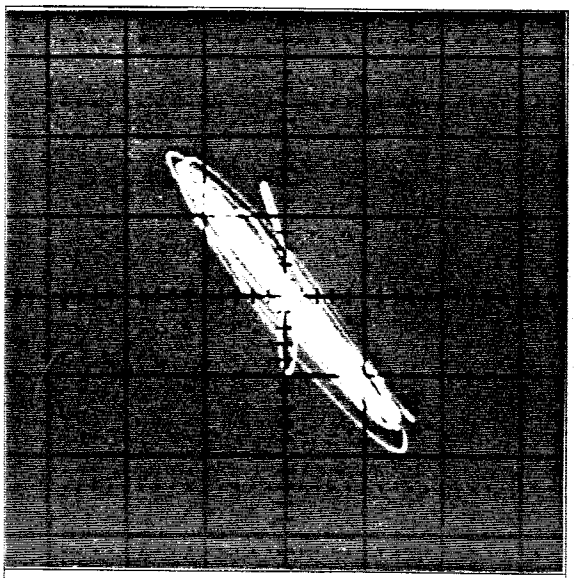

Test Antenna Orientation:215 deg.
X-Y Plot
H: TEST V at .1 v/div.
V: TEST H at .1 v/div.

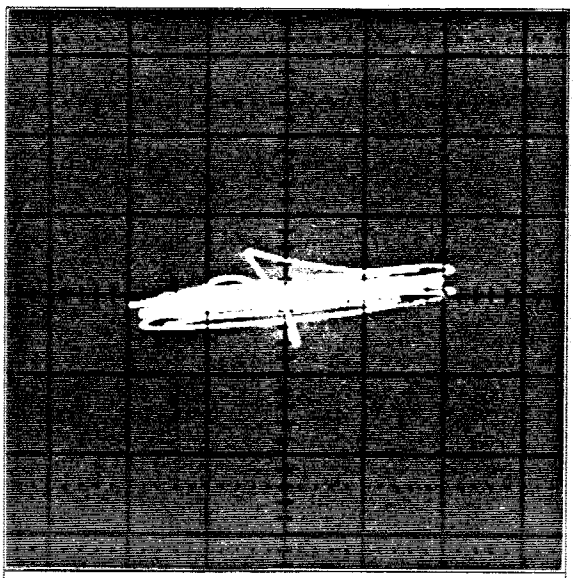

Test Antenna Orientation:270 deg.
X-Y Plot
H: TEST V at .1 v/div.
V: TEST H at .1 v/div.

Figure 5-10: X-Y Plots of Linearly Polarized Signals

5.2.3.3. Tests Using An Elliptically Polarized Transmitting Antenna

To verify that the polarimeter would give a correct indication of circularly polarized components a helical antenna was constructed [20]. The polarization pattern for this antenna was measured in the lab using a network analyzer to generate and measure power, a linear horn as a receiver, and the helical antenna as a transmitter. Results from the characterization of this antenna are given in Appendix D. They show that the helical antenna exhibits an elliptical polarization response with an ellipticity angle of 35.5 degrees. The major axis of its polarization pattern makes an angle of 50 degrees with a reference line drawn on the back of the antenna.

The helical antenna was used as the antenna illuminating the radars in Figure 5-5. Measurements of the IF outputs vs orientation angle of the antenna were again taken and the polarization ratio, ellipticity angle and orientation angle calculated for various orientations. The tabular data from these measurements and calculations is given in Appendix E. Graphical presentations are shown in Figures 5-11 and 5-12.

The plots of the power ratios and polarization ratios show values in excess of one. This is again attributed to the variations in the IF filters as was discussed in section 5.2.3.2.

The calculated values for the ellipticity angle range from -32 to -43 degrees. A cyclical pattern is again observed with respect to the test antenna orientation as would be expected from the multipath interference. The values are however close to the 35.5 degree ellipticity value determined from the antenna characterization of Appendix D.

The polarization pattern of the helical antenna indicated that the orientation of the major axis was 60 degrees. The measured values of the orientation angle indicated by the polarimeter should therefore correspond to the test antenna orientation with a 60 degree offset. Significant variations from these expected values are observed in the plot of Figure 5-12. This is

not surprising since the polarization ellipse is very close to a circle. Small levels of additive linear polarization with the correct orientation angle will be sufficient to swing the major axis of the ellipse over large angles. Multipath is again considered to be the culprit.

Pictures of X-Y oscilloscope traces were also taken of the signals from the helical antenna. They are shown in Figure 5-13. They show that the polarization ellipse is not clean, but varies considerably from cycle to cycle. This is in part due to the fact that the IF signals are blanked during the downsweep portion of the modulating cycle. The transient response of the test filters will not allow instananeous changes in the test outputs, so when the signal is blanked, the oscilloscope trace will spiral in toward the origin. Similarly, when the signal is again allowed to pass, the trace will spiral out to the location of the steady state ellipse. The traces quite clearly show the elliptical nature of the polarization state, and also indicate that the ellipse is quite close to being circular.

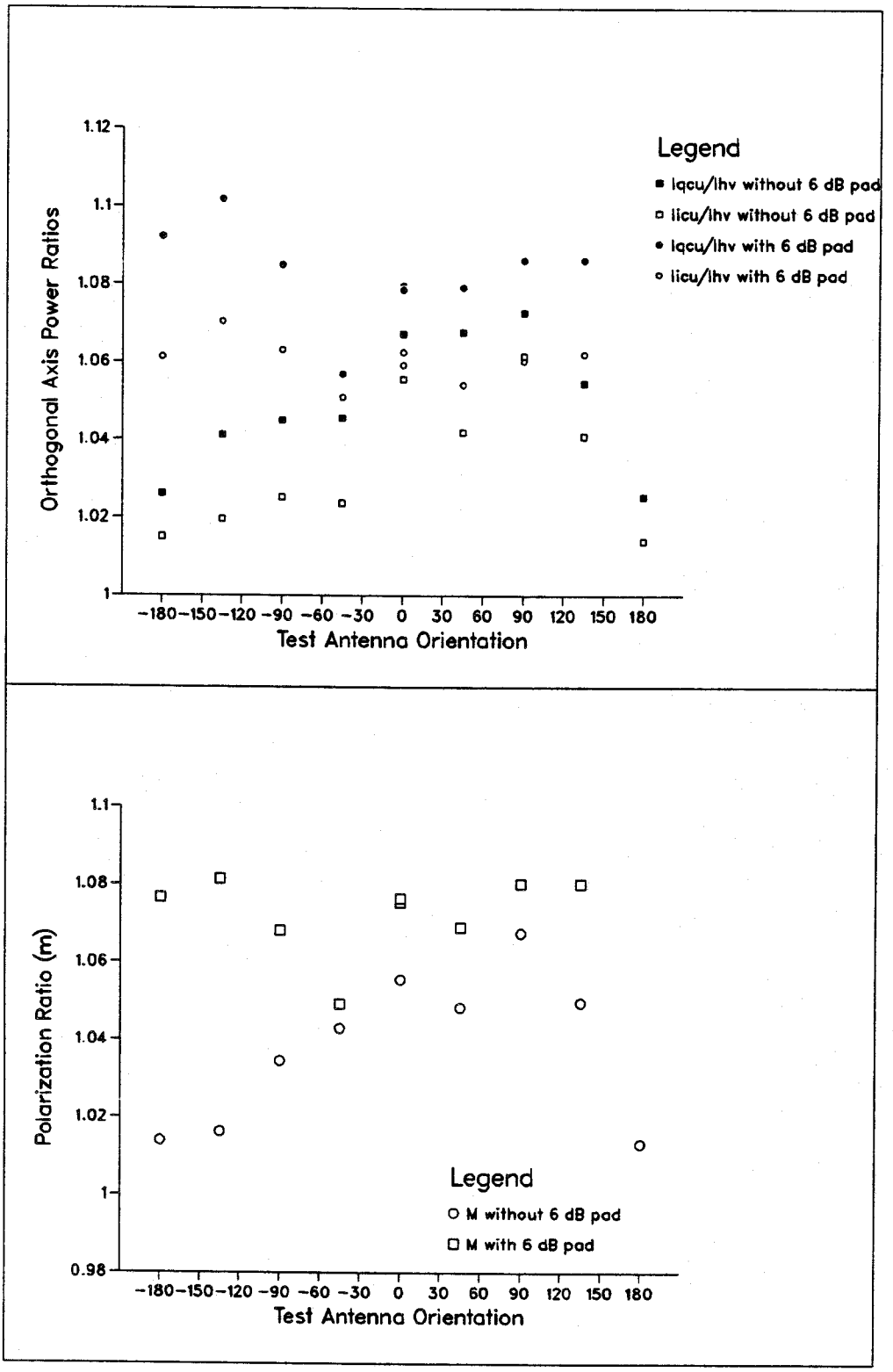

Figure 5-11: Results of Tests Using Helical Antenna

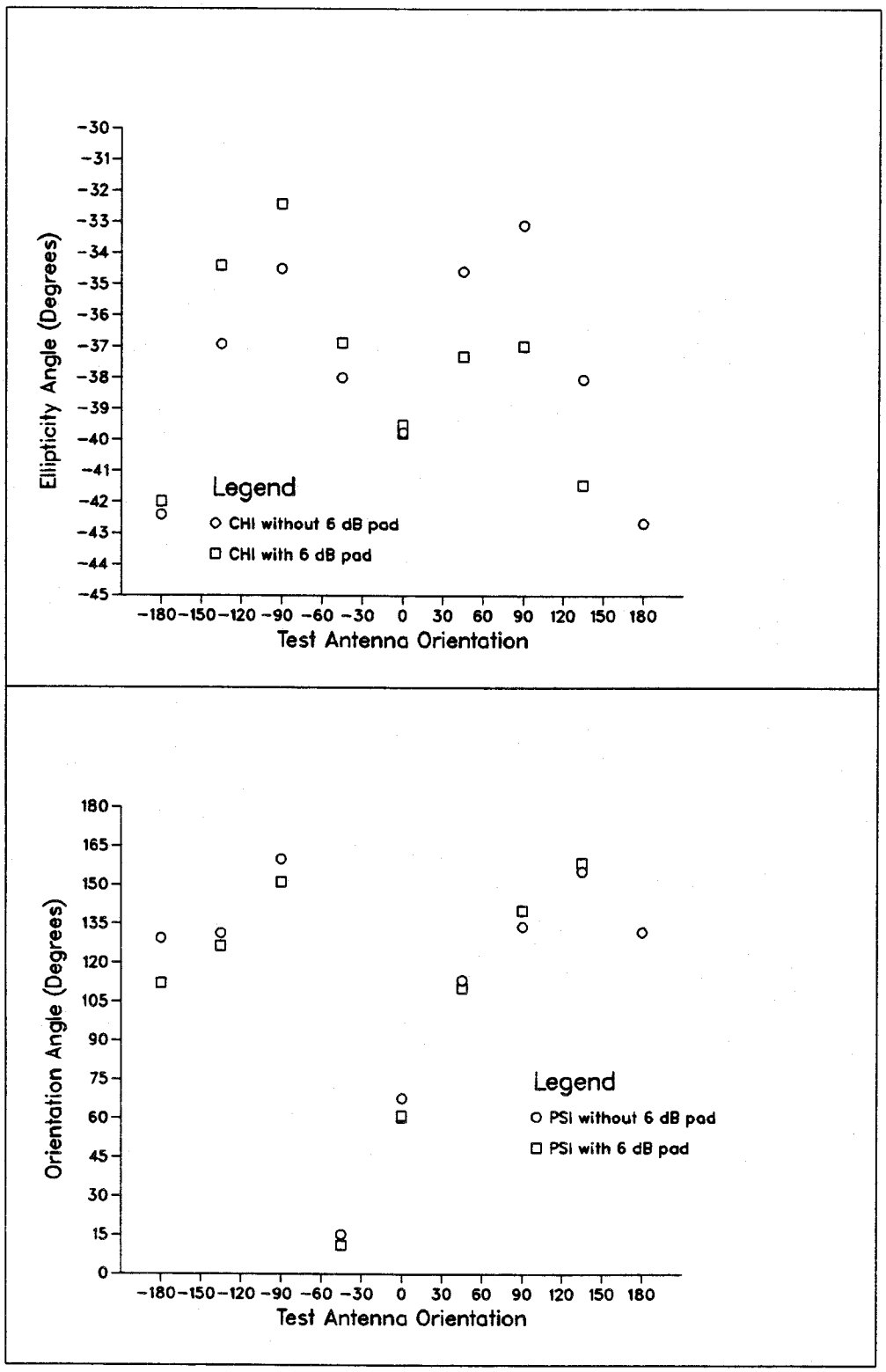

Figure 5-12: Results of Tests Using Helical Antenna

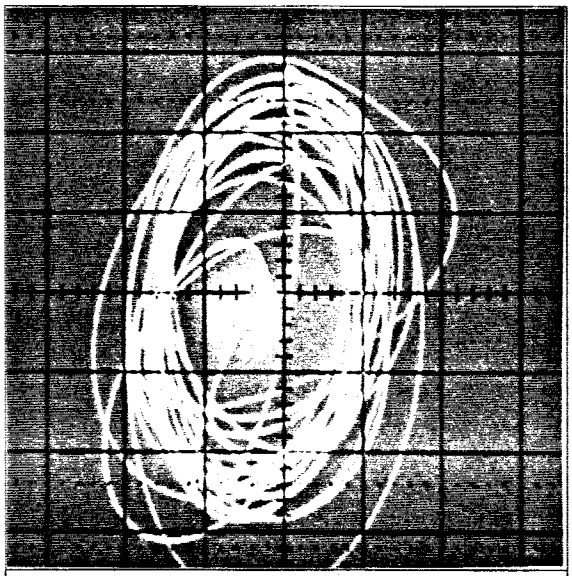

Test Antenna Orientation:-60 deg.
X-Y Plot
H: TEST V at .1 v/div.
V: TEST H at .1 v/div.

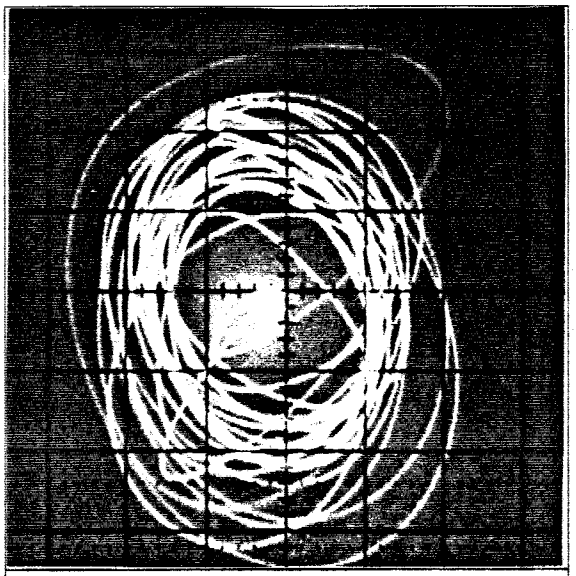

Test Antenna Orientation: 0 deg.
X-Y Plot
H: TEST V at .1 v/div.
V: TEST H at .1 v/div.

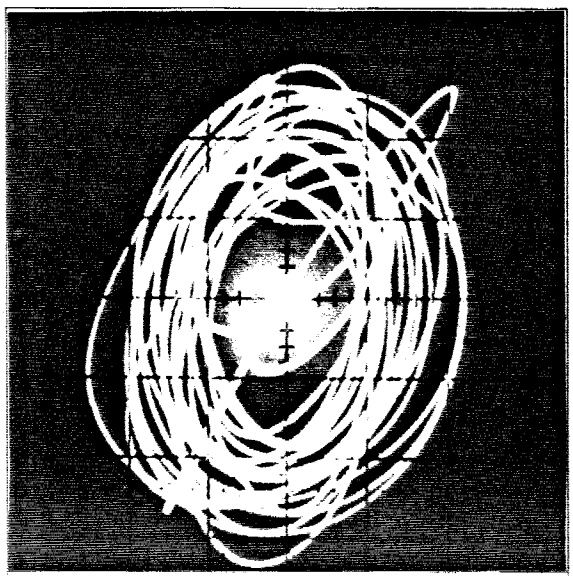

Test Antenna Orientation: 90 deg.
X-Y Plot
H: TEST V at .1 v/div.
V: TEST H at .1 v/div.

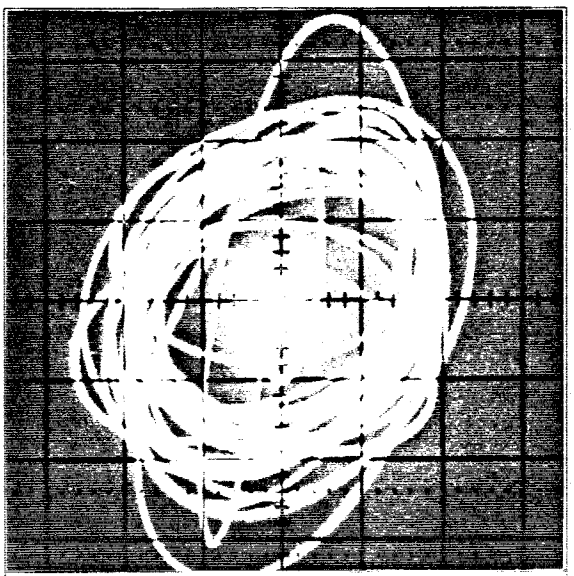

Test Antenna Orientation:225 deg.
X-Y Plot
H: TEST V at .1 v/div.
V: TEST H at .1 v/div.

Figure 5-13: X-Y Plots of Elliptically Polarized Signals

5.2.4. Field Tests of the Completed Polarimeter

After the tests described in the previous sections had been carried out, the radar transceivers were mounted at the end of a boom on the truck and the unit taken to the field. The radars were used to illuminate both an active radar calibrator (ARC) and a trihedral corner reflector, and the polarimetry circuits were used to measure the returning signals. While the radars were illuminating the corner reflector, both the time waveforms and the spectra of the received signals were recorded. As a final field test, the radars were pointed at the sky and the voltages caused by internal reflections were recorded.

The active radar calibrator was supplied by Applied Microwave Corp. It consists of a pyramidal receiving horn antenna, a *K*-band amplifier, an adjustable attenuator and a pyramidal transmitting horn. Signals intercepted by the receiving horn are amplified, attenuated and retransmitted by the transmitting horn. The two antennas are pointed in the same direction. Received signals are therefore retransmitted back towards their source. The antennas are oriented with the E plane axis making a 45 degree angle from the vertical. They will thus receive either vertically or horizontally polarized radiation, but will always transmit linearly polarized signals with the electric field vector at 135 degrees from the horizontal. Schematic diagrams and calibration details for the ARC are given with the scatterometer documentation [21].

The *K*-band active radar calibrator was placed on the ground approximatedly 10 meters from the radars and the *K*-band radar was oriented towards it. A spirit level was used to ensure that the ARC was as level as possible. After adjustments of both the ARC and radar to maximize the power returned, measurements were taken and the polarimetry data examined. The line stretcher in the radar was adjusted such that the orientation angle read by the radar was as close as possible to -45 degrees and the ellipticity angle as close as possible to zero degrees. Another set of

measurements was then taken and recorded.

The results of the recorded measurements are given in Table 5-2 for the case of horizontally polarized illuminating radiation, and in Table 5-3 for vertically polarized illumination. The tables together show the results of ten trials. Each trial represents the results of a single set of the six IF processor output voltage measurements. The trials were carried out sequentially with no adjustments between them. The averages shown for the individual IF processor outputs were derived by calculating the average power of the individual outputs across the number of trials, then taking the square root. The remaining entries in the average column are then calculated from the individual output averages.

The results show good consistency between trials, and indicate that the measured orientation angles (psi) lie within ± 1 degree of the ideal value of -45 degrees. The measured ellipticity (chi) values indicate that the received radiation is very close to being linearly polarized, which would be indicated by an ellipticity of zero degrees. Some variability is seen in the power ratios (I_{icu}/I_{hv} and I_{qcu}/I_{hv}) and the polarization ratios (m) as a result of the IF filter mismatches, but is not as severe as was seen in the tests of sections 5.2.3.2 and 5.2.3.3.

Following the tests using the active radar calibrators, the *K*-band radar transceiver was pointed at a trihedral corner reflector [22]. The reflector was mounted on a tower constructed from ABS plastic pipe to minimize background reflections. Another set of measurements was then taken and recorded for both vertically and horizontally polarized illuminating signals. The results are given in Tables 5-4 and 5-5. The averages shown are again obtained as described in the previous paragraph.

The corner reflector will return incident radiation without changing its polarization. The signals received by the transceiver should thus have an orientation angle of 90 degrees when a vertically polarized illuminating signal

Table 5-2: Field Test Data Using *K*-Band ARC, Horizontal Transmit Polarity

TESTS OF *K*-BAND POLARIMETER USING ACTIVE RADAR CALIBRATOR

Trial #	1	2	3	4	5
Tx Pol.	H	H	H	H	H
Tx Power	-0.501	-0.501	-0.501	-0.501	-0.501
H (volts)	-1.846	-1.871	-1.837	-1.838	-1.834
V (volts)	-1.867	-1.921	-1.885	-1.821	-1.884
Dq(volts)	-2.625	-2.657	-2.626	-2.634	-2.625
Sq(volts)	-2.510	-2.528	-2.572	-2.526	-2.522
Di(volts)	-0.243	-0.255	-0.238	-0.244	-0.245
Si(volts)	-3.620	-3.678	-3.686	-3.595	-3.664
M	0.947	0.938	0.977	0.962	0.968
PSI (deg)	-45.342	-45.807	-45.756	-44.723	-45.797
CHI (deg)	1.296	1.422	0.594	1.240	1.135
Iqcu/Ihv	0.957	0.935	0.975	0.995	0.958
Iicu/Ihv	0.955	0.945	0.985	0.970	0.975

Trial #	6	7	8	9	10	AVG H
Tx Pol.	H	H	H	H	H	
Tx Power	-0.501	-0.501	-0.501	-0.501	-0.501	-0.501
H (volts)	-1.871	-1.840	-1.817	-1.838	-1.827	-1.842
V (volts)	-1.920	-1.884	-1.857	-1.861	-1.825	-1.873
Dq (volts)	-2.655	-2.619	-2.666	-2.634	-2.646	-2.639
Sq (volts)	-2.529	-2.513	-2.563	-2.494	-2.516	-2.527
Di (volts)	-0.249	-0.237	-0.257	-0.245	-0.245	-0.246
Si (volts)	-3.684	-3.595	-3.680	-3.606	-3.645	-3.645
M	0.941	0.929	0.999	0.947	0.993	0.960
PSI (deg)	-45.788	-45.729	-45.625	-45.377	-44.968	-45.491
CHI (deg)	1.383	1.210	1.144	1.587	1.452	1.246
Iqcu/Ihv	0.935	0.950	1.013	0.962	1.000	0.968
Iicu/Ihv	0.949	0.936	1.008	0.955	1.001	0.968

NOTE: AVERAGES ARE POWER AVERAGES

DATA IS FROM FILE 4C890I00 OF JUNE 5,1987

Table 5-3: Field Test Data Using *K*-Band ARC, Vertical Transmit Polarity

Trial #	1	2	3	4	5
Tx Pol.	V	V	V	V	V
Tx Power	-0.501	-0.501	-0.501	-0.501	-0.501
H (volts)	-1.804	-1.807	-1.813	-1.833	-1.805
V (volts)	-1.810	-1.810	-1.804	-1.831	-1.788
Dq (volts)	-2.530	-2.555	-2.527	-2.626	-2.569
Sq (volts)	-2.479	-2.539	-2.523	-2.566	-2.505
Di (volts)	-0.226	-0.224	-0.219	-0.230	-0.231
Si (volts)	-3.587	-3.575	-3.543	-3.714	-3.581
M	0.981	0.973	0.956	1.024	0.990
PSI (deg)	-45.097	-45.049	-44.851	-44.969	-44.726
CHI (deg)	0.571	0.183	0.046	0.649	0.728
Iqcu/Ihv	0.961	0.992	0.975	1.004	0.997
Iicu/Ihv	0.989	0.981	0.963	1.031	0.997

Trial #	6	7	8	9	10	AVG V
Tx Pol.	V	V	V	V	V	
Tx Power	-0.501	-0.501	-0.501	-0.501	-0.501	-0.501
H (volts)	-1.797	-1.834	-1.808	-1.801	-1.803	-1.811
V (volts)	-1.773	-1.832	-1.813	-1.804	-1.782	-1.805
Dq (volts)	-2.555	-2.585	-2.548	-2.576	-2.569	-2.564
Sq (volts)	-2.559	-2.538	-2.537	-2.581	-2.528	-2.536
Di (volts)	-0.241	-0.220	-0.226	-0.248	-0.238	-0.230
Si (volts)	-3.610	-3.601	-3.572	-3.623	-3.595	-3.600
M	1.018	0.961	0.969	1.005	1.001	0.988
PSI (deg)	-44.622	-44.967	-45.082	-45.047	-44.665	-44.908
CHI (deg)	-0.045	0.534	0.126	-0.057	0.465	0.320
Iqcu/Ihv	1.026	0.976	0.986	1.023	1.011	0.995
Iicu/Ihv	1.027	0.968	0.977	1.015	1.010	0.996

NOTE: AVERAGES ARE POWER AVERAGES

DATA IS FROM FILE 4C890I00 OF JUNE 5,1987

is used, and either 0 or 180 degrees if the illuminating radiation is horizontally polarized. The tables show a deviation of less than two degrees from these expected values. The measured ellipticity angles are also within two degrees of the expected value of zero degrees for linearly polarized radiation.

The waveforms recorded while the *K*-band transceiver was illuminating the corner reflector are shown in Figures 5-14 and 5-15. The signals were recorded at the P1-5 points on the schematics of pages 75 to 79. They show both that there is a significant slope to the signals across the width of an RF sweep and that the transient responses of the filters are not significantly different (the filter decay times are quite similar).

The spectra measured at the P1-5 points on the horizontal and vertical IF processor cards are shown in Figure 5-16. These spectra again result from the signals returned from the *C*-band corner reflector. Some asymmetry is present about the peak of the response. The peak response is also offset somewhat from the desired value of 22 KHz.

The results from the measurements of the voltages caused by internal reflections are shown in Table 5-6. These voltages correspond to the values measured at the outputs of the *K*-band IF processor cards when the transceiver antenna is pointing at the sky, and the modulation frequency is set to the value corresponding to a range of 9.5 meters.

Table 5-4: Field Test Data Using *C*-Band Corner Reflector, Vertical Transmit Polarity

Trial #	1	2	3	4	5
Tx Pol.	V	V	V	V	V
Tx Power	-0.508	-0.508	-0.508	-0.508	-0.508
H (volts)	-0.175	-0.175	-0.175	-0.175	-0.175
V (volts)	-4.683	-4.683	-4.683	-4.683	-4.684
Dq (volts)	-5.201	-5.202	-5.201	-5.200	-5.199
Sq (volts)	-4.950	-4.951	-4.948	-4.949	-4.948
Di (volts)	-5.128	-5.128	-5.128	-5.127	-5.126
Si (volts)	-4.912	-4.911	-4.910	-4.911	-4.908
M	1.000	1.000	1.000	1.000	1.000
PSI (deg)	88.583	88.576	88.570	88.583	88.571
CHI (deg)	1.663	1.663	1.675	1.662	1.661
Iqcu/Ihv	1.174	1.174	1.173	1.173	1.172
Iicu/Ihv	1.148	1.148	1.148	1.148	1.146

Trial #	6	7	8	9	10	AVG V
Tx Pol.	V	V	V	V	V	
Tx Power	-0.508	-0.508	-0.508	-0.508	-0.508	-0.508
H (volts)	-0.175	-0.175	-0.175	-0.175	-0.175	-0.175
V (volts)	-4.683	-4.682	-4.682	-4.683	-4.684	-4.683
Dq (volts)	-5.199	-5.199	-5.201	-5.200	-5.203	-5.201
Sq (volts)	-4.948	-4.948	-4.950	-4.949	-4.950	-4.949
Di (volts)	-5.126	-5.125	-5.129	-5.125	-5.127	-5.127
Si (volts)	-4.910	-4.908	-4.912	-4.909	-4.910	-4.910
M	1.000	1.000	1.000	1.000	1.000	1.000
PSI (deg)	88.583	88.577	88.575	88.584	88.577	88.578
CHI (deg)	1.662	1.663	1.663	1.662	1.675	1.665
Iqcu/Ihv	1.173	1.173	1.174	1.173	1.174	1.173
Iicu/Ihv	1.147	1.147	1.149	1.147	1.147	1.147

NOTE: AVERAGES ARE POWER AVERAGES

DATA IS FROM FILE 4F790K00 OF JUNE 8,1987

Table 5-5: Field Test Data Using *C*-Band Corner Reflector, Horizontal Transmit Polarity

TESTS OF *K*-BAND POLARIMETER USING *C*-BAND CORNER REFLECTOR

Trial #	1	2	3	4	5
Tx Pol.	H	H	H	H	H
Tx Power	-0.508	-0.508	-0.508	-0.508	-0.508
H (volts)	-4.987	-4.989	-4.989	-4.989	-4.990
V (volts)	-0.167	-0.168	-0.168	-0.168	-0.168
Dq (volts)	-5.072	-5.070	-5.069	-5.070	-5.069
Sq (volts)	-5.393	-5.395	-5.392	-5.393	-5.393
Di (volts)	-5.265	-5.265	-5.265	-5.264	-5.264
Si (volts)	-5.141	-5.140	-5.140	-5.140	-5.139
M	1.000	1.000	1.000	1.000	1.000
PSI (deg)	0.744	0.749	0.749	0.743	0.749
CHI (deg)	-1.933	-1.956	-1.943	-1.943	-1.948
Iqcu/Ihv	1.101	1.100	1.099	1.099	1.099
Iicu/Ihv	1.087	1.086	1.086	1.086	1.085

Trial #	6	7	8	9	10	AVG H
Tx Pol.	H	H	H	H	H	
Tx Power	-0.508	-0.508	-0.508	-0.508	-0.508	-0.508
H (volts)	-4.990	-4.992	-4.993	-4.991	-4.992	-4.990
V (volts)	-0.168	-0.168	-0.168	-0.168	-0.167	-0.168
Dq (volts)	-5.069	-5.069	-5.068	-5.069	-5.068	-5.069
Sq (volts)	-5.392	-5.391	-5.391	-5.391	-5.390	-5.392
Di (volts)	-5.264	-5.264	-5.264	-5.264	-5.264	-5.264
Si (volts)	-5.141	-5.139	-5.140	-5.138	-5.139	-5.140
M	1.000	1.000	1.000	1.000	1.000	1.000
PSI (deg)	0.737	0.748	0.742	0.754	0.748	0.746
CHI (deg)	-1.942	-1.935	-1.940	-1.935	-1.934	-1.941
Iqcu/Ihv	1.099	1.097	1.097	1.098	1.097	1.099
Iicu/Ihv	1.086	1.085	1.084	1.085	1.085	1.086

NOTE: AVERAGES ARE POWER AVERAGES

DATA IS FROM FILE 4F790K00 OF JUNE 8,1987

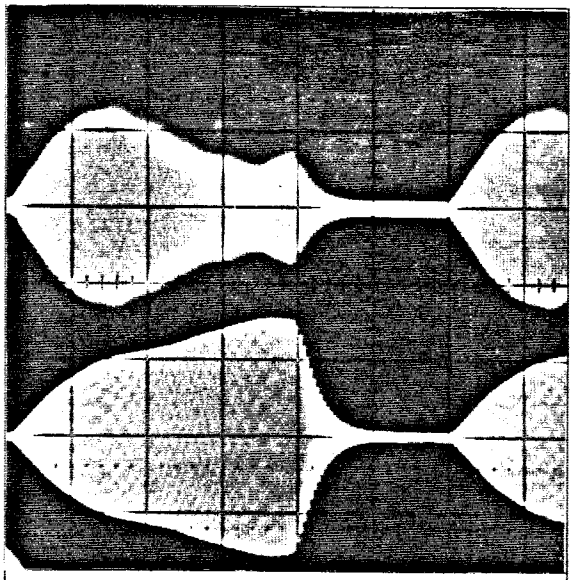

Corner Reflector Returns
Top: Flout V, .2 v/div.
Bottom:Flout H, 5 v/div.
Time Scale: 1 mS/div.
Tx Polarization: Horizontal

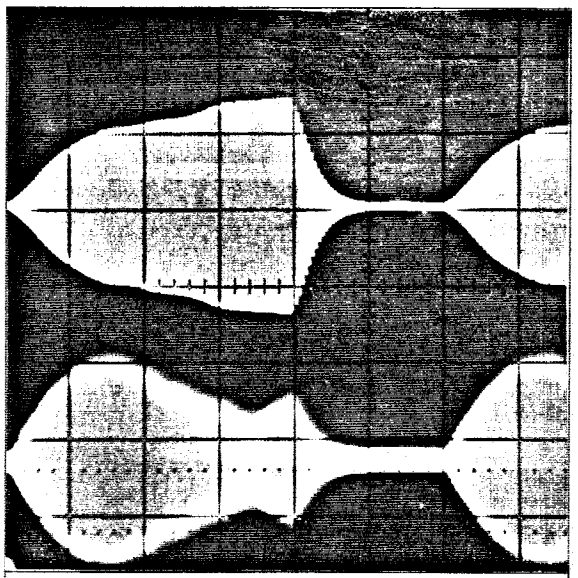

Corner Reflector Returns
Top: Flout V, 5 v/div.
Bottom:Flout H, .2 v/div.
Time Scale: 1 mS/div.
Tx Polarization: Vertical

Figure 5-14: Traces of Corner Reflector Returns

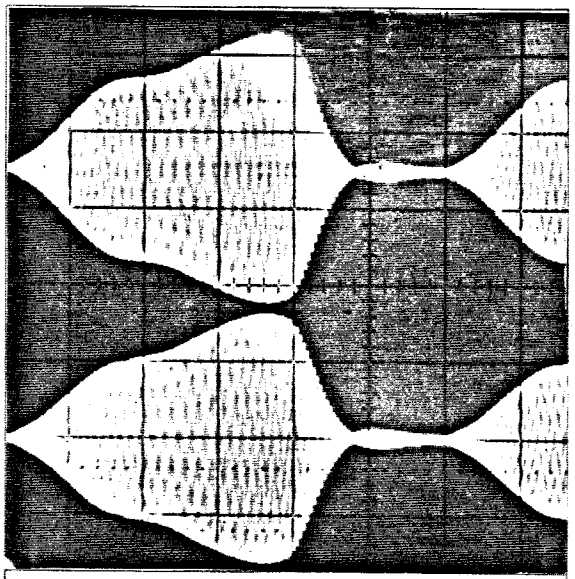

Corner Reflector Returns
Top: Flout A, 5 v/div.
Bottom:Flout B, 5 v/div.
Time Scale: 1 mS/div.
Tx Polarization: Horizontal

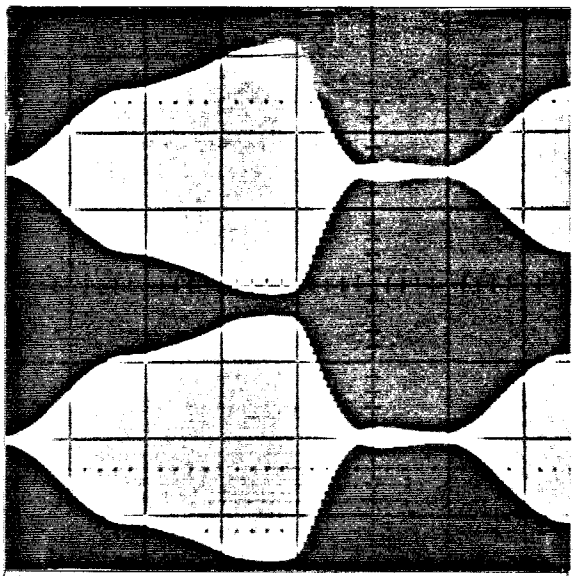

Corner Reflector Returns
Top: Flout A, 5 v/div.
Bottom:Flout B, 5 v/div.
Time Scale: 1 mS/div.
Tx Polarization: Vertical

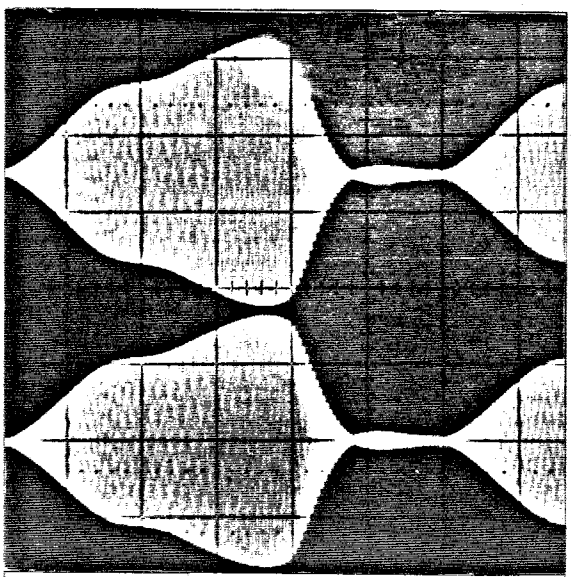

Corner Reflector Returns
Top: Flout C, 5 v/div.
Bottom:Flout D, 5 v/div.
Time Scale: 1 mS/div.
Tx Polarization: Horizontal

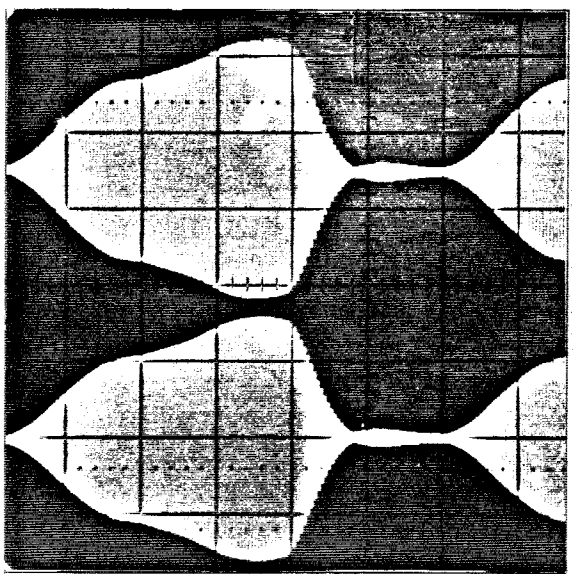

Corner Reflector Returns
Top: Flout C, 5 v/div.
Bottom:Flout D, 5 v/div.
Time Scale: 1 mS/div.
Tx Polarization: Vertical

Figure 5-15: Traces of Corner Reflector Returns

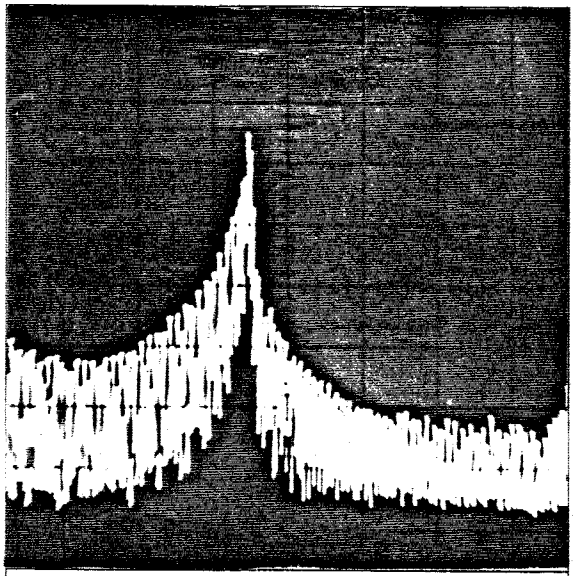

Corner Reflector Spectrum
at P1-5 on Board H
Center line is 25 KHz.
5 KHz./Div., 10 dB/Div.
Tx Polarization: Horizontal

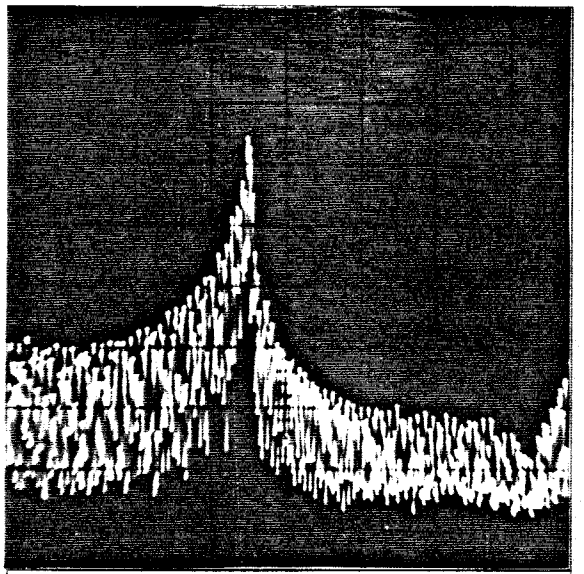

Corner Reflector Spectrum
at P1-5 on Board V
Center line is 25 KHz.
5 KHz./Div., 10 dB/Div.
Tx Polarization: Vertical

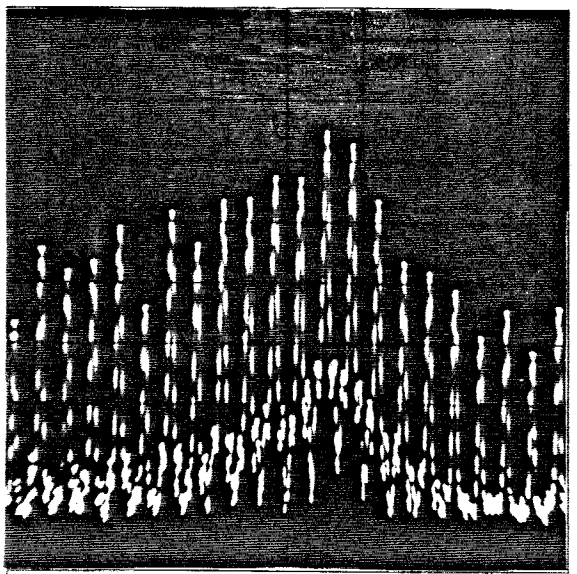

Corner Reflector Spectrum
at P1-5 on Board H
Center line is 22 KHz.
500 Hz./Div., 10 dB/Div.
Tx Polarization: Horizontal

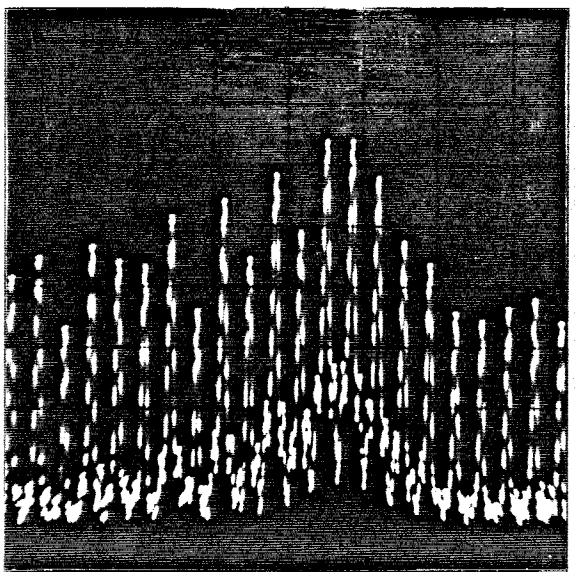

Corner Reflector Spectrum
at P1-5 on Board V
Center line is 22 KHz.
500 Hz./Div., 10 dB/Div.
Tx Polarization: Vertical

Figure 5-16: Spectra of Corner Reflector Returns

Table 5-6: IF Outputs due to Internal Reflections

Transmit Polarization	H (volts)	V (volts)	Si (volts)	Di (volts)	Sq (volts)	Dq (volts)
Horizontal	.013	.001	.018	.013	.016	.015
Vertical	.004	.008	.014	.009	.012	.010

Data is from file 4C990T00.RW2 of June 5, 1987

5.3. External Calibration

5.3.1. Theoretical Considerations

External calibration relies on the use of an external target with a known scattering cross section to allow determination of the system gain constants. The radar equation for a monostatic radar was given previously (equation (3.5) on page 28) as:

$$P_r = \frac{\lambda^2}{(4\pi)^3} \frac{P_t G^2}{R^4} \sigma$$

where the antenna gain G corresponds to some fixed azimuth and elevation angles representing the relative positions of the radar antenna and the target. For these fixed angles, and in particular if both azimuth and elevation are zero degrees (on boresight) the equation can be rewritten as:

$$P_r = \frac{P_t K}{R^4} \sigma \tag{5.2}$$

Should sigma be known, as in the case of a calibration target, measurements of P_r, P_t and R will be sufficient to determine the system gain constant K. Some discussion is required regarding each of these parameters.

5.3.2. Measurement of Transmit Power

The microwave scatterometer measures the transmit power using a power detector connected to one of the ports of the power splitter at the output of the YIG oscillator (see Figure 3-5 on page 43). Before reaching the antenna the signal must pass through the transmit relay, one of the H or V circulators, and the orthomode transducer. Losses in these components are therefore not accounted for in the measured transmit power. Furthermore, the power detector output must itself be multiplied by a constant before indicating absolute power. All of these factors may be taken into account by

using the measured transmit power as the value for P_t in equation (5.2) while letting the gain constant K absorb the losses mentioned above.

Differences in the gain factors between the possible combinations of transmitted polarization and receiving channel can be handled by defining a separate gain constant for each of the transmit/receive combinations. The system gain constant corresponding to the case using horizontally polarized transmitted signals and the vertically polarized receiving channel would then be designated as K_{hv} with similar definitions for K_{hh}, K_{vh} and K_{vv}.

5.3.3. Measurement of Received Power

When a calibration target of known cross section is illuminated by the scatterometer, the receiver will measure backscatter from the background in addition to the backscatter from the target. Returns from the target and background can add in phase, out of phase or somewhere in between, depending on the relative configurations of target to background and the range to each. Mathematically, if $\mathbf{V}_t$ is a phasor representing the voltage induced at the terminals of a linearly polarized antenna due to backscatter from a target, and $\mathbf{V}_b$ a phasor representing the voltage induced by the background, the resultant voltage measured at the antenna terminals ($\mathbf{V}_m$) will be:

$$\mathbf{V}_m = \mathbf{V}_t + \mathbf{V}_b.$$

The peak value of the resultant will be given by

$$V_m = \sqrt{V_t^2 + V_b^2 + 2V_t V_b \cos\phi}$$

where V_m is the magnitude of the phasor $\mathbf{V}_m$, V_t is the magnitude of the phasor $\mathbf{V}_t$, V_b is the magnitude of the phasor $\mathbf{V}_b$, and where ϕ is the phase angle between $\mathbf{V}_t$ and $\mathbf{V}_b$. Since ϕ can be any value, it can be seen that the measured value of V_m can differ from V_t by as much as $\pm V_b$.

Translating this to a power indication results in the following bounds for an indication of the power received due to the target:

$$P_t = \frac{V_t^2}{2}$$

$$P_{t\,max} = \frac{(V_m + V_b)^2}{2} \tag{5.3}$$

$$P_{t\,min} = \frac{(V_m - V_b)^2}{2}. \tag{5.4}$$

This inaccuracy in the measurement of received power from the calibration target implies that the gain constant K determined using the received power measurements will have the same inaccuracy. To more precisely determine the constant, a series of measurements can be taken at varying ranges. Different measurements will then correspond to different values of ϕ, allowing a value to be chosen which minimizes the effect of the background radiation.

5.3.3.1. Measurement of the Range to the Target

The development of the radar equation makes use of Frii's transmission formula, which assumes that the free space path loss is given as [23]:

$$L_{FS} = (\frac{4\pi R}{\lambda})^2$$

The dimension R is defined as the distance between a hypothetical isotropic point source radiator and the measurement point. For any real system however, the transmitting/receiving antenna will not be a point source. This causes confusion regarding the point on the antenna to measure the range from (and to). The antennas mounted on the radar use parabolic reflectors. Reflector antennas are typically analyzed by assuming an electric field

distribution across the aperture. The range to the measurement point is then taken to be the center of the aperture. Since this point was also used by the radar manufacturer when calibrating, it will be used as the zero range location.

A second problem is associated with the corner reflector as is illustrated by Figure 5-17.

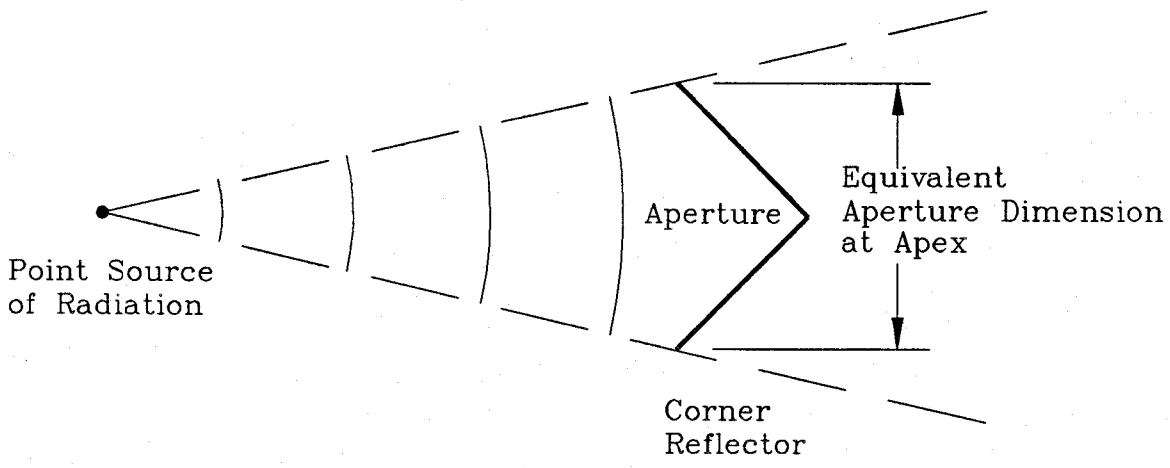

Figure 5-17: Illumination of Corner Reflector by Point Source

Radiation reaching the reflector must travel a distance equal to twice the aperture to apex dimension before emerging through the aperture on the way back to the source. Robertson [22] has claimed that the corner reflector can be replaced with a flat plate located at the apex of the corner reflector and having the same effective area as the corner reflector. This would seem to be born out by considering the length of travel for the wavefront, but as can be seen from Figure 5-17, a flat plate with the same effective area as the corner reflector and placed at the apex would intercept less radiation due to the increased distance from the source, and hence would reflect a smaller amount of power. At ranges large compared to the depth of the corner reflector this

effect would be small, but for ground based systems with shorter ranges it can be appreciable. If a calibration was carried out at a range of 15 meters and using an *L*-band corner reflector with a depth of .46 meters, the discrepancy in received power would amount to 12.7 percent.

Since as Robertson has shown, any ray entering the aperture and within the effective area of the reflector will be returned to the source, the depth of the reflector will be immaterial insofar as attenuation measurements are concerned, and the range should be measured to the aperture of the corner reflector instead of the apex.

The calibrations undertaken in this chapter therefore measure the range from the aperture of the transmitting antenna to the aperture of the corner reflector (i.e. the front face of the reflector).

5.3.3.2. Corner Reflector Cross Sections

When calibrating externally, it is necessary to know the cross section of the target being measured if the calibration constants are to be determined. Any error in the assumed cross section of the target will translate directly into an error in the calibration constant.

The radar cross sections of corner reflectors have been studied by Robertson. He has shown that for a trihedral corner reflector, the radar cross section can be calculated theoretically as:

$$\sigma = \frac{4\pi}{\lambda^2} A^2_{eff} \tag{5.5}$$

where A_{eff} is the effective area of the reflector and λ is the wavelength of the incident radiation, and where the corner reflector face is perpendicular to the transmitting source. Brown, Newman and Crispin [24] show that the effective area for the trihedral corner reflector can be described as:

$$A_{eff} \approx (\frac{1}{\sqrt{3}})\,(1-0.00076\,\delta^2)b^2; \qquad \text{for small } \delta \quad (5.6)$$

where δ is the angle in degrees between the corner reflector axis of symmetry and the transmitter, and b is the inner dimension of the corner reflector. Use of these two equations results in the conclusion that the cross section on the axis of symmetry (ie. for δ=0) is given as:

$$\sigma = \frac{\pi\, l^4}{3\lambda^2} \qquad (5.7)$$

where l is the front face dimension of the reflector. In addition, equation (5.6) shows that a five degree pointing error will result in a 3.9% reduction in cross section, while a ten degree error will cause a 17.1% reduction (.69 dB).

Robertson also points out that inaccuracies in the central angles of the corner reflector due to construction variances can significantly affect the cross section. For example, an angular error causing a change in the aperture dimension (l) of .4 wavelengths is sufficient to reduce the cross section by 5 dB. If it is assumed that the corner reflector dimensions are accurate to within 2 mm, it is possible to have an error of up to .083 wavelengths at *K*-band, .034 wavelengths at *C*-band, and .01 wavelengths at *L*-band. Using Robertson's curves, this would result in cross section reductions of approximately .4 dB, .2 dB and .1 dB respectively.

5.3.4. External Calibration Test Results

The calibration tests described in this section were carried out at the Kernen farm, located approximately two miles east of Saskatoon. A calibration tower has been erected on the farm property to facilitate the calibration process. The tower consists of a plywood platform four feet wide by sixteen feet long mounted sixteen feet above the ground. The support

structure for the tower consists of wooden beams held together with lag bolts. Two towers made from ABS plastic pipe are situated at the opposing ends of this platform, each having a four foot by four foot support structure which is six feet high. The ABS towers are capped with four foot square plywood platforms on which the corner reflectors can be mounted with wooden pivot pins. The long side of the tower is oriented in a north-east/ south-west direction.

When calibrating, the radar truck is parked to the south-east of the tower. The radars are positioned with the *K*-band unit approximately four feet above ground level. All radar antennas therefore look well above the horizon when pointing at the corner reflectors, thereby minimizing ground reflections.

Calibration data was taken on two dates, and using two separate corner reflectors. In addition various ranges were used so that the effects of background scatter could be analyzed.

Three different computer programs were used to control the radar circuitry during the course of this testing. The major data gathering was carried out using the MANSCAN4 program, a program written specifically for calibration purposes. This program automatically gathers the data for one scan, consisting of ten individual sets of measurements using first horizontally polarized illuminating radiation, then vertically polarized. OVERHEAD is a program which reads the current center frequency, transmit power and temperature for each of the three radars. The section of this program which reads the center frequencies uses an integrating voltmeter to sample the signal controlling the frequency of the RF oscillator. The average value of this signal is an indication of the radar center frequency. Unfortunately, the integration time of the voltmeter as set by the program is insufficient to completely average out the variations in the sweeping control line, so several OVERHEAD readings were taken and averaged. AUTOPEAK is a program which determines the range that produces the largest measured power in the fourth range cell for a specified radar. The listings and documentation for

these programs are maintained at the Institute for Space and Atmospheric Studies at the University of Saskatchewan.

A detailed explanation of the testing sequence is described in Appendix F. Measurements for all three radar transceivers (*K*, *C*, and *L*-band) were carried out. The results for the *K*-band unit are shown in Table 5-7, while the results for the *C* and *L*-band units are given in Appendix F. Explanations of the row headings and the calculations are given below.

- **Trial Number** is the trial from which the data results. Each scan consists of ten separate trials.

- **Center Freq.** is the center frequency of the selected radar, in GHz. It is calculated using the values measured by the OVERHEAD program and the data supplied with the RF oscillators.

- **Size of Corner Reflector** is the front face dimension (l) of the corner reflector being used. The *C*-band corner reflector has an l of .714m, while the *L*-band corner reflector has an l of 1.117m.

- **Sigma of Corner Reflector** is the radar cross section of the corner reflector being used. It is calculated from equation (5.7) using the current center frequency and corner reflector size.

- **Tx Power** is the measured transmit power as described in section 5.3.2.

- **Measured Range** is the range as measured from the front face of the corner reflector to the disk at the end of the feed waveguide on the radar antenna.

- **Range Offset** is the dimension from the antenna aperture (ie. the plane touching the front edge of the parabolic antenna) to the disk at the end of the feed waveguide.

- **True Range** is the range from antenna aperture to corner reflector aperture, as discussed in section 5.3.3.1. It is calculated as the **Measured Range** plus the **Range Offset**.

- **Indicated Range** is the value supplied by the AUTOPEAK program as the range for which the maximum received power occurs.

- **Rx HH Voltage** is the voltage measured at the detector output when the radar is both transmitting and receiving with the horizontally polarized antenna.

- **Rx VV Voltage** is the voltage measured at the detector output when the radar is both transmitting and receiving with the vertically polarized antenna.

- **Rx H Background Voltage** is the voltage at the output of the radar's horizontal channel detector when the corner reflector has been removed, but the radar is still looking at the same spot as when the reflector was in place.

- **Rx V Background Voltage** is the voltage at the output of the radar's vertical channel detector when the corner reflector has been removed, but the radar is still looking at the same spot as when the reflector was in place.

- **Kh (max)** is the maximum value for the calibration constant based on the measured values of **Rx HH Voltage, Rx H Background Voltage** , equation (5.3) and equation (5.2).

- **Kh (min)** is the minimum value for the calibration constant based on the measured values of **Rx HH Voltage, Rx H Background Voltage**, equation (5.4) and equation (5.2).

- **Kv (max)** is the maximum value for the calibration constant based on the measured values of **Rx VV Voltage, Rx V Background Voltage**, equation (5.3) and equation (5.2).

- **Kh (min)** is the minimum value for the calibration constant based on the measured values of **Rx VV Voltage, Rx V Background Voltage**, equation (5.4) and equation (5.2).

- **Average Kh** is the average of all values for Kh. It represents the best approximation to the horizontal channel calibration constant.

- **Average Kv** is the average of all values for Kv. It represents the best approximation to the vertical channel calibration constant.

- **Average Khv or Kvh** is the average of all values for Kh and Kv. It is used as the approximate calibration constant for the cross polarized channels.

Several points should be brought out with regard to the data in the tables. On June 16 an incomplete set of tower backscatter measurements was

obtained. Rather than ignore the tower backscatter, estimated values were used based on the backscatter information obtained on July 11. On July 11, on the other hand, OVERHEAD readings were not taken. An examination of the overhead values for June 16 showed only small variations, so values for center frequencies for the July 11 data were estimated from the June 16 data.

Table 5-7: *K*-Band Calibration Test Results

Test Date (1987)	July 11	July 11	June 16	June 16	June 16
Trial Number	1	1	1	1	1
Center Freq. (GHz.)	12.810	12.810	12.810	12.807	12.814
Size of Corner Reflector (m)	0.714	1.117	0.714	0.714	0.714
Sigma of Corner Reflector (m*m)	496.223	2972.330	496.223	495.991	496.533
Tx Power (v)	0.504	0.503	0.503	0.505	0.503
Measured Range (m)	17.500	28.920	17.690	22.100	27.050
Range Offset (m)	0.081	0.081	0.081	0.081	0.081
True Range (m)	17.581	29.001	17.771	22.181	27.131
Indicated Range (m)	17.140	30.400	17.690	22.450	28.270
Rx HH Voltage (v)	-3.329	-2.887	-3.189	-2.024	-1.358
Rx VV voltage (v)	-3.195	-2.903	-3.067	-1.937	-1.313
Rx H Background Voltage (v)	-0.019	-0.023	-0.025	-0.025	-0.025
Rx V Background Voltage (v)	-0.010	-0.017	-0.015	-0.015	-0.015
Kh (max)	4281.9	4006.6	4127.6	4057.4	4149.5
Kh (min)	4185.3	3880.9	4000.1	3861.8	3854.8
Kv (max)	3923.9	4034.2	3795.5	3682.3	3826.0
Kv (min)	3875.1	3940.8	3722.0	3570.0	3655.1
Average Kh	4040.6				
Average Kv	3802.5				
Average Khv or Kvh	3921.5				

Chapter 6

PERFORMANCE EVALUATION

6.1. General

Chapter 4 of this document discussed the extension of the theory of polarization to the FM-CW radar case and presented designs which would allow an FM scatterometer to provide an indication of the polarization state of the radiation backscattered from a target. The testing of those designs was described in Chapter 5 along with some characterizations of the original scatterometer circuitry. An analysis of these results indicates some problem areas which impinge on the ability of the equipment to correctly predict the desired polarization parameters, but which were not discussed in Chapter 4. This chapter discusses those areas and attempts to predict the expected degradations which they will cause. The specific areas to be discussed are the effects of insufficient antenna cross polarization isolation, the effects of residual phase imbalances, the effects of poorly matched IF filters, the effects of improper power measurement, the effects of internally generated interference, and the effects of sampling the channel outputs at different points in time. The chapter concludes with a summary of the important effects regarding the application of these concepts to the field data.

6.2. Cross Polarization Effects

The assumption up to this point has been that the radar antennas are polarized in the vertical and horizontal directions, and that for either polarization state, the antenna's polarization state will be ideal. If, for example, a vertically polarized signal is being transmitted, no component of

the radiated signal will be horizontally polarized, and if a vertically polarized signal is being received, no voltage will be present at the terminals of the horizontally polarized antenna. Practical antennas will allow some of the energy from one polarization state to spill over into the other. This is termed cross polarization [10]. If cross polarized components caused by limitations in the antenna's operation are present either in the radiated field or in the voltages sensed at the antenna terminals the polarization state measured by the equipment will be in error [25]. A discussion of how much error can be attributed to the cross polarization effects is therefore in order.

Measurements of the co-polar (i.e. the same transmit and receive polarizations) and cross-polar (orthogonal transmit and receive polarizations) radiation power patterns for all three of the antennas used in the radar system were undertaken by Applied Microwave Corp. The results were supplied with the documentation for the scatterometer [21]. Reference to these measurements showed that at boresight, a cross polarization isolation in excess of 40 dB can be expected for the *K*-band antenna, but that the isolation can be as low as 24 dB at the beamwidth edge. Since under normal scatterometer operation, the received signals will be due to many scatterers spread throughout the antenna's beamwidth, a value corresponding to the integrated value across the beamwidth is the most appropriate for determining the errors in the measured polarization state. This value was estimated to be 30 dB[12].

Cross polarization effects will manifest themselves both during transmission and reception. The cross polarized components in the transmitted signal will be scattered by the target and be intercepted by the appropriately polarized receiving antenna. If a vertically polarized signal is being transmitted, some of it will be radiated with a horizontal polarization, and if not modified by

---

[12]This value for the integrated cross polarization isolation was determined both from a review of the curves mentioned and a discussion with Dr. D. Brunfeld of Applied Microwave Corp.

the scatterer will return to be received by the horizontally polarized antenna. At the same time, some vertically polarized signals returning from the target will be translated to horizontally polarized radiation and will be received by the same antenna. The combined effect of these two contributions will be considered to be equivalent to the transmission of a perfectly polarized signal, followed by reception by an antenna with a cross polarization isolation of only 27 dB, rather than the 30 dB estimated above.

This situation can now be applied to the measurement apparatus. Linearly polarized radiation incident on the antenna can be represented by its component vectors in the horizontal and vertical directions. Cross polarization effects will translate some of the power in the horizontal axis to the vertical axis and vice versa. The amount of power translated will be a function of the magnitude of the incident radiation and the cross polarization isolation of the antenna. The largest percentage change in an individual component will occur when the magnitude of the incident radiation is zero in that direction, and maximum in the orthogonal direction. Such a case is examined below.

It will be assumed that horizontally polarized radiation is incident on the receiver to produce a sinusiodal voltage at the terminals of the horizontally polarized antenna which can be symbolized by $h(t)$. Cross polarization effects will then cause a voltage $v(t)$ to appear at the terminals of the vertically polarized antenna, the magnitude and phase of which will be dictated by the cross polarization characteristic between the two antennas. In equation form,

$$h(t) = \cos \omega t, \qquad v(t) = a \cos (\omega t + \phi)$$

where a is the square root of the cross polarization isolation and ϕ is an unknown phase. Substitution of these values into eqns (4.7), (4.8) and (4.9) results in:

$$\tan 2\psi = \frac{2a\cos\phi}{1-a^2}$$

$$\sin 2\chi = \frac{2a\sin\phi}{1+a^2}$$

$$m = 1$$

Since the horizontally polarized radiation at the antenna should result in an orientation angle of 0 degrees with an ellipticity of 0 degrees, the solution of these equations using the value of ϕ which maximizes the right hand side will yield the possible measurement error for a given cross polarization isolation. For the isolation of 27 dB estimated above (a=.0447) the error in either the orientation angle or the ellipticity can be up to 2.56 degrees. The measurement of the polarization ratio does not depend on the cross polarization isolation.

6.3. Phase Imbalances

The phase matching described in section 4.4.1 did not completely remove the differential phase shift between the horizontal and vertical receiving channels. The residual component varied over a ± 12 degree range when measured at the inputs to the IF filters. To determine the effect that this residual phase error may have on the validity of the measured polarization parameters, a simple case will be analysed.

The inputs to the IF sections are assumed to be single frequency sinusoids. Any phase differences caused by the microwave receiving sections are combined and referred to the horizontal IF signal. Descriptions of these signals are thus given by:

$$h(t)=A_h\cos\left[\omega_{IF}t + \phi_h + \phi_e(t)\right] \qquad v(t)=A_v\cos\left[\omega_{IF}t + \phi_v\right]$$

where

- $h(t)$ and $v(t)$ are the voltage waveforms at the inputs to the horizontal and vertical IF sections,
- A_h and A_v are the constant magnitudes of the waveforms,
- ϕ_h and ϕ_v are the ideal phases of the horizontal and vertical waveforms, and
- $\phi_e(t)$ is a time varying error term describing the differential phase errors between the horizontal and vertical microwave receiving sections.

The powers in the six intensity channels can then be calculated in a straight forward manner. Using the notation of sections 2.2.1.2 and 2.2.3.2,

$$I(0,0) = A_h{}^2/2$$

$$I(90,0) = A_v{}^2/2$$

$$I(45,0) = A_h{}^2/2 + A_v{}^2/2 + \frac{A_h A_v}{T}\int \cos\left[\phi_h - \phi_v + \phi_e(t)\right]dt$$

$$I(135,0) = A_h{}^2/2 + A_v{}^2/2 - \frac{A_h A_v}{T}\int \cos\left[\phi_h - \phi_v + \phi_e(t)\right]dt$$

$$I(45,\frac{\pi}{2}) = A_h{}^2/2 + A_v{}^2/2 + \frac{A_h A_v}{T}\int \sin\left[\phi_h - \phi_v + \phi_e(t)\right]dt$$

$$I(135,\frac{\pi}{2}) = A_h{}^2/2 + A_v{}^2/2 - \frac{A_h A_v}{T}\int \sin\left[\phi_h - \phi_v + \phi_e(t)\right]dt$$

If the phase error term is now assumed to be a linear function of time, and to equal zero at the midpoint of the integration interval, the following

results are obtained.

$$\phi_e(t) = k_e t$$

$$I(45,0) - I(135,0) = \frac{2A_h A_v}{T}\int_{-T/2}^{T/2} \cos\left[\delta + k_e t\right] dt$$

$$= A_h A_v \cos\delta \ \frac{\sin\left(k_e T/2\right)}{\left(k_e T/2\right)}$$

$$I(45,\frac{\pi}{2}) - I(135,\frac{\pi}{2}) = \frac{2A_h A_v}{T}\int_{-T/2}^{T/2} \sin\left[\delta + k_e t\right] dt$$

$$= A_h A_v \sin\delta \ \frac{\sin\left(k_e T/2\right)}{\left(k_e T/2\right)}$$

The polarization parameters can then be calculated using the relations given in section 2.2.3.2:

$$\tan 2\psi = \frac{2A_h A_v \cos\delta}{\left(A_h{}^2 - A_v{}^2\right)} \ \frac{\sin\left(k_e T/2\right)}{\left(k_e T/2\right)}$$

$$\sin 2\chi = \frac{2A_h A_v \sin\delta}{\left(A_h{}^2 + A_v{}^2\right)} \ \frac{\sin\left(k_e T/2\right)}{\left(k_e T/2\right)}$$

$$m = \frac{2\sqrt{\left(A_h{}^2 - A_v{}^2\right)^2 + 4A_h{}^2 A_v{}^2 \operatorname{sinc}^2\left(k_e T/2\right)}}{\left(A_h{}^2 + A_v{}^2\right)}$$

Solution of these equations using a value for $k_e T/2$ corresponding to 12 degrees and at typical horizontal to vertical amplitude ratios (25 dB) reveals that errors due to the phase imbalance will amount to only a small fraction

of a degree in angle (.001 degrees) and .00015 in polarization ratio. These errors are so small that they can be ignored, even if the effects due to many spectral lines are considered.

6.4. IF Filter Mismatches

The derivation presented in section 4.3.2 showed that the intensity method for determining the polarization parameters relied on the use of filters that were matched in amplitude as well as phase. Examination of the magnitude responses of the filters presented in Figures 5-3 and 5-4 reveals that there are significant differences between them. The possible repercussions of these differences are discussed in this section.

The IF filter frequency responses reveal that the filters in the A,B,C and D channels are quite well matched, and that the H and V channel filters are quite similar, but that these two sets differ quite markedly. The shape of the responses even suggests that the order of the filter is different between the two sets. This was in fact verified by designing a second order Bessel bandpass filter and a third order Butterworth bandpass filter and showing that the predicted response characteristics matched the measured characteristics of Figures 5-3 and 5-4. The third order filter was mistuned slightly to cause its magnitude response to more closely match the A,B,C and D channel filters. Schematic diagrams for these filters along with the response characteristics predicted by the Micro-cap II circuit analysis program [26] are shown in Figures 6-1 and 6-2.

It was assumed that since the magnitude responses shown in Figures 6-1 and 6-2 matched the responses of the H,V,A,B,C and D channel filters, the phase responses would also be similar. An analysis of the effects due to the differences between filters could then be carried out using the more complete set of characteristics.

To determine what these effects might be in terms of the values at the

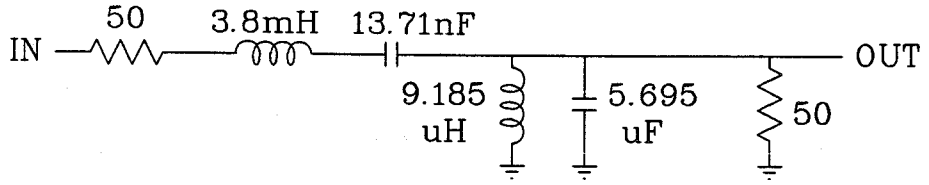

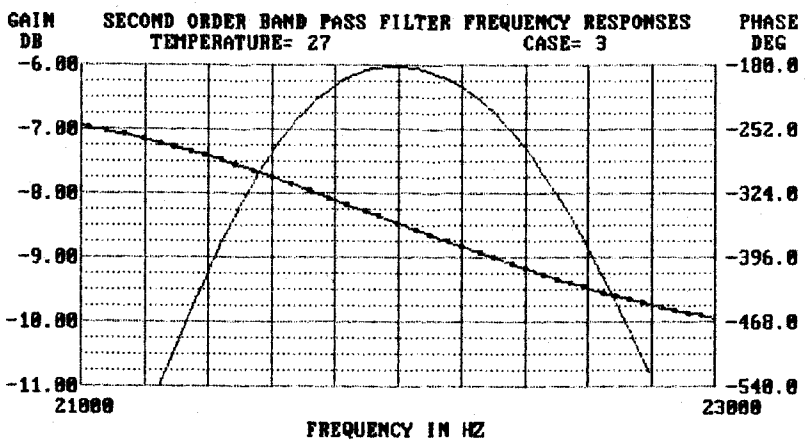

Figure 6-1: Second Order Bandpass Filter Details

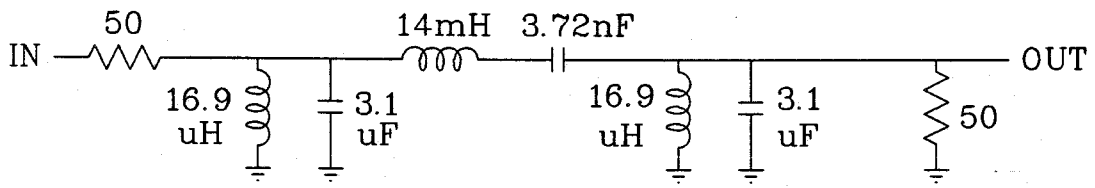

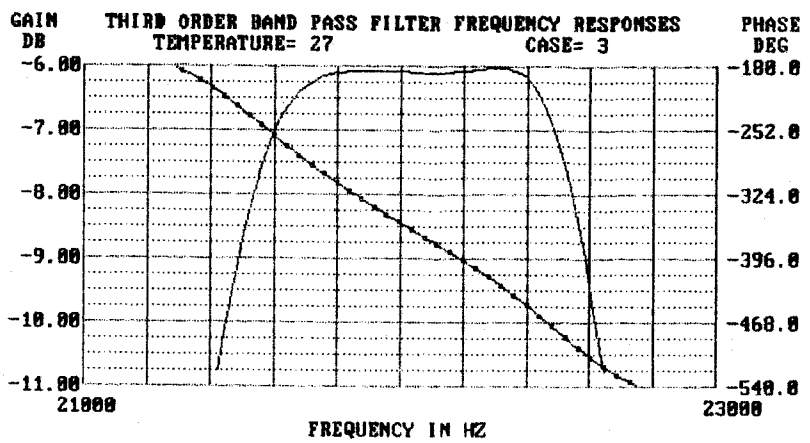

Figure 6-2: Third Order Bandpass Filter Details

outputs of the H,V,A,B,C and D channels, a computer simulation was

carried out. In this simulation a signal consisting of a collection of spectral lines was applied to the inputs of the two filters of Figures 6-1 and 6-2. The resulting outputs were full wave rectified by taking the absolute value, and averaged by numerically integrating over a period corresponding to the positive going portion of the RF sweep. The simulation closely modelled the actual operation of the H and C channels of the scatterometer system when a horizontally polarized signal is received. The simulation assumed that five spectral lines would be contained within the three dB bandwidths of the filters, and that the frequencies of these spectral lines would be fixed. The phases of the spectral lines were assumed to be constant in a manner consistent with the description of the IF waveform in equation (4.5). The values for the square of the average value of the output and the average power vs the magnitudes of the spectral lines were calculated as the amplitudes of the spectral lines were stepped over all combinations between 0 and 1 in steps of .2. The integration period was taken to be two thirds of the period corresponding to the frequency of the spacing between the spectral lines. A listing of this program is given in Appendix G.

The results of the simulation show that the ratio of the squares of the averaged outputs from the two filters (C/H) varies from .776 to 2.427 as the input spectrum is varied.

This variation of the power ratios will cause drastic errors in the measurement of the polarization state, which depends upon these ratios to determine the required quantities (see section 4.5). Although the only sure method of reducing these effects is to ensure that all of the IF filters in the system are properly matched, it is possible to reduce the error in processing the data which was acquired using the unmatched filters if an assumption regarding the spectrum can be made.

If it can be assumed (as was done in Chapter 4) that the shape of the IF spectrum at the input to the horizontal channel is identical to that at the input to the vertical channel except for its overall magnitude, and

furthermore that the phase difference between any spectral line in the horizontal channel and the corresponding spectral line in the vertical channel is the same, the IF filters need only be matched in sets of two. In such a case, the ratios of the two powers being measured by a matched filter set will be valid, although the sum of these two powers may not match the sum of the powers from a different matched set. Since the sum of the powers measured in any set of orthogonal axes must be equal to the sum of the powers measured in any other orthogonal set, the sets of measurements can then be normalized to a common value, while retaining the correct ratio.

Examination of the filter responses of Figures 5-3 and 5-4 reveals that the H and V channel filters are quite well matched and that all of the A,B,C and D channel filters are matched. Matched pairs could thus be used for the H and V channels, the A and B channels and the C and D channels.

6.5. Detector Performance

The theoretical developments in Chapters 2 and 4 relied on the measurement of power to determine the quantities of interest. The equipment as constructed, however does not measure the power in the waveforms. It measures the time average of the full wave rectified signal. If the waveform being measured consists of a single sinusoid and the measurement interval is long compared to the period of the sinusoid, the ratio of the square of the full wave rectified average to the power average will be $8/\pi^2$ (.81), giving a direct relationship between the two values. Unfortunately, under normal operation of this scatterometer system the input waveform consists of the superposition of a number of sinusoids, each having a different frequency. It is therefore not clear that the measured value will be a proper indication of the power in the waveform.

A computer simulation similar to the one described in section 6.4 above provided a comparison between the square of the averaged, full wave rectified values and the true power in the waveform when the input signal consisted

of the sum of five sinusoids. A listing of the program used for this simulation is given in Appendix G. The sinusoids were assumed to be equally spaced in frequency across a bandwidth of 5% of the normal IF frequency of 22 KHz, and were assumed to have equal fixed phase terms. Such a situation would arise when the scatterometer is set to measure the backscatter from a target at a range of approximately 12.5 meters. The results showed that the ratio of the square of the rectified average to the power average as a function of the magnitudes of the input sinsusoids varied from .293 to .81. As a power indication, the square of the rectified average can thus be in error by as much as -4.4 dB.

While the above result has significant implications on the accuracy of the measured radar cross sections, it does not significantly affect the measurement of the polarization parameters. If as assumed in section 6.4 the shape of the horizontal IF spectrum is the same as the IF vertical spectrum, the resulting spectra for the sum, difference, quadrature sum and quadrature difference channels will also have the same shape. Any error in the power measurement will then be common to all channels. When the erroneous values are used to predict the polarization parameters via equations (4.7), (4.8) and (4.9) the common error factors will cancel, leaving only the desired ratios to be translated to the quantities of interest.

6.6. Effects Due To System Generated Interference

The section describing transceiver operation in Chapter 3 noted that internal reflections of the transmitted signal would cause interference falling within the bandwidth of the IF filters. This interference can be considered to have originated from a point target at extremely short range, and the spectral contributions due to it can therefore be described by equation (3.15). From this equation it is seen that the spectral lines within the filter bandwidth will all have the same fixed phase offset. The envelope of their magnitudes will have only a slight magnitude slope across the filter passband, being larger at the low frequency passband edge.

The spectral lines due to scattering from a target, however have phases determined both by the range to the scatterers and by the scattering matrix of those scatterers. Since the range to the scatterers will vary as measurements are made[13], it can be assumed that the phase of the scattered contributions will be distributed over the full range of phase angles.

For situations where the spectral lines from the scatterers have greater magnitudes than the spectral lines due to internal reflections, the resultant of these two components will have a magnitude lying between the extremes given by the sum and difference of the component magnitudes. The phase of the resultant will differ from the phase of the spectral contribution from the scatterers by an amount that can be as high as the inverse tangent of the ratio of the two magnitudes.

If only the magnitudes of the spectral lines were considered, many measurements could be taken and averaged to arrive at a value approaching the contribution from the scatterers alone. The phase shifting of the signal however, will result in variations in the voltage waveform at the output of the IF filters that can cause large fluctuations in the power measured over short time intervals, as was discussed in section 6.4. Although this effect will not be analysed in detail it is noted that an amplitude ratio of ten between the magnitude of a scattered spectral contribution and an interfering contribution (or a power ratio of 20 dB) can result in a phase change of up to 5.7 degrees in the phase of the resultant spectral line, which would already be expected to affect the measured power.

Any measurements which show that the measured power in one of the channels is less than 20 dB above the value expected from the measurement of the noise alone should therefore be expected to contain error.

---

[13]The measurements are taken while slowly driving the truck on which the radars are mounted.

Measurements of the IF processor outputs voltages due to the internal reflections were carried out and given in Chapter 5 as Table 5-6. Only one set of voltages is given, corresponding to the values resulting when the antenna is pointing at the sky and attempting to measure the signal backscattered from a range of 9.5 meters. The field measurements are typically gathered using a boom height of eleven meters and antenna elevation angles (look angles) of 10 through 70 degrees, corresponding to ranges of eleven to thirty-two meters. An extension of the data from internal reflection measurements is thus required to allow comparison of the internally reflected signals to the externally reflected signals at larger ranges.

The spectrum of the IF voltage due to the internal reflections has its peak very close to DC. The portion of the spectrum lying within the IF filter passband will therefore consist of the higher order harmonics. This allows the approximation of equation (4.4) to be employed. Examination of this equation along with the definition for the constant K_n on page 52 shows that for small r (i.e. at short ranges) and large n, the magnitude of the spectral lines follows a $1/n$ relationship.

The harmonic number n will also be given (approximately) as the ratio of the IF frequency to the modulation frequency. If the fact that the upsweep portion of the modulating waveform is approximately two-thirds of the total period is taken into account, equation (3.4) can be solved for n as well, yielding

$$n \approx \frac{f_{IF}}{f_m} = \frac{3BR}{c} \tag{6.2}$$

Combination of these two relationships results in the conclusion that the magnitude of the spectral lines lying within the IF passband varies inversely with range.

At the same time, equation (6.2) shows that the modulation frequency will

itself vary inversely with range. As the range increases, the number of spectral lines within the passband of the IF will increase. The magnitude of the spectral lines varying inversely with range, and the number of lines in the passband varying directly with range results in the total power in the IF passband due to the internal reflections varying inversely with range.

Values corresponding to the power level of internal reflections for any range may therefore be calculated by multiplying the square of the values in Table 5-6 with the ratio of the original range (9.5 m) to the desired range.

6.7. Effects Of Non-Simultaneous Channel Sampling

The derivations presented in Chapters 3 and 4 of this document assumed that the target being illuminated by the scatterometer consisted of some number of fixed point targets, and that there was no relative motion between these scatterers and the scatterometer. Field data is obtained however, by driving the truck on which the scatterometer is mounted along the side of crop being illuminated. The measured power in the individual scatterometer channels is then read by the data acquisition unit sequentially. Since there are no sample and hold circuits in the equipment, this motion implies that the measured value from each channel corresponds to a different set of scatterers and thus that the underlying assumptions are being violated.

A total of ten channels are sampled by the data acquisition unit. The first set of six measurements samples the horizontal channel for each of the L, C, and K-band units, followed by the vertical channel for each. The four sum and difference channels are sampled last. The measurement of the ten channels takes approximately two seconds. Assuming that each measurement takes the same amount of time, a total of 1.4 seconds will ellapse from the time the K-band horizontal channel is sampled to the time the last sampled channel is read. Estimating the speed of the truck to be one foot per second, this implies a total movement of 1.4 feet (.43 meters).

The width of the illuminated area is controlled by the antenna beamwidth, the height of the antenna above the ground, and the radar look angle (elevation angle of the antenna). For the *K*-band transceiver, it will range from .66 meters (at a 10 degree look angle) to 1.91 meters (at a 70 degree look angle). The .43 meter displacement between the first and last measurements thus represents a major change in the target.

The effect that this motion will have on the validity of the polarization parameters has not been completely analysed. If the scattering properties of the target change significantly across the total illuminated area, the results will obviously be in error. On the other hand, if the scattering properties are fairly uniform so that the measured power in any given channel remains fairly constant regardless of the area being illuminated, the results would still be valid. At this time, the data gathered has not been analysed for variations in time, so valid conclusions cannot be reached.

6.8. Application To Interpretation Of Field Measurements

The discussions in this chapter have indicated that significant performance degradations can be expected from several factors. The largest degradation by far can be caused by the non-simultaneous sampling of the individual channel outputs. The presence of major degradations from this source will be indicated by variations in the trial to trial channel measurements. Should significant variations be discovered here, it would seem to be most suitable to average the values across the total number of trials before attempting to calculate the polarization parameters.

A second degradation will result from mismatches in the IF bandpass filters. This will be signified in the data by differences in the total power as measured by the sum of the H and V channel powers, the sum of the in phase sum and in phase difference channel powers, and the sum of the quadrature sum and quadrature difference channel powers, even when the degradation due to non-simultaneous sampling is not present. Processing of

the data should therefore provide these three powers for comparison.

If the trial to trial measurements are fairly constant and the assumptions stated in section 6.4 hold, the effects of the IF filter mismatches can be removed by normalizing the three sets of powers mentioned above. In such a case, the degradations caused by insufficient antenna cross polarization isolation and possibly internal reflections will come into play. Since the expected value of the antenna cross polarization isolation is on the order of 27 dB, any ratio of the measured horizontal channel power to vertical channel power which approaches this value will indicate the presence of a degradation. At the same time, any measured value for the horizontal or vertical channel power which is less than 20 dB above the expected power contribution from internal reflections will signify that an error can be expected. Recognizing that these errors may be present requires that the processed data provide the horizontal to vertical channel power ratio, and the absolute power of the smallest of the horizontal and vertical channel powers.

Chapter 7

RESULTS FROM THE MEASUREMENT OF WHEAT

7.1. General

The testing carried out in Chapter 5 measured the signals returning from three different sources: a linearly polarized antenna, a circularly polarized antenna, and the Active Radar Calibrator. In each of these cases, the radiation can be considered to have originated from a point source. This chapter will present the results of measurements on a field of wheat, representing a distributed target.

7.2. Description Of The Data Gathering Process

The data was gathered by using the modified scatterometer (now a polarimeter) to measure a field of Hard Red Spring wheat. This field was designated as plot 11 in the CCRS measurement campaign. It was planted on May 8^{th}, 1987 with a density of 90 pounds per acre (designated as high density), and was swathed on August 21^{st}, 1987. This plot was examined several times over the course of the growing season. The data to be used for illustration in this chapter has been selected from two of these measurement occasions, June 29^{th} and August 4^{th}.

Before measurements were taken, the radar transceivers were raised to a height of 11 meters. The look angle was adjusted to the desired value and the range to the crop determined using the *C*-band radar transceiver. This range was then assumed to be the range of maximum return for all three of the transceivers. Measurements were then taken while slowly driving the

truck on which the radars are mounted along the perimeter of the field. Data was gathered for three range cells: the range of maximum return, the range 5% less than this, and the range 5% more. Each set of three range cell measurements was carried out using first a horizontally polarized illuminating radiation, then a vertically polarized radiation and constituted a trial. At least ten trials were carried out for any given look angle. The data gathered was stored on floppy disks for later analysis.

This process was repeated for look angles of 10, 15, 20, 25, 30, 35, 40, 50, 60 and 70 degrees. The entire process was repeated while driving parallel to the row furrows, perpendicular to the row furrows, and parallel to the furrows with the boom turret rotated at a 45 degree angle (the incident radiation is then also a 45 degree angle to the furrows). On June 29 th thirty trials were carried out at the 10 degree look angle, and twenty trials were carried out at 15 and 20 degree look angles. At all other look angles on June 29th and for all look angles on August 4th ten trials were carried out.

7.3. Processing The Raw Data

The data presented in this chapter represents only the *K*-band measurements, and only those measurements taken while driving parallel to the row furrows with the boom turret rotated to a 45 degree angle. It was taken in its raw form (i.e. corresponding to the voltages at the six IF processor outputs) and used to calculate the maximum, average, and minimum values of:

- the ratio of the total power present at the outputs of the in phase combination unit to the total power present in the horizontal and vertical IF processor outputs and
- the ratio of the total power present at the outputs of the quadrature combination unit to the total power present in the horizontal and vertical IF processor outputs

for both horizontally and vertically polarized transmitted signals and at each

of the look angles measured. The average values were calculated by first calculating the average value of the square of the individual IF processor outputs, then by calculating the ratios using the averages. This was done to ensure that the signals were averaged on a power basis, rather than a voltage basis. The maximum and minimum values shown are based on the individual ratio calculations for each trial. The values were calculated from the data in range cell 3 only[14].

The raw data was then normalized to ensure that the total power from the in phase and quadrature combination units was equal to the total power in the horizontal and vertical IF processor outputs. This step will remove the effects of the IF filter mismatches as discussed in section 6.8. The normalized data was used to calculate the polarization ratio (m), ellipticity angle (χ) and orientation angle (ψ) as a function of the look angle. Maximum, average and minimum values were calculated for each quantity. The maximum and minimum values correspond to the outer limits of the quantity of interest over the range of trials in range cell 3, while the average corresponds to the value that the quantity of interest takes on if it is calculated from the values determined by power averaging the normalized raw data over the range of trials for range cell 3.

---

[14]Data from three range cells is normally collected. The first and shortest range cell corresponds to the vegetation top, the middle cell to the body of the vegetation and the third and longest to the underlying soil. The changes to the local oscillator line length discussed in section 4.4.1 had the effect of shortening the measured range, thus causing the first range cell to measure a space above the top of the vegetation and the third range cell to measure the body of the vegetation. The data shown here from range cell three thus results from measurement of the vegetation itself rather than the soil as would have been expected.

7.4. Processed Data

The results of the processing described in section 7.3 are shown in the figures on pages 157 to 162. The lower horizontal line on these plots shows the minimum value resulting from the calculations, the solid dot the average of all trials taken at the look angle in question, and the upper horizontal line the maximum value found during calculations. Also shown are the maximum, average and minimum values for the powers in the horizontal and vertical IF processor channel outputs (Figures 7-5 through 7-8 on pages 153 to 156).

Figures 7-1, 7-2, 7-3 and 7-4 show the minimum, average and maximum values for the ratios of the total power measured at the outputs of the in phase and quadrature combination units to the total power measured at the outputs of the horizontal and vertical channels. The ratios show considerable variability ranging from small values up to almost 5 on an individual trial basis. Such large ratios cannot be explained on the basis of differences in the IF filters alone. They therefore indicate that the movement of the measurement system with respect to the target is resulting in channel to channel power fluctuations.

The average values of these ratios trend from smaller to larger values as the radar look angle increases. This indicates that the peak of the spectrum of the returning signals is not properly centered in the IF bandwidth. The higher order (and steeper skirts) of the filters in the in phase and quadrature combination units reject more of the out of band power than the filters in the horizontal and vertical channels, thereby decreasing the power ratio. The effect decreases with increasing look angle because the spectrum tends to spread out as the illuminated area increases, thus resulting in more in band power.

Figures 7-5 to 7-8 show the total powers measured in the horizontal and vertical channels along with the estimated value of power present due to

internal reflections in the equipment. These plots show both that the variation in the measurements between trials is quite large (up to a factor of 25) and that the received power is quite close to the values expected from internal reflections alone. The variation in the power indicates that polarization parameters calculated on an individual trial basis will be affected quite severely by the motion of the equipment with respect to the scatterers. The fact that the measured powers are close to the expected values from the internal reflections shows that some degree of error would be present even without that relative motion.

The calculated values for the polarization parameters are given in the plots on pages 157 to 162. They show the expected variability in the individual trial calculations, with the orientation angles ranging over a 130 degree range when using vertically polarized illumination, and a 30 degree range when using horizontally polarized illumination. The ellipticity calculations are somewhat less flighty, showing variations across trials of 50 degrees for vertically polarized illumination and 25 degrees for horizontally polarized illumination. The polarization ratio shows similar fluctuations.

Of special interest is the observation that the polarization parameters calculated from the across trial power averages of the data are quite close to the expected values. The orientation angles are close to 0 degrees for horizontally polarized illumination and close to 90 degrees for vertically polarized. The ellipticity angles range about 0 degrees indicating linearly polarized scattered radiation, and the polarization ratio is always less than one, as it should be. These observations indicate that averaging the data across the number of trials before normalizing to remove the effects of IF filter variations and calculating the polarization parameters may yield more reliable results.

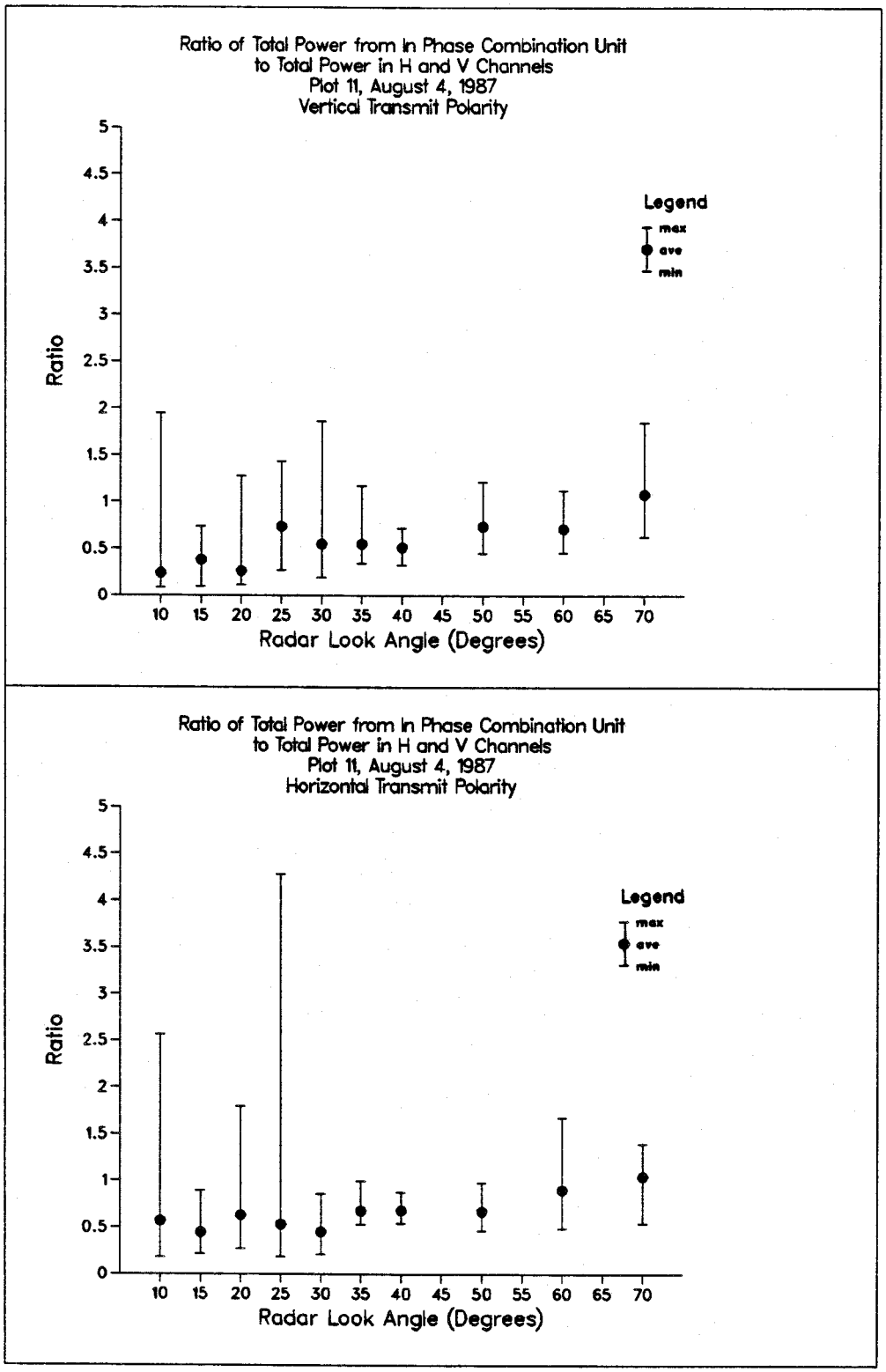

Figure 7-1: In Phase Combination Unit Power Ratios, August 4

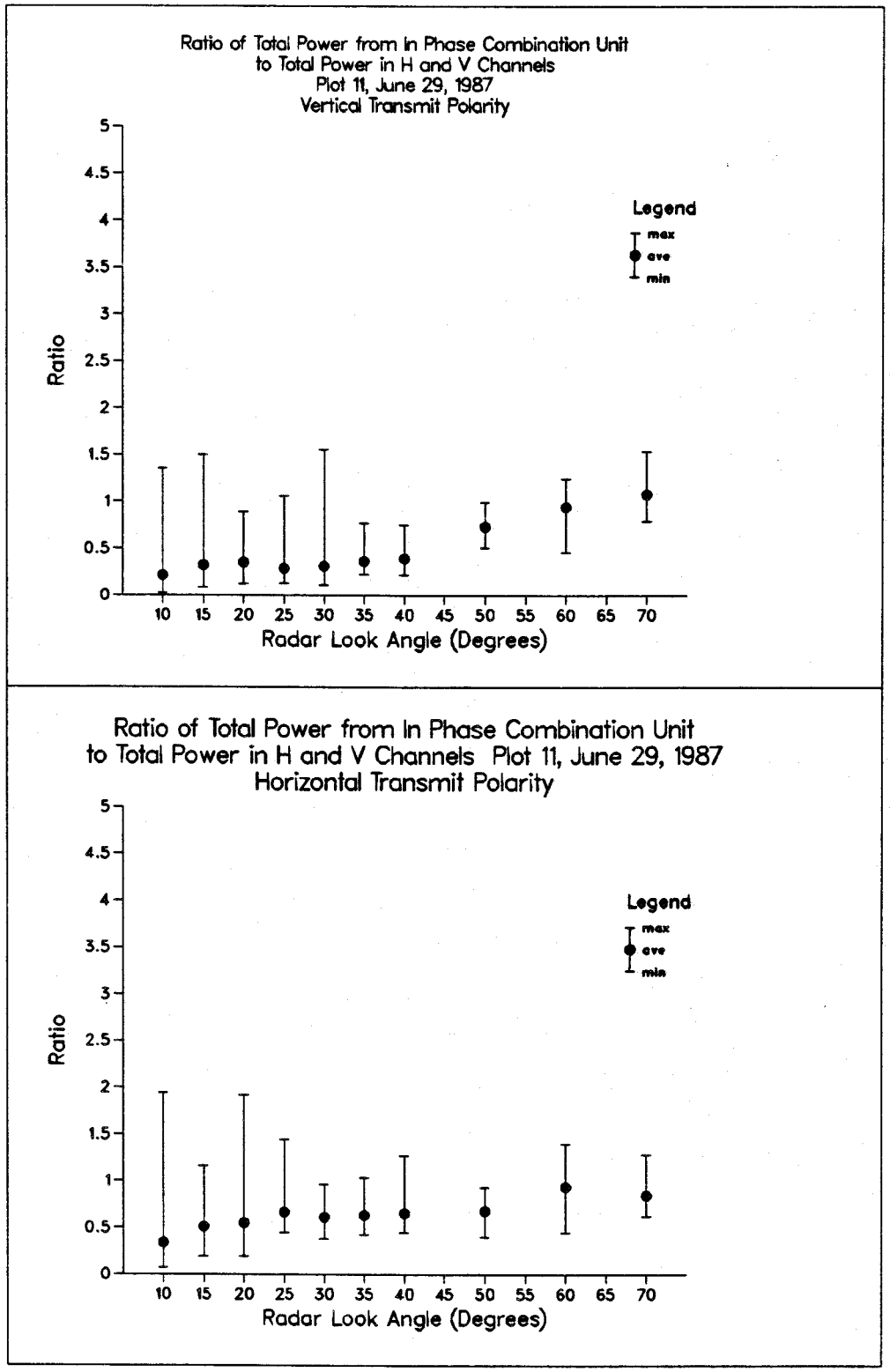

Figure 7-2: In Phase Combination Unit Power Ratios, June 29

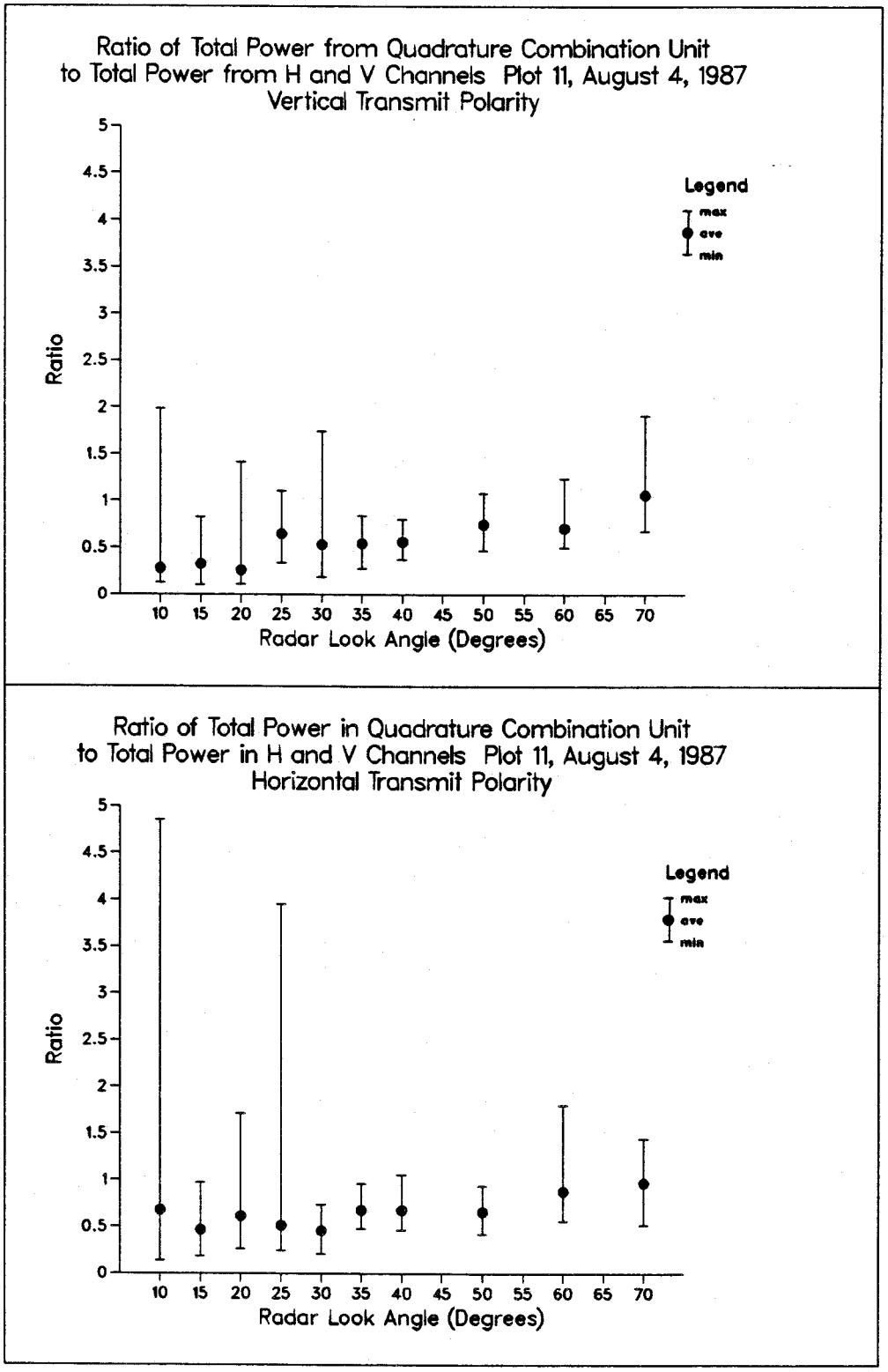

Figure 7-3: Quadrature Combination Unit Power Ratios, August 4

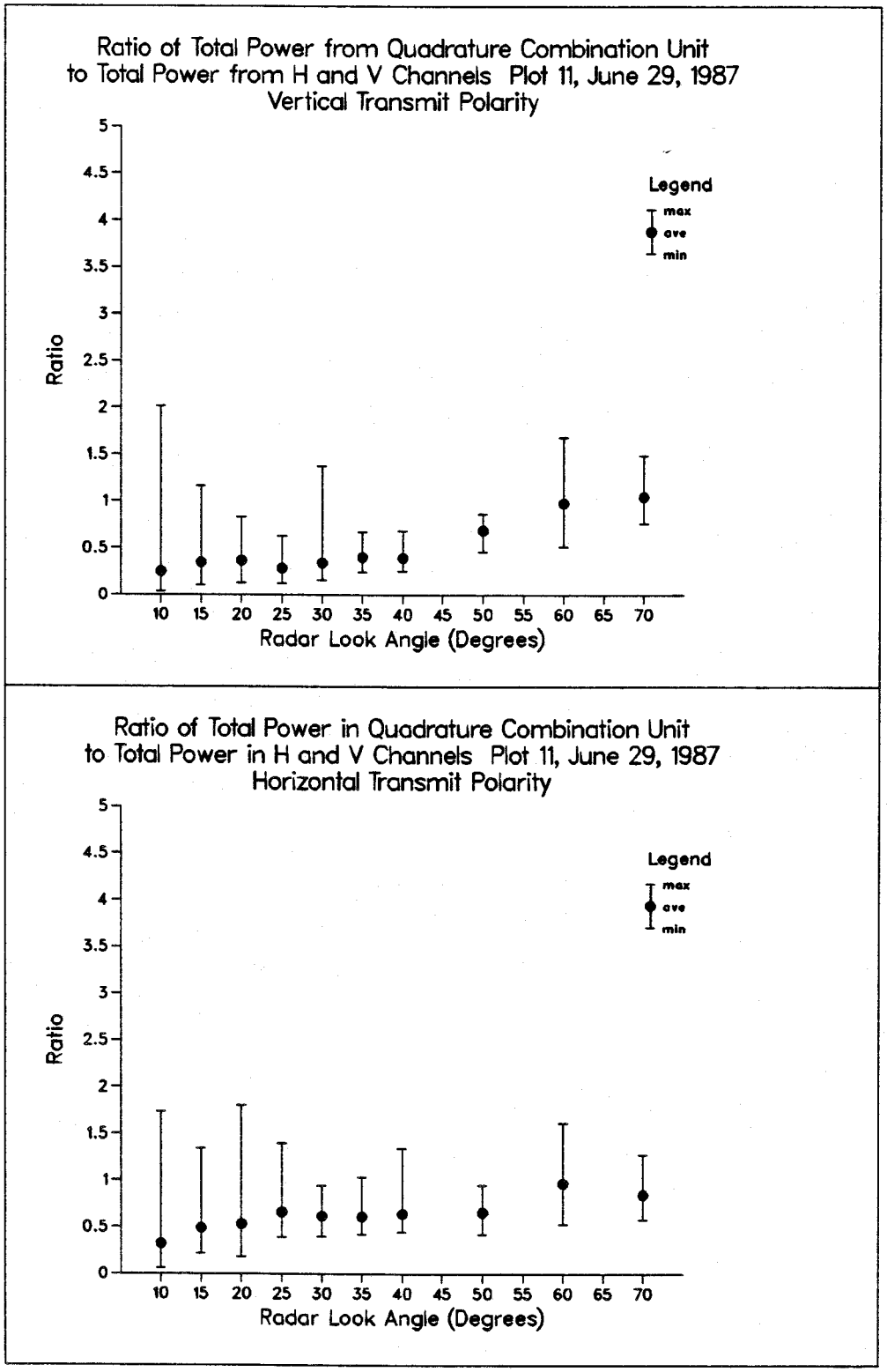

Figure 7-4: Quadrature Combination Unit Power Ratios, June 29

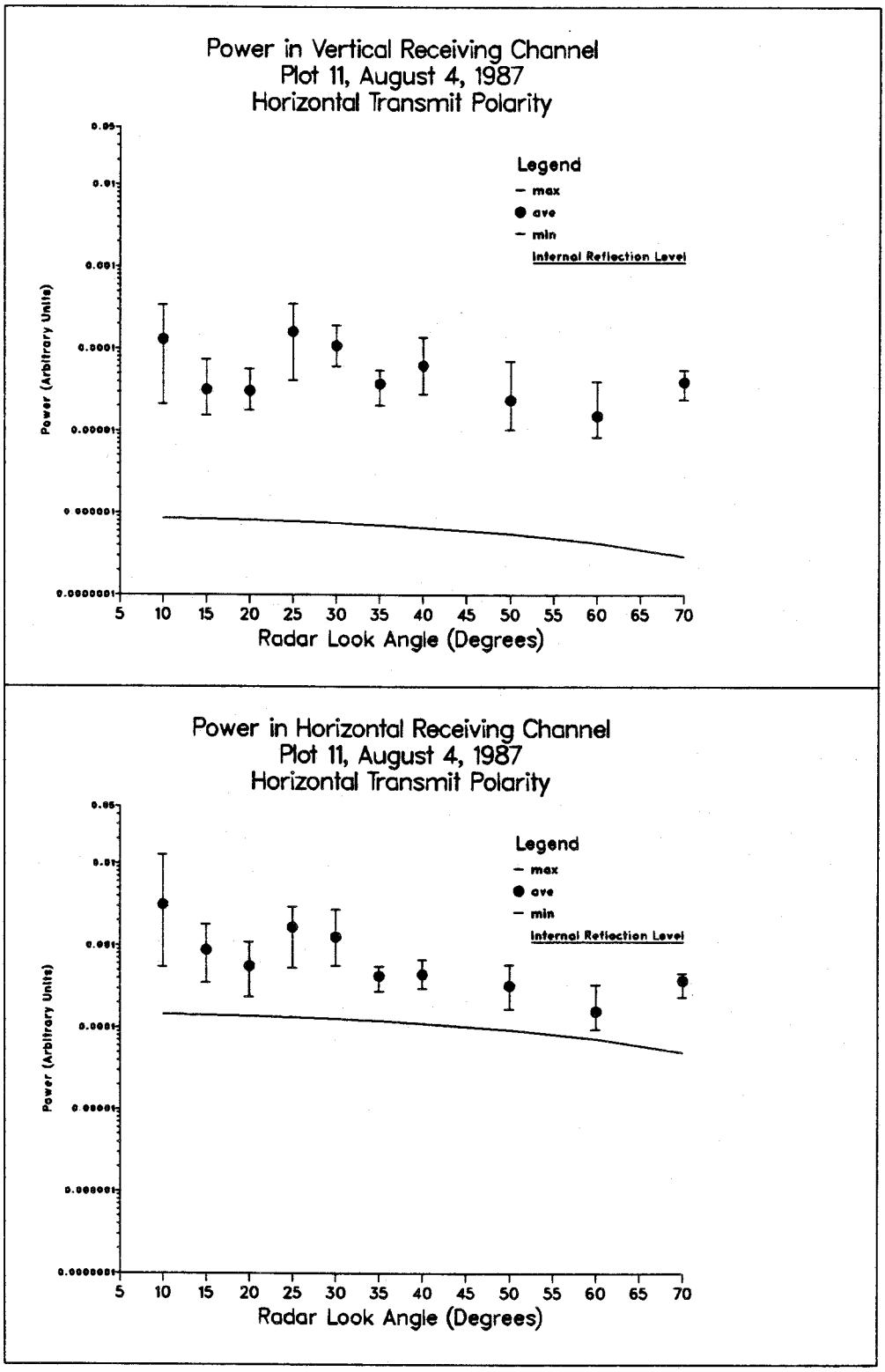

Figure 7-5: Received Power, August 4

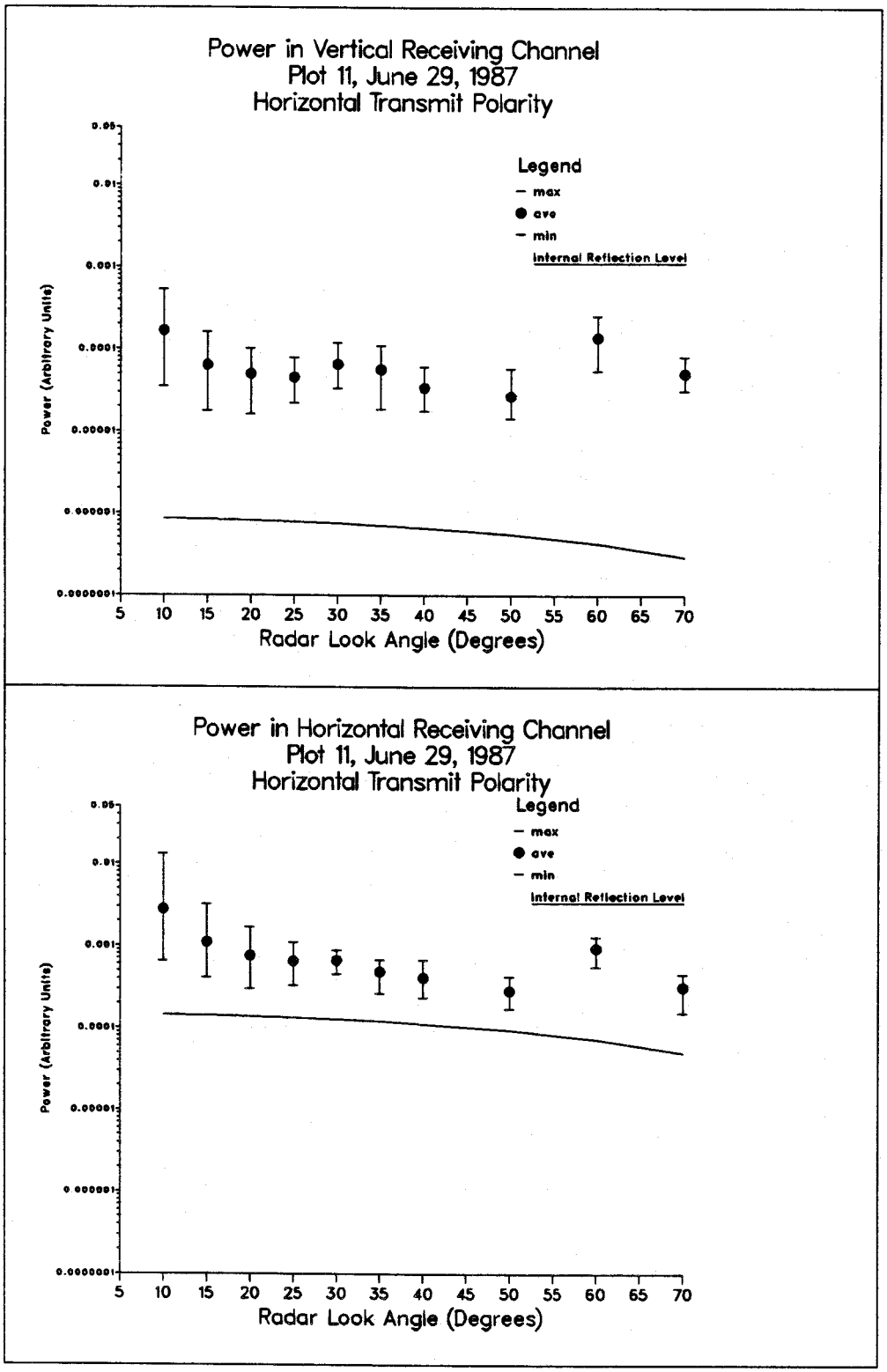

Figure 7-6: Received Power, June 29

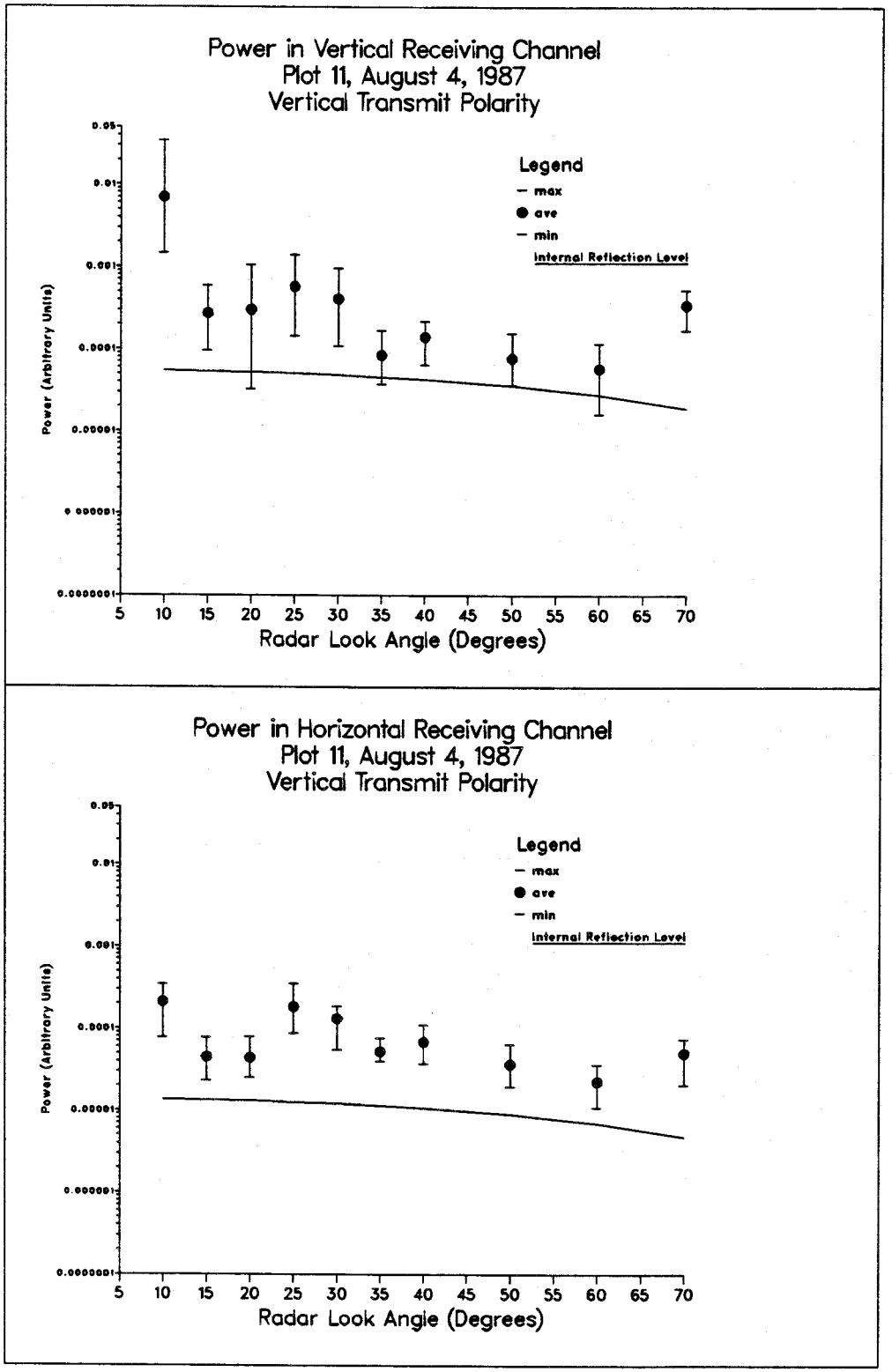

Figure 7-7: Received Power, August 4

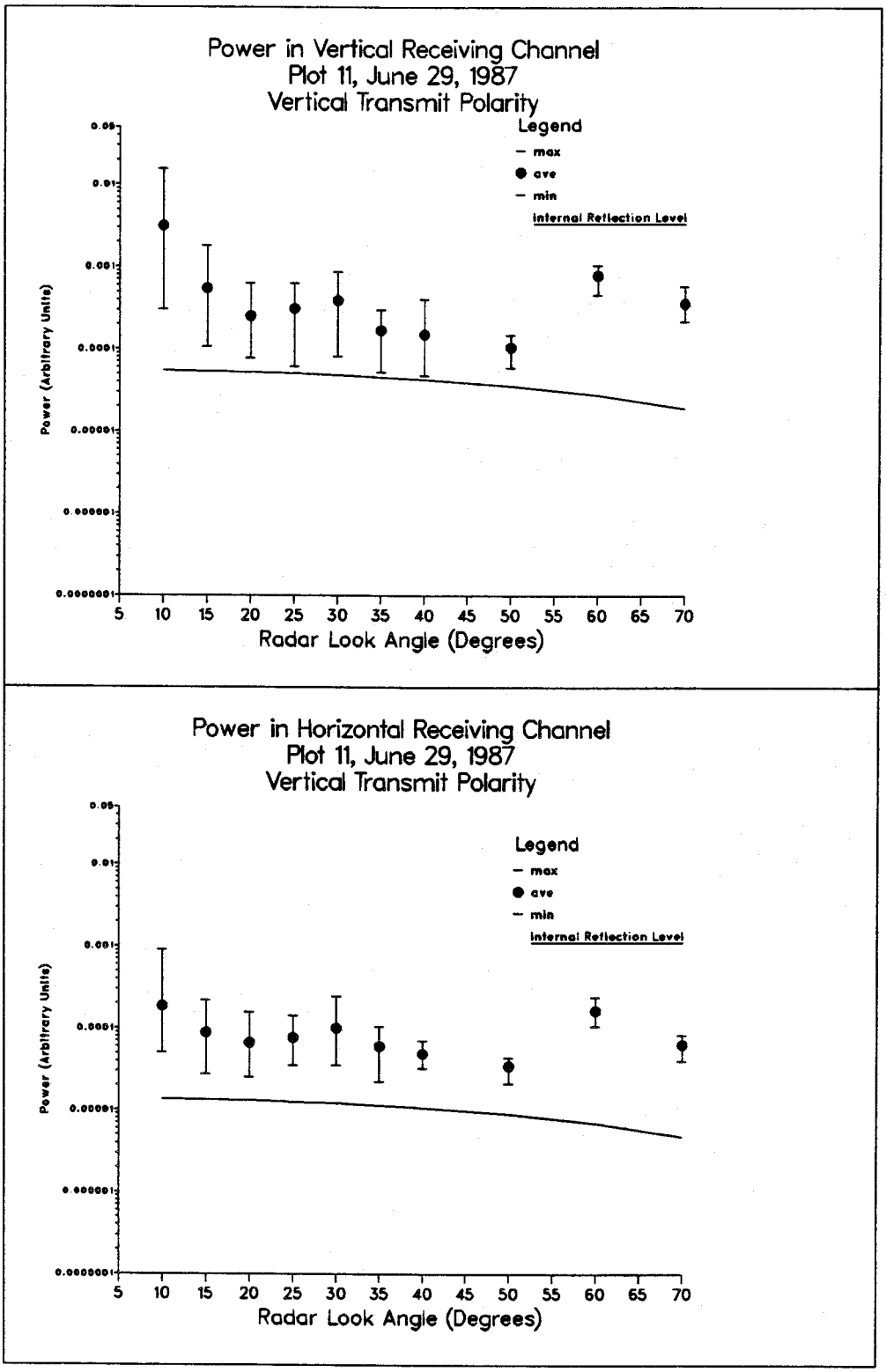

Figure 7-8: Received Power, June 29

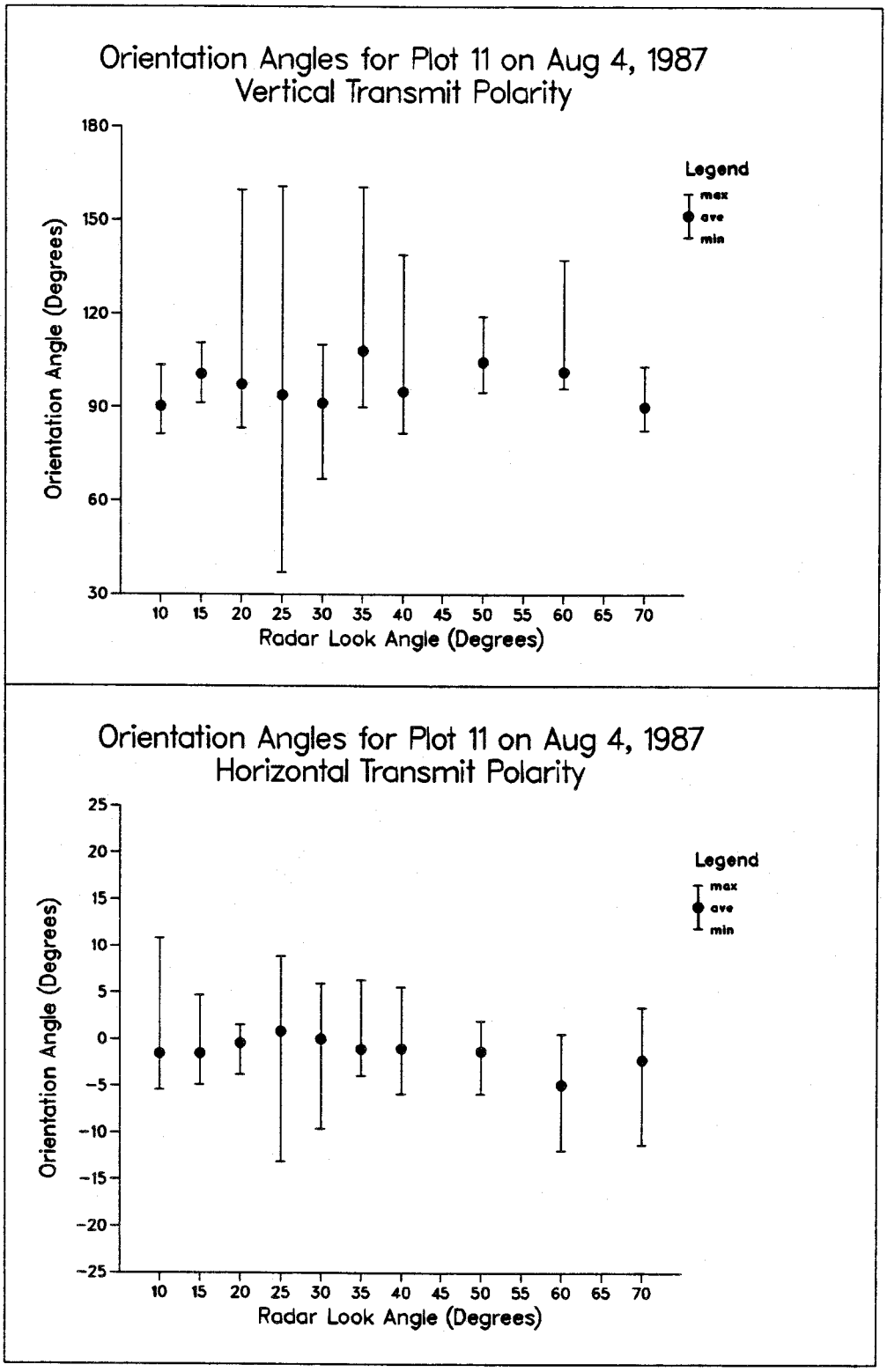

Figure 7-9: Orientation Angle, August 4

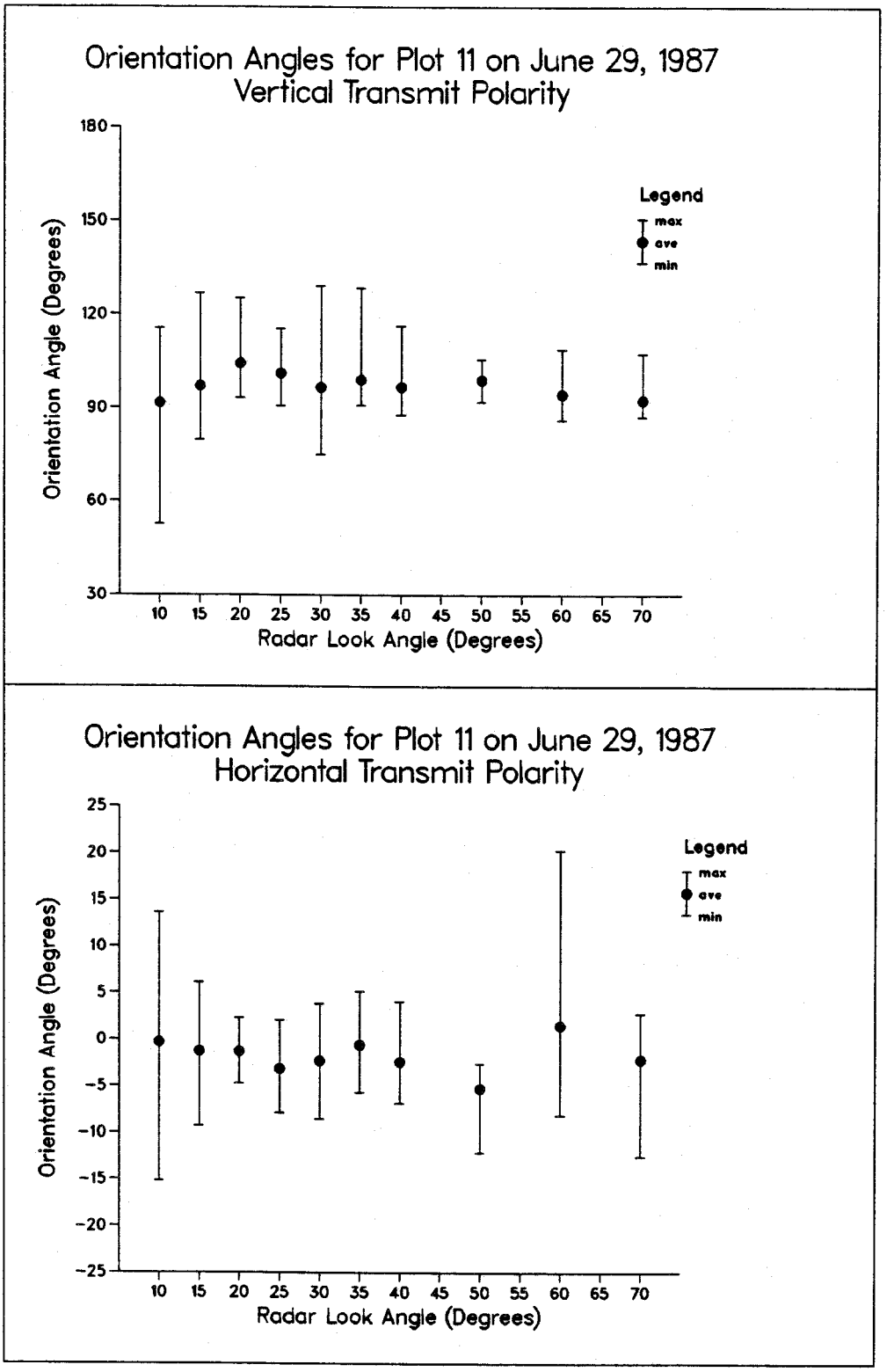

Figure 7-10: Orientation Angle, June 29

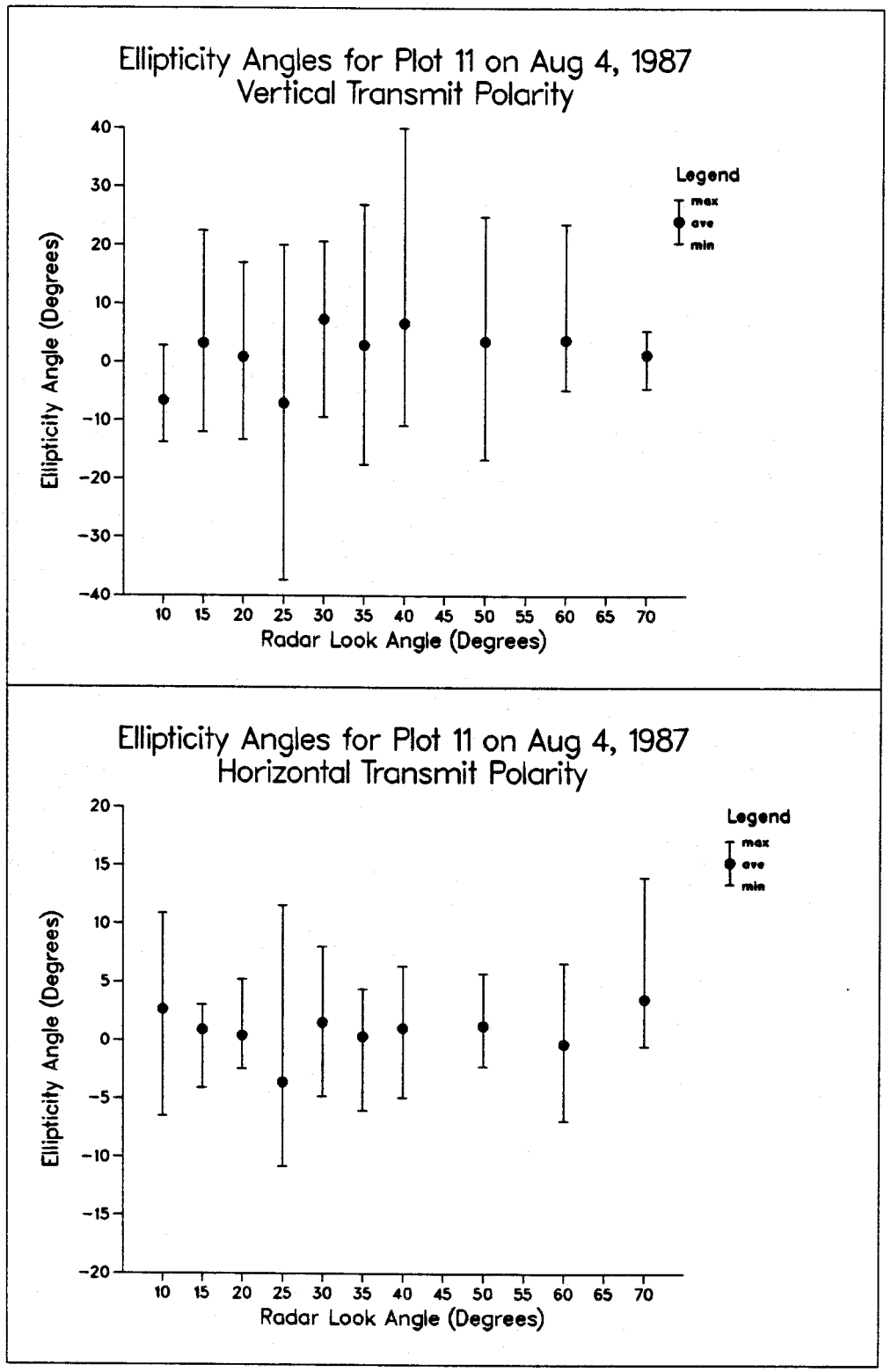

Figure 7-11: Ellipticity Angle, August 4

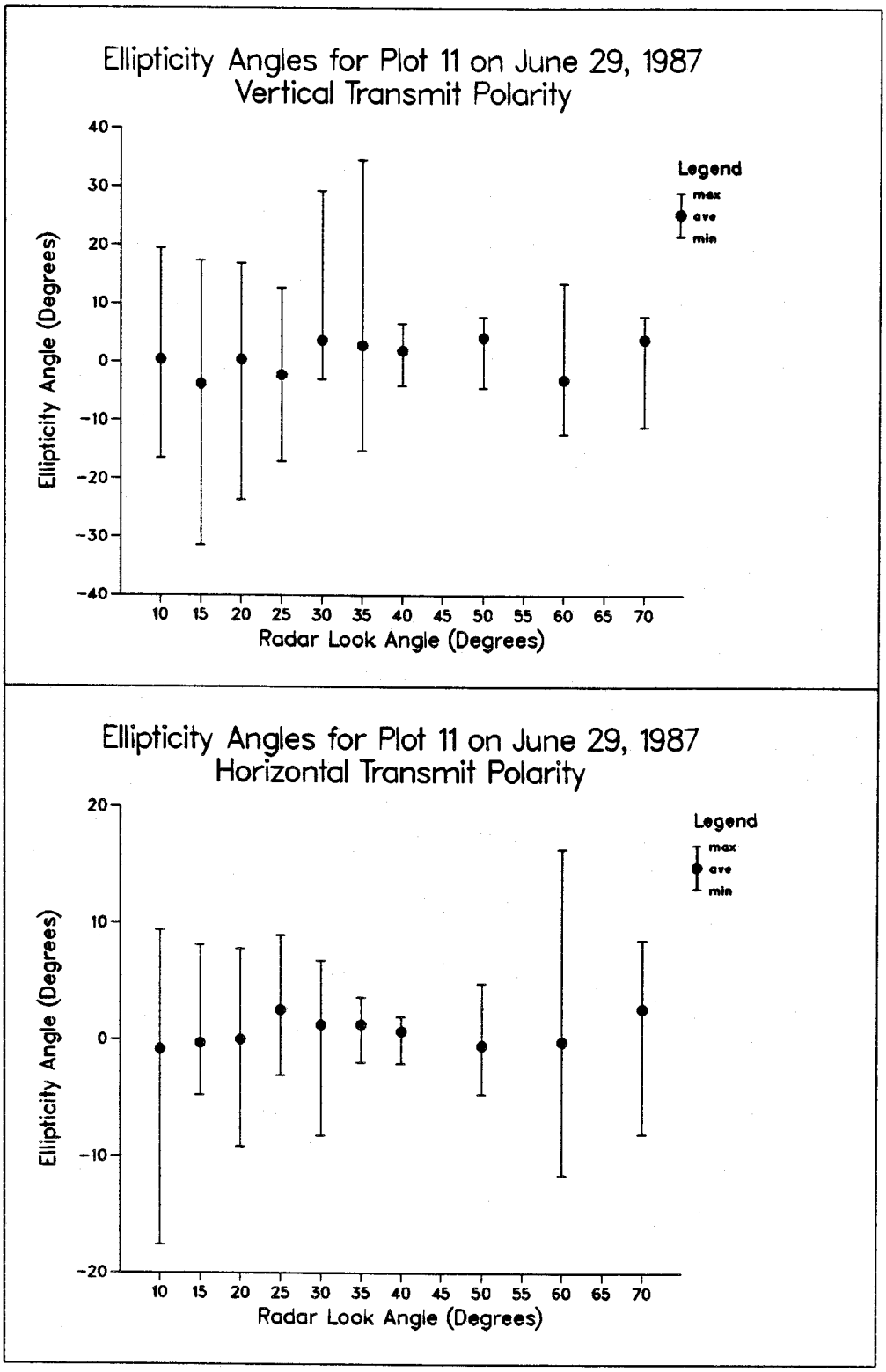

Figure 7-12: Ellipticity Angle, June 29

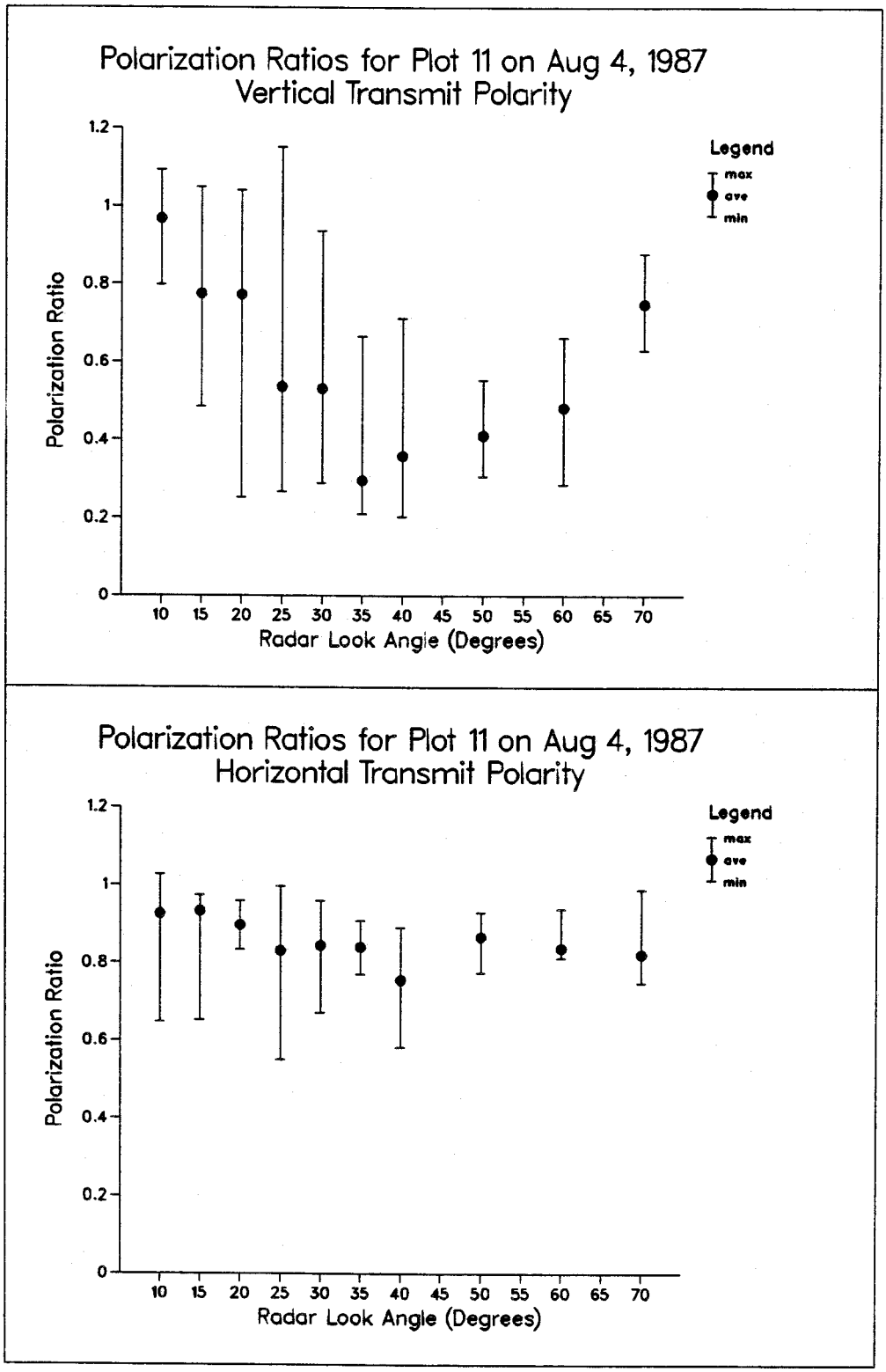

Figure 7-13: Polarization Ratio, August 4

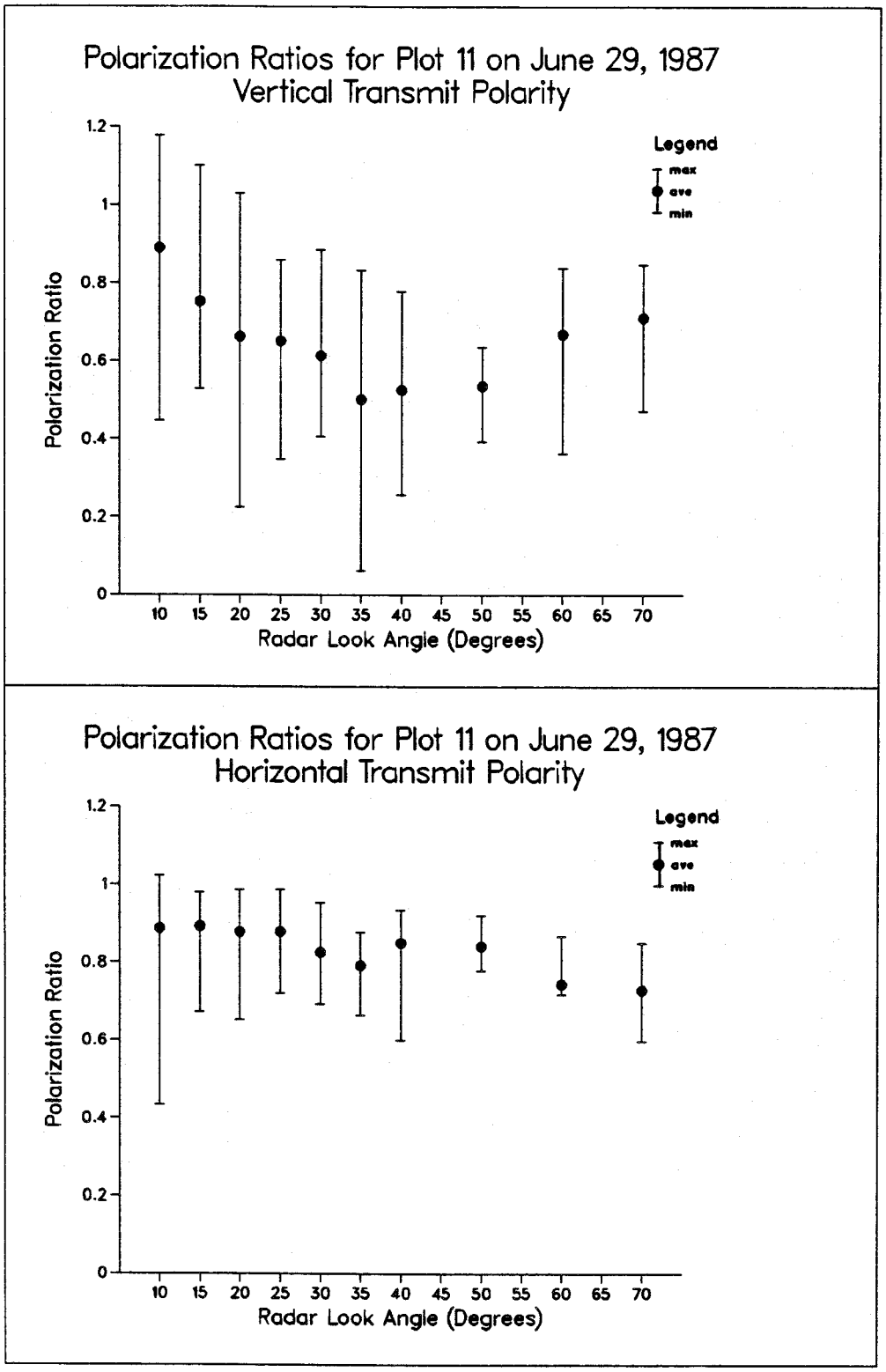

Figure 7-14: Polarization Ratio, June 29

Chapter 8

SUMMARY AND CONCLUSIONS

This document has described the theory and implementation details of circuitry added to a K band scatterometer to allow its use as a polarimeter. Results of testing carried out on the modified unit to ensure correct operation are presented along with a select set of data obtained by using the system to measure a field of wheat.

The expansion of the intermediate frequency radar signal resulting from the illumination of a point target in the form of a Fourier series showed that each spectral line in the IF spectrum contains information describing the polarization state of the radiation at the antenna terminals. Differences between the received and transmitted polarization states can be directly attributed to the properties of the target. The same statements will apply with respect to a collection of scatterers if those scatterers are fixed in space, and have scattering properties which are both independent of frequency over the bandwidth of the illuminating radiation and uniform between scatterers.

A single spectral line in the IF spectrum was shown to be equivalent to a monochromatic signal, allowing the application of conventional polarization theory for monochromatic radiation to the FM radar case. A parallel was drawn between quasi-monochromatic radiation and the IF spectrum resulting from the superposition of many individual (and possibly time varying) scatterers, showing that quasi-monochromatic polarization theory and the coherency matrix would also apply. The theory was extended by showing that equivalent results could be obtained through the examination of a collection of spectral lines at the IF, thus easing some of the problems

associated with implementing the circuitry.

Circuitry allowing the K band scatterometer to function as a polarimeter was designed, implemented and tested. Tests in the lab showed that the equipment could be expected to characterize the polarization to an accuracy within $\pm$ 5 degrees for the orientation and ellipticity angles of the polarization ellipse, and within 9 percent for the polarization ratio. Field tests using fixed targets gave much better results, yielding errors of only 2 degrees in the angular parameters and 7.1 percent for the polarization ratio.

An analysis of the system indicated several problem areas. The most severe of these is the fact that individual channel outputs are sampled at different points in time. Movement of the measuring system while reading these outputs thus implies that sequentially measured values correspond to different sets of scatterers. This invalidates the basic theory, which assumes that all channels are measured simultaneously.

The filters used in the IF processing sections were also found to show significant frequency response variations. This again violates an underlying assumption and causes most of the measurement error in the polarization ratio for the lab tests mentioned above.

The power detection circuitry was found to be dependent on the shape of the IF spectrum and can yield values that are in error by as much as 4.4 dB. While this does not affect the measurement of the polarization state, it does cast suspicion on the measured scattering cross sections.

Reflections internal to the equipment provide a noise floor for the measurements and affect both the polarization measurements and the measured cross sections. Interpretation of the results must therefore take into account the ratio of the measured power to the expected value of the power present due to these unwanted reflections.

The cross polarization isolation of the antennas introduces an error of up to 2.56 degrees in the measured values of the angles of the polarization ellipse, but does not affect the polarization ratio.

The presence or effects of several of these performance degradations can be seen in the data collected from the illumination of a field of wheat. Large variations in the measured values result from sampling the outputs at different times. This combines with the IF filter mismatches to yield polarization ratios that are sometimes in excess of one, an impossible situation. The measured values of the channel powers are sometimes below the values expected from internal reflections alone, indicating that large errors may be present.

Several of these performance degradations may be removed by modifying the equipment. The inclusion of sample and hold circuits at each IF processor output will allow all channels to be sampled simultaneously and should remove much of the variation present in the measurements. Replacing the filters in the IF processor units with a matched set will ensure that all measured powers will be directly comparable. Replacing the detector circuits with true rms reading circuits will ensure that the measured cross sections are correct. With these modifications only minor effects will be left to cause error in the measurements, allowing the results to be examined much more closely for correlation to agricultural parameters and temporal effects.

References

1. Curlander, J.C., "Utilization of Spaceborne SAR Data for Mapping", *IEEE Transactions on Geoscience and Remote Sensing*, Vol. GE-22, 1984, pp. 106-112.

2. Long, A.E. and Trizna, D.B., "Mapping of North Atlantic Winds by HF Radar Sea Backscatter Interpretation", *IEEE Transactions on Antennas and Propagation*, Vol. AP-21, 1973 , pp. 680-685.

3. Blume, H.-J.C. and Kendall, B.M., "Passive Microwave Measurements of Temperature and Salinity in Coastal Areas", *IEEE Transactions on Geoscience and Remote Sensing*, Vol. GE-20, 1982, pp. 394-404.

4. Ulaby, F.W., "Radar Measurements of Soil Moisture Content", *IEEE Transactions on Antennas and Propagation*, Vol. AP-22, 1974, pp. 257-265.

5. Rosenthal, W.D. and Blanchard, B.J., "Active Microwave Responses: An Aid in Improved Crop Classification", *PERS*, Vol. 50, No. 4, 1984, pp. 461-468.

6. Shepherd, Paul R., "Crop Separability using a 3-Band Microwave Scatterometer", Master's thesis, University of Saskatchewan, 1987.

7. Ulaby, F.T., "Radar Response of Vegetation", *IEEE Transactions on Antennas and Propagation*, Vol. 23, No. 1, 1975, pp. 36-45.

8. Ulaby, F.T., Held, D., Dobson, M.C., McDonald, K.C., and Senior, T.B.A., "Relating Polarization Phase Difference of SAR Signals to Scene Properties", *IEEE Transactions on Remote Sensing*, Vol. 25, No. 1, 1987, pp. 83-92.

9. Born, M. and Wolf, E., *Principles of Optics*, Pergamon Press, 1970.

10. Antenna Standards Committee of the IEEE Antennas and Propagation Society, "IEEE Standard Definitions of Terms for Antennas".

11. Sofko, G.J., *Polarization of Auroral Backscatter at 42 MHz.*, PhD dissertation, University of Saskatchewan, 1968.

12. Cohen, M.N., "Radio Astronomy Polarization Measurements", *Proceedings of the IRE*, January 1958, pp. 172-183.

13. Ulaby, F.T., Moore, R.K. and Fung, A.K., *Microwave Remote Sensing, Active and Passive,* Addison-Wesley Publishing Company, Vol. 2, 1982.

14. Ziemer, R.E. and Tranter, W.H., *Principles of Communications: Systems, Modulation and Noise,* Houghton Mifflin Company, Boston, Mass., 1985.

15. Blachman, N.M. and McAlpine, G.A., "The Spectrum of a High Index FM Waveform: Woodwards Theorem Revisited", *IEEE Transactions on Communication Technology,* Vol. Com-17, No. 2, April 1969, pp. 201-207.

16. Morton, C.M., "Backscattering Behavior of Agricultural Crops in the Microwave Region", Master's thesis, University of Saskatchewan, 1987.

17. Graves, C.D., "Radar Polarization Power Scattering Matrix", *Proceedings of the IRE,* February 1956, pp. 248-252.

18. Bedrosian, S.D., "Normalized Design of 90 Degree Phase-Difference Networks", *IRE Transactions on Circuit Theory,* Vol. CT7, June 1960.

19. Williams, A.B., *Electronic Filter Design Handbook,* McGraw-Hill Book Company, 1981.

20. Orr, W.I., *Radio Handbook,* Howard W. Sams and Co. Inc., Indianapolis, Ind., 1981.

21. Applied Microwave Corp., Lawrence, Kansas, "Documentation for Microwave Scatterometer".

22. Robertson, Sloan D., "Targets for Microwave Radar Navigation", *The Bell System Technical Journal,* 1957.

23. Ulaby, F.T., Moore, R.K. and Fung, A.K., *Microwave Remote Sensing, Active and Passive,* Addison-Wesley Publishing Company, Vol. 1, 1981.

24. Crispin, J.W. and Siegel, K.M., editors, *Methods of Radar Cross-Section Analysis,* Academic Press, New York and London, 1968.

25. Blanchard, A.J. and Jean, B.R., "Antenna Effects in Depolarization Measurements", *IEEE Trans. on Geoscience and Remote Sensing,* Vol. GE-21, No. 1, January 1983, pp. 113-117.

26. *MICRO-CAP II Electronic Circuit Analysis Program,* 1021 S. Wolfe Rd., Sunnyvale, CA 94086, 1986.

Appendix A

Derivation of Intensities

The following equations show the derivation of the intensities referred to in section 4.3.2 of the text.

$$I(0,0) = \frac{2}{T}\int_0^T \left[\sum_{n=p}^{q} K_n \sqrt{\sigma_{hh}} \cos\left(n\omega_0 t + \omega_c \tau + \phi_h\right) \right]^2 dt$$

$$= \frac{2}{T}\int_0^T \sum_{n=p}^{q}\sum_{m=p}^{q} K_n K_m \sigma_{hh} \cos\left(n\omega_0 t + \omega_c \tau + \phi_h\right) \cos\left(m\omega_0 t + \omega_c \tau + \phi_h\right)\, dt$$

$$= \frac{1}{T}\int_0^T \sum_{n=p}^{q}\sum_{m=p}^{q} K_n K_m \sigma_{hh} \{\cos\left([n-m]\omega_0 t + \omega_c \tau + \phi_h\right) + \cos\left([n+m]\omega_0 t + \omega_c \tau + \phi_h\right)\} dt$$

$$= \frac{1}{T}\int_0^T \sum_{n=p}^{q}\sum_{m=p}^{q} K_n K_m \sigma_{hh} \cos\left([n-m]\omega_0 t\right)\, dt$$

$$I(0,0) = \sigma_{hh}\left[\sum_{n=p}^{q} K_n^{\,2} + \frac{2}{T}\int_0^T \sum_{mn} K_n K_m \cos\left([n-m]\omega_0 t\right)\, dt \right]$$

where $\{mn\}$ is taken to be the set of all values of m and n between p and q such that the value of $(m\text{-}n)$ ranges from one to $q\text{-}p$.

$$I(90,0) = \sigma_{vv}\left[\sum_{n=p}^{q} K_n^{\,2} + \frac{2}{T}\int_0^T \sum_{mn} K_n K_m \cos\left([n-m]\omega_0 t\right)\, dt \right]$$

$$I(45,0) = < [V_{IFh}(t) + V_{IFv}(t)\,]^2 >$$

$$= \frac{1}{T}\int_0^T [\,V_{IFh}{}^2(t) + 2V_{IFh}(t)V_{IFv}(t) + V_{IFv}{}^2(t)\,]\;dt$$

$$= J_{xx} + J_{yy} + \frac{2}{T}\int_0^T \left[\sum_{n=p}^{q} K_n\sqrt{\sigma_{hh}}\cos(n\omega_0 t + \omega_c\tau + \phi_h) \times \sum_{m=p}^{q} K_m\sqrt{\sigma_{hv}}\cos(m\omega_0 t + \omega_c\tau + \phi_v)\right] dt$$

$$= J_{xx} + J_{yy} + \frac{2\sqrt{\sigma_{hh}\sigma_{hv}}}{T}\int_0^T \sum_{n=p}^{q}\sum_{m=p}^{q} K_m K_n\cos(n\omega_0 t + \omega_c\tau + \phi_h)\times\cos(m\omega_0 t + \omega_c\tau + \phi_v)\;dt$$

$$= J_{xx} + J_{yy} + \frac{\sqrt{\sigma_{hh}\sigma_{hv}}}{T}\int_0^T \sum_{n=p}^{q}\sum_{m=p}^{q} K_m K_n\{\cos([n-m]\omega_0 t + \delta) + \cos([n+m]\omega_0 t + 2\omega_c\tau + \phi_h + \phi_v)\}\;dt$$

$$= J_{xx} + J_{yy} + \frac{\sqrt{\sigma_{hh}\sigma_{hv}}}{T}\int_0^T \sum_{n=p}^{q}\sum_{m=p}^{q} K_m K_n\cos([n-m]\omega_0 t + \delta)\;dt$$

$$= J_{xx} + J_{yy} + \frac{\sqrt{\sigma_{hh}\sigma_{hv}}}{T}\left[\int_0^T \sum_{n=p}^{q} K_n{}^2\cos\delta + \sum_{mn} K_m K_n\{\cos([n-m]\omega_0 t + \delta) + \cos([m-n]\omega_0 t + \delta)\}\;dt\right]$$

$$= J_{xx} + J_{yy} + \sqrt{\sigma_{hh}\sigma_{hv}}\left[\sum_{n=p}^{q} K_n{}^2\cos\delta + \frac{2}{T}\int_0^T \sum_{mn} K_m K_n\cos([n-m]\omega_0 t)\cos(\delta)dt\right]$$

$$I(45,0) = J_{xx} + J_{yy} + \sqrt{\sigma_{hh}\sigma_{hv}}\cos(\delta)\left[\sum_{n=p}^{q} K_n{}^2 + \frac{2}{T}\int_0^T \sum_{mn} K_m K_n\cos([n-m]\omega_0 t)\,dt\right]$$

$$I(135,0) = J_{xx} + J_{yy} - \sqrt{\sigma_{hh}\sigma_{hv}}\cos\delta\left[\sum_{n=p}^{q} K_n{}^2 + \frac{2}{T}\int_0^T \sum_{mn} K_m K_n\cos([n-m]\omega_0 t)dt\right]$$

$$I(45,\frac{\pi}{2}) = < [V_{IFh}(t) + V_{IFv}(t,\frac{\pi}{2})]^2 >$$

$$= \frac{1}{T}\int_0^T [\, {V_{IFh}}^2(t) + 2V_{IFh}(t)V_{IFv}(t,\frac{\pi}{2}) + {V_{IFv}}^2(t) \,]\, dt$$

$$= J_{xx} + J_{yy} + \frac{2}{T}\int_0^T \left[\sum_{n=p}^{q} K_n \sqrt{\sigma_{hh}} \cos(n\omega_0 t + \omega_c \tau + \phi_h) \times \sum_{m=p}^{q} K_m \sqrt{\sigma_{hv}} \cos(m\omega_0 t + \omega_c \tau + \phi_v - \pi/2) \right]$$

$$= J_{xx} + J_{yy} - \frac{2\sqrt{\sigma_{hh}\sigma_{hv}}}{T}\int_0^T \sum_{n=p}^{q}\sum_{m=p}^{q} K_m K_n \cos(n\omega_0 t + \omega_c \tau + \phi_h) \times \sin(m\omega_0 t + \omega_c \tau + \phi_v)\, dt$$

$$= J_{xx} + J_{yy} - \frac{\sqrt{\sigma_{hh}\sigma_{hv}}}{T}\int_0^T \sum_{n=p}^{q}\sum_{m=p}^{q} K_m K_n \{\sin([n-m]\omega_0 t + \delta) + \sin([n+m]\omega_0 t + 2\omega_c \tau + \phi_h + \phi_v)\}\, dt$$

$$= J_{xx} + J_{yy} + \frac{\sqrt{\sigma_{hh}\sigma_{hv}}}{T}\int_0^T \sum_{n=p}^{q}\sum_{m=p}^{q} K_m K_n \sin([n-m]\omega_0 t + \delta)\, dt$$

$$= J_{xx} + J_{yy} + \frac{\sqrt{\sigma_{hh}\sigma_{hv}}}{T}\left[\int_0^T \sum_{n=p}^{q} {K_n}^2 \sin\delta + \sum_{mn} K_m K_n \{\sin([n-m]\omega_0 t + \delta) + \sin([m-n]\omega_0 t + \delta)\}\, dt \right]$$

$$= J_{xx} + J_{yy} + \sqrt{\sigma_{hh}\sigma_{hv}}\left[\sum_{n=p}^{q} {K_n}^2 \sin\delta + \frac{2}{T}\int_0^T \sum_{mn} K_m K_n \cos([n-m]\omega_0 t)\sin(\delta) dt \right]$$

$$I(45,\frac{\pi}{2}) = J_{xx} + J_{yy} + \sqrt{\sigma_{hh}\sigma_{hv}}\sin(\delta)\left[\sum_{n=p}^{q} {K_n}^2 + \frac{2}{T}\int_0^T \sum_{mn} K_m K_n \cos([n-m]\omega_0 t)\, dt \right]$$

$$I(135,\frac{\pi}{2}) = J_{xx} + J_{yy} - \sqrt{\sigma_{hh}\sigma_{hv}}\sin\delta\left[\sum_{n=p}^{q} {K_n}^2 + \frac{2}{T}\int_0^T \sum_{mn} K_m K_n \cos([n-m]\omega_0 t) dt \right]$$

Appendix B

Phase Shifter Test Data

To verify the correct operation of the phase shifter, tests were carried out to determine its phase vs frequency response. These tests were done by measuring the time difference between the two output signals when a sinusiodal signal was applied at the input. The measured time difference was converted to phase by dividing by the period of the input sinusiod.

Although this test is simple in concept, it was quite difficult to carry out accurately due to distortions present in the applied sinusoid and the input offset voltages in the counters used to measure time.

The true value of the period can be obtained from any of:

$$\begin{aligned} \text{Period} &= \uparrow \text{A:}\uparrow \text{B} + \uparrow \text{B:}\uparrow \text{A} \\ &= \downarrow \text{A:}\downarrow \text{B} + \downarrow \text{B:}\downarrow \text{A} \\ &= \uparrow \text{A:}\downarrow \text{B} + \downarrow \text{B:}\uparrow \text{A} \\ &= \downarrow \text{A:}\uparrow \text{B} + \uparrow \text{B:}\downarrow \text{A} \end{aligned}$$

where:

- $\uparrow$ A:$\uparrow$ B is the period from the rising edge of A to the rising edge of B
- $\uparrow$ B:$\uparrow$ A is the period from the rising edge of B to the rising edge of A
- $\downarrow$ A:$\downarrow$ B is the period from the falling edge of A to the falling edge of B
- $\downarrow$ B:$\downarrow$ A is the period from the falling edge of B to the falling edge of A

- ↑ A:↓ B is the period from the rising edge of A to the falling edge of B
- ↓ B:↑ A is the period from the falling edge of B to the rising edge of A
- ↓ A:↑ B is the period from the falling edge of A to the rising edge of B
- ↑ B:↓ A is the period from the falling edge of B to the rising edge of A

The value for any individual measurement of time delay between the waveforms will be corrupted by the counter input offset voltages. Specifically it is noted that:

$$\uparrow A{:}\uparrow B = (\uparrow A{:}\uparrow B)_{meas.} + T_a - T_b$$
$$\downarrow A{:}\downarrow B = (\downarrow A{:}\downarrow B)_{meas.} - T_a + T_b$$

where:

- T_a is the time offset due to the input offset voltage of the A channel
- T_b is the time offset due to the input offset voltage of the B channel

The effects of these offset voltages can be eliminated by using the sum of the two time periods itemized above as the estimate for twice the time delay between the two waveforms. In addition to eliminating the effects of the offset voltages this will also average any distortions in the waveform which act to cause the values of ↑ A:↑ B and ↓ A:↓ B to differ.

The test results from a series of measurements to determine the phase shifter characteristics are given below. The source used in the measurements had a tendency to drift, so frequency was measured both at the start of a series of measurements (Strt. Freq.) and at the end of the series (End Freq.). The other terms used are:

$$TOTAL\ A = \uparrow A \uparrow B + \uparrow B \uparrow A + \downarrow A \downarrow B + \downarrow B \downarrow A$$

$$TOTAL\ B = \uparrow A \downarrow B + \uparrow B \downarrow A + \downarrow A \uparrow B + \downarrow B \uparrow A$$

$$PHASE\ A = \frac{\text{Sum of lowest two of measurements in } TOTAL\ A}{TOTAL\ A}$$

$$PHASE\ B = \frac{\text{Sum of lowest two of measurements in } TOTAL\ B}{TOTAL\ B}$$

The measurements show an absolute error in phase which varies from the ideal by .671 to .787 degrees over the 20 to 24Khz frequency range. Also shown is the average of the rising to rising/ falling to falling value and the rising to falling/falling to rising value. This indicates that the measurement integrity is to within .05 degrees.

TESTS ON 90 DEGREE PHASE SHIFTER

MEASURED DATA

Strt Freq.	End Freq.	↑ A:↑ B	↓ A:↓ B	↑ A:↓ B	↓ A:↑ B
19930	19940	37.408	37.461	12.339	12.506
20242	20245	36.942	36.996	12.182	12.350
20511	20513	36.463	36.510	12.024	12.189
20758	20762	36.025	36.072	11.880	12.043
21017	21017	35.592	35.622	11.733	11.895
21266	21268	35.172	35.203	11.595	11.754
21493	21496	34.800	34.829	11.471	11.629
21735	21740	34.410	34.440	11.342	11.497
21993	21994	34.007	34.038	11.209	11.363
22310	22310	33.521	33.552	11.048	11.199
22500	22493	33.249	33.262	10.960	11.104
22770	22764	32.856	32.869	10.831	10.973
23000	22988	32.529	32.546	10.723	10.864
23250	23248	32.176	32.188	10.606	10.744
23770	23755	31.475	31.489	10.375	10.510
24000	23987	31.169	31.183	10.274	10.406

MEASURED DATA

Strt Freq.	End Freq.	↑ B:↑ A	↓ B:↓ A	↑ B:↓ A	↓ B:↑ A
19930	19940	12.590	12.615	37.516	37.692
20242	20245	12.437	12.458	37.052	37.225
20511	20513	12.276	12.296	36.570	36.742
20758	20762	12.130	12.148	36.132	36.301
21017	21017	11.992	11.994	35.695	35.863
21266	21268	11.852	11.852	35.237	35.438
21493	21496	11.726	11.729	34.902	35.064
21735	21740	11.596	11.598	34.511	34.672
21993	21994	11.462	11.466	34.113	34.273
22310	22310	11.301	11.302	33.630	33.787
22500	22493	11.199	11.220	33.358	33.508
22770	22764	11.065	11.086	32.961	33.111
23000	22988	10.956	10.977	32.639	32.786
23250	23248	10.835	10.857	32.277	32.422
23770	23755	10.605	10.625	31.587	31.729
24000	23987	10.504	10.523	31.285	31.424

CALCULATED DATA

AVG.FREQ	PERIOD	TOTAL A	TOTAL B	PHASE A	PHASE B	AVG. PHASE
19935.0	50.163	100.074	100.053	90.671	89.395	90.033
20243.5	49.399	98.833	98.809	90.680	89.380	90.030
20512.0	48.752	97.545	97.525	90.686	89.379	90.032
20760.0	48.170	96.375	96.356	90.688	89.380	90.034
21017.0	47.581	95.200	95.186	90.703	89.363	90.033
21267.0	47.021	94.079	94.024	90.705	89.399	90.052
21494.5	46.524	93.084	93.066	90.712	89.356	90.034
21737.5	46.003	92.044	92.022	90.716	89.349	90.032
21993.5	45.468	90.973	90.958	90.731	89.337	90.034
22310.0	44.823	89.676	89.664	90.739	89.321	90.030
22496.5	44.451	88.930	88.930	90.755	89.318	90.036
22767.0	43.923	87.876	87.876	90.746	89.324	90.035
22994.0	43.490	87.008	87.012	90.749	89.313	90.031
23249.0	43.013	86.056	86.049	90.745	89.321	90.033
23762.5	42.083	84.194	84.201	90.776	89.293	90.035
23993.5	41.678	83.379	83.389	90.787	89.278	90.032

Appendix C

Results of Tests Using Horn Antenna

Table C-1: Test Using Linearly Polarized Transmitting Antenna

TESTS WITH 6 dB PADS TERMINATING MIXERS MAY 14, 1987

MEASURED VALUES

(all values in volts)

Angle	H	V	D_q	S_q	D_i	S_i
0	-0.4270	-0.0138	-0.4360	-0.4580	-0.4540	-0.4350
-15	-0.4250	-0.0940	-0.4540	-0.4600	-0.3450	-0.5400
-30	-0.3870	-0.1960	-0.4650	-0.4490	-0.1990	-0.6070
-45	-0.3240	-0.2790	-0.4690	-0.4340	-0.0550	-0.6300
-60	-0.2420	-0.3620	-0.4870	-0.4310	-0.1320	-0.6260
-75	-0.1350	-0.4120	-0.4800	-0.4340	-0.2920	-0.5670
-90	-0.0250	-0.4500	-0.4840	-0.4610	-0.4430	-0.4900
-105	-0.1040	-0.4440	-0.4730	-0.4800	-0.5690	-0.3510
-120	-0.2230	-0.4070	-0.4660	-0.5020	-0.6550	-0.1910
-135	-0.3330	-0.3370	-0.4650	-0.5240	-0.6970	-0.0410
-150	-0.4110	-0.2520	-0.4710	-0.5340	-0.6890	-0.1730
-165	-0.4720	-0.1290	-0.4880	-0.5360	-0.6250	-0.3600
-180	-0.4880	-0.0150	-0.5050	-0.5190	-0.5210	-0.4950
0	-0.4580	-0.0130	-0.4730	-0.4870	-0.4870	-0.4660

CALCULATED VALUES

Angle	M	PSI(ψ)	CHI(χ)	I_{qcu}/I_{hv}	I_{icu}/I_{hv}
0	1.0004	1.3274	-1.5436	1.0954	1.0830
-15	1.0148	166.6651	-0.4086	1.1024	1.0837
-30	1.0560	152.0535	1.0544	1.1101	1.0842
-45	1.0908	138.9225	2.2724	1.1167	1.0938
-60	1.0675	124.4186	3.6479	1.1153	1.0793
-75	1.0282	108.9686	3.1223	1.1139	1.0820
-90	1.0011	93.0993	1.5317	1.0998	1.0741
-105	1.0176	75.8551	-0.4516	1.0919	1.0747
-120	1.0614	60.2832	-2.1856	1.0892	1.0807
-135	1.0863	45.3172	-3.4361	1.0933	1.0859
-150	1.0676	32.3194	-3.6648	1.0907	1.0856
-165	1.0242	16.1693	-2.8759	1.0973	1.0864
-180	1.0001	1.5887	-0.8615	1.0999	1.0833
0	1.0000	1.3667	-0.9171	1.0977	1.0821

Table C-2: Test Using Linearly Polarized Transmitting Antenna

TESTS WITH 6 dB PADS TERMINATING MIXERS MAY 15, 1987
MEASURED VALUES
(all values in volts)

Angle	H	V	D_q	S_q	D_i	S_i
0	-0.4420	-0.0200	-0.4290	-0.4700	-0.4540	-0.4430
-15	-0.4330	-0.1030	-0.4510	-0.4610	-0.3340	-0.5480
-30	-0.3920	-0.2080	-0.4650	-0.4460	-0.1870	-0.6130
-45	-0.3240	-0.2970	-0.4730	-0.4310	-0.0410	-0.6330
-60	-0.2330	-0.3620	-0.4690	-0.4180	-0.1380	-0.6080
-75	-0.1260	-0.4060	-0.4640	-0.4140	-0.2910	-0.5430
-90	-0.0230	-0.4180	-0.4500	-0.4130	-0.4160	-0.4410
-105	-0.1040	-0.4000	-0.4340	-0.4180	-0.5190	-0.3050
-120	-0.2010	-0.3660	-0.4270	-0.4310	-0.5810	-0.1680
-135	-0.2980	-0.2950	-0.4220	-0.4420	-0.6100	-0.0210
-150	-0.3650	-0.2160	-0.4220	-0.4470	-0.5920	-0.1540
-165	-0.4130	-0.1100	-0.4310	-0.4460	-0.5350	-0.3110
-180	-0.4300	-0.0090	-0.4450	-0.4390	-0.4470	-0.4330
165	-0.4170	-0.1030	-0.4600	-0.4260	-0.3210	-0.5330
150	-0.3780	-0.1960	-0.4670	-0.4130	-0.1910	-0.5890
135	-0.3100	-0.2830	-0.4670	-0.4010	-0.0540	-0.6080
120	-0.2290	-0.3460	-0.4620	-0.3990	-0.1290	-0.5890
105	-0.1280	-0.3920	-0.4470	-0.4080	-0.2730	-0.5340
90	-0.0230	-0.4040	-0.4230	-0.4210	-0.3950	-0.4400
75	-0.0960	-0.3960	-0.4020	-0.4400	-0.5040	-0.3110
60	-0.1950	-0.3600	-0.3870	-0.4550	-0.5670	-0.1800
45	-0.2910	-0.2950	-0.3810	-0.4670	-0.5980	-0.0590
30	-0.3600	-0.2130	-0.3870	-0.4720	-0.5890	-0.1640
15	-0.4140	-0.1160	-0.4090	-0.4760	-0.5420	-0.3130
0	-0.4340	-0.0190	-0.4270	-0.4670	-0.4490	-0.4420

Table C-3: Values Calculated From the Data in Table C-1

	CALCULATED DATA				
Angle	M	PSI(ψ)	CHI(χ)	I_{qcu}/I_{hv}	I_{icu}/I_{hv}
0	1.0007	0.7248	-2.6991	1.0343	1.0277
-15	1.0123	165.9590	-0.6515	1.0498	1.0395
-30	1.0320	151.4693	1.2204	1.0540	1.0429
-45	1.0410	137.4020	2.7083	1.0598	1.0414
-60	1.0398	123.1775	3.3702	1.0648	1.0487
-75	1.0161	107.6005	3.4329	1.0699	1.0501
-90	1.0000	91.7595	2.6134	1.0644	1.0486
-105	1.0153	74.7084	1.1262	1.0628	1.0607
-120	1.0368	60.5843	-0.2720	1.0556	1.0490
-135	1.0581	44.7258	-1.3309	1.0620	1.0594
-150	1.0296	31.0408	-1.6811	1.0504	1.0401
-165	1.0114	15.4381	-1.0201	1.0529	1.0482
-180	0.9998	0.9545	0.4108	1.0562	1.0469
165	1.0152	165.4978	2.3062	1.0653	1.0491
150	1.0403	151.9709	3.6186	1.0719	1.0574
135	1.0573	137.4950	4.4225	1.0752	1.0573
120	1.0477	123.9175	4.3241	1.0823	1.0559
105	1.0222	108.7467	2.7520	1.0770	1.0576
90	1.0002	93.2937	0.1476	1.0876	1.0676
75	1.0119	75.9747	-2.7320	1.0697	1.0562
60	1.0350	61.1780	-4.7490	1.0643	1.0556
45	1.0529	45.3792	-5.8179	1.0578	1.0515
30	1.0543	31.1188	-5.7070	1.0646	1.0682
15	1.0179	15.8961	-4.5326	1.0653	1.0596
0	1.0008	0.4752	-2.7161	1.0609	1.0517

Table C-4: Test Using Linearly Polarized Transmitting Antenna

TESTS WITH MIXERS DRIVING IF PROCESSORS DIRECTLY

MEASURED VALUES
(all values in volts)

Angle	H	V	D_q	S_q	D_i	S_i
0	-0.8420	-0.0200	-0.8480	-0.8650	-0.8550	-0.8490
-15	-0.7930	-0.1990	-0.8610	-0.8400	-0.6120	-1.0250
-30	-0.7240	-0.3610	-0.8680	-0.8210	-0.3780	-1.1200
-45	-0.5900	-0.5120	-0.8480	-0.7830	-0.0960	-1.1370
-60	-0.3080	-0.4830	-0.6260	-0.5610	-0.1860	-0.8080
-75	-0.1580	-0.5280	-0.6030	-0.5420	-0.3860	-0.7030
-90	-0.0310	-0.5180	-0.5600	-0.5170	-0.5280	-0.5380
-105	-0.1370	-0.4930	-0.5420	-0.5220	-0.6510	-0.3660
-120	-0.2630	-0.4430	-0.5300	-0.5340	-0.7270	-0.1850
-135	-0.3790	-0.3550	-0.5210	-0.5520	-0.7560	-0.0410
-150	-0.4740	-0.2700	-0.5480	-0.5830	-0.7720	-0.2140
-165	-0.5330	-0.1460	-0.5610	-0.5860	-0.7030	-0.4000
-180	-0.5600	-0.0170	-0.5810	-0.5760	-0.5850	-0.5700
165	-0.5430	-0.1300	-0.5980	-0.5630	-0.4260	-0.6930
150	-0.4980	-0.2480	-0.6100	-0.5470	-0.2590	-0.7680
135	-0.4150	-0.3640	-0.6140	-0.5340	-0.0760	-0.8020
120	-0.3060	-0.4440	-0.6020	-0.5220	-0.1530	-0.7700
105	-0.1810	-0.4990	-0.5800	-0.5260	-0.3320	-0.6990
90	-0.0410	-0.5170	-0.5450	-0.5320	-0.4910	-0.5720
75	-0.1170	-0.5210	-0.5350	-0.5700	-0.6520	-0.4200
60	-0.2270	-0.4530	-0.4870	-0.5590	-0.6970	-0.2400
45	-0.3420	-0.3680	-0.4720	-0.5610	-0.7280	-0.0720
30	-0.4290	-0.2750	-0.4780	-0.5680	-0.7200	-0.1700
15	-0.4890	-0.1480	-0.4840	-0.5650	-0.6490	-0.3570
0	-0.5170	-0.0220	-0.5160	-0.5510	-0.5470	-0.5150

Table C-5: Values Calculated from the Data in Table C-3

CALCULATED VALUES

Angle	M	PSI(ψ)	CHI(χ)	I_{qcu}/I_{hv}	I_{icu}/I_{hv}
0	0.9991	0.2067	-0.5886	1.0343	1.0233
-15	1.0166	165.0790	0.7530	1.0823	1.0660
-30	1.0425	152.6622	1.6674	1.0905	1.0674
-45	1.0646	138.8142	2.3400	1.0915	1.0668
-60	1.0388	122.9390	3.2489	1.0766	1.0475
-75	1.0171	107.1085	3.2454	1.0821	1.0588
-90	0.9968	90.5710	2.4744	1.0786	1.0551
-105	1.0207	73.5654	1.1409	1.0814	1.0652
-120	1.0471	58.6056	-0.2194	1.0663	1.0601
-135	1.0604	43.2311	-1.6671	1.0683	1.0628
-150	1.0579	30.5567	-1.8023	1.0757	1.0783
-165	1.0207	16.2267	-1.3181	1.0774	1.0711
-180	0.9986	0.7919	0.2644	1.0662	1.0627
165	1.0143	165.8719	1.8420	1.0819	1.0613
150	1.0441	152.7548	3.2379	1.0845	1.0612
135	1.0647	138.5528	4.0683	1.0865	1.0649
120	1.0534	125.0123	4.2204	1.0917	1.0598
105	1.0252	110.5913	2.9668	1.0879	1.0626
90	1.0007	94.6034	0.7452	1.0783	1.0564
75	1.0060	77.1225	-1.9328	1.0717	1.0548
60	1.0370	62.8350	-4.0657	1.0704	1.0583
45	1.0580	47.0121	-4.9563	1.0648	1.0602
30	1.0467	33.0541	-4.9865	1.0612	1.0539
15	1.0177	17.0327	-4.6016	1.0602	1.0510
0	1.0008	1.8220	-1.9976	1.0641	1.0539

Appendix D

Helical Antenna Characterization

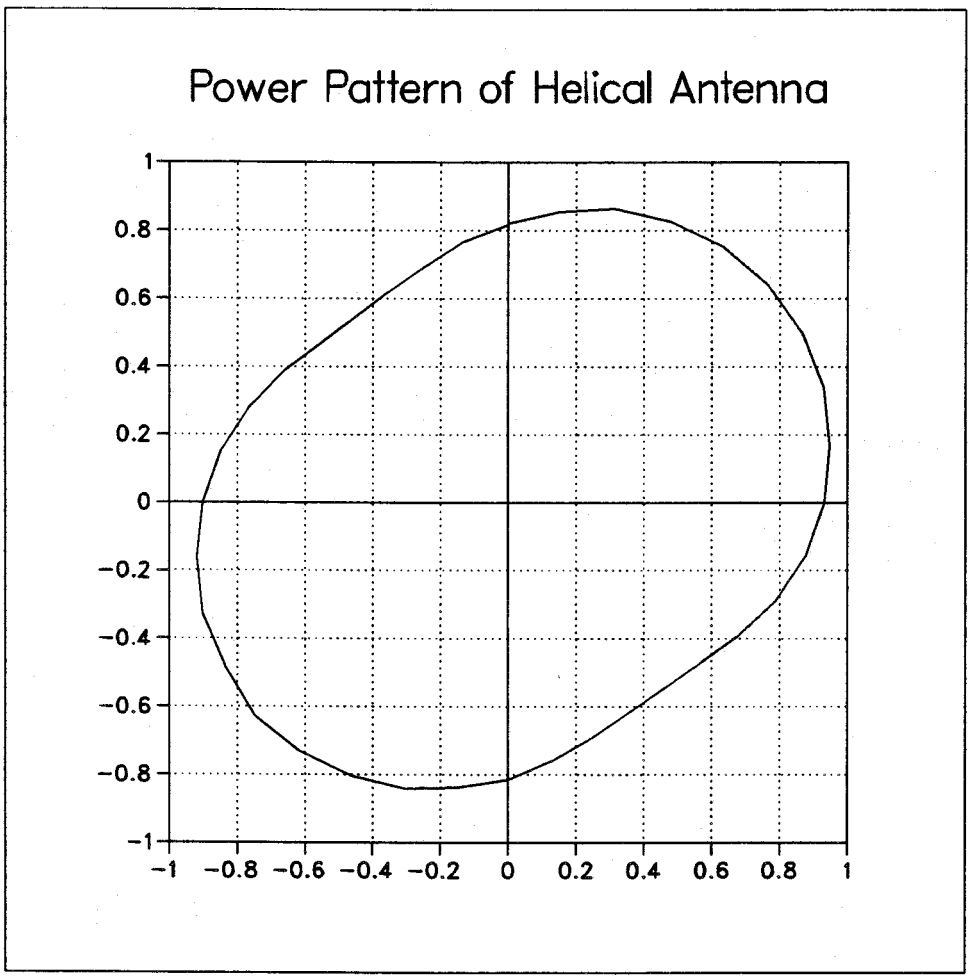

Figure D-1: Polarization Pattern for Helical Antenna

CHARACTERIZATION OF HELICAL ANTENNA
POLARIZATION PATTERN

ANGLE	S21(dB)	S21(LIN)	S21(MAX)
90	-39.60	0.822	-37.9
80	-39.13	0.868	
70	-38.63	0.919	
60	-38.30	0.955	
50	-38.05	0.983	
40	-37.92	0.998	
30	-37.90	1.000	
20	-37.98	0.991	
10	-38.23	0.963	
0	-38.50	0.933	
350	-38.90	0.891	
340	-39.41	0.840	
330	-40.03	0.783	
320	-40.56	0.736	
310	-40.82	0.714	
300	-40.84	0.713	
290	-40.60	0.733	
280	-40.18	0.769	
270	-39.68	0.815	
260	-39.31	0.850	
250	-38.86	0.895	
240	-38.55	0.928	
230	-38.29	0.956	
220	-38.10	0.977	
210	-38.22	0.964	
200	-38.27	0.958	
190	-38.51	0.932	
180	-38.80	0.902	
170	-39.19	0.862	
160	-39.67	0.816	
150	-40.19	0.768	
140	-40.69	0.725	
130	-40.91	0.707	
120	-40.83	0.714	
110	-40.57	0.735	
100	-40.08	0.778	
90	-39.65	0.818	

Appendix E

Helical Antenna Test Results

Table E-1: Tests on Radar using Helical Antenna

TESTS WITH MIXERS DRIVING IF SECTIONS DIRECTLY
CIRCULAR POLARIZATION MAY 15, 1987

MEASURED VALUES
(all values in volts)

Angle	H	V	D_q	S_q	D_i	S_i
180	-0.1130	-0.1140	-0.0200	-0.2290	-0.1550	-0.1680
135	-0.1250	-0.1060	-0.0310	-0.2360	-0.1510	-0.1820
90	-0.1200	-0.1220	-0.0530	-0.2450	-0.1360	-0.2090
45	-0.1070	-0.1390	-0.0520	-0.2510	-0.1540	-0.2010
0	-0.1150	-0.1320	-0.0300	-0.2540	-0.1910	-0.1680
-45	-0.1360	-0.1090	-0.0320	-0.2500	-0.1870	-0.1650
-90	-0.1310	-0.0980	-0.0460	-0.2320	-0.1450	-0.1840
-135	-0.1090	-0.1130	-0.0400	-0.2230	-0.1350	-0.1790
-180	-0.1100	-0.1120	-0.0200	-0.2240	-0.1510	-0.1650

CALCULATED VALUES

Angle	M	PSI(ψ)	CHI(χ)	I_{qcu}/I_{hv}	I_{icu}/I_{hv}
180	1.0132	131.91	-42.68	1.0254	1.0140
135	1.0496	155.19	-38.05	1.0546	1.0410
90	1.0675	133.90	-33.11	1.0728	1.0616
45	1.0483	113.33	-34.59	1.0677	1.0419
0	1.0555	67.74	-39.76	1.0672	1.0556
-45	1.0429	15.17	-38.00	1.0456	1.0237
-90	1.0345	159.84	-34.51	1.0450	1.0252
-135	1.0163	131.34	-36.93	1.0412	1.0196
-180	1.0140	129.33	-42.41	1.0261	1.0150

Table E-2: Tests on radar using helical antenna

TESTS WITH 6 dB PADS TERMINATING MIXERS
CIRCULAR POLARIZATION MAY 15, 1987

MEASURED VALUES
(all values in volts)

Angle	H	V	D_q	S_q	D_i	S_i
0	-0.0950	-0.1060	-0.0210	-0.2080	-0.1580	-0.1340
-45	-0.1110	-0.0840	-0.0310	-0.2000	-0.1500	-0.1350
-90	-0.1100	-0.0860	-0.0480	-0.2000	-0.1150	-0.1680
-135	-0.0980	-0.1100	-0.0450	-0.2140	-0.1230	-0.1770
-180	-0.1060	-0.1150	-0.0230	-0.2300	-0.1550	-0.1670
135	-0.1180	-0.1070	-0.0190	-0.2340	-0.1570	-0.1710
90	-0.1160	-0.1100	-0.0350	-0.2330	-0.1400	-0.1860
45	-0.0940	-0.1170	-0.0330	-0.2180	-0.1400	-0.1670
0	-0.0950	-0.1050	-0.0210	-0.2070	-0.1570	-0.1340

CALCULATED VALUES

Angle	M	PSI(ψ)	CHI(χ)	I_{qcu}/I_{hv}	I_{icu}/I_{hv}
0	1.0764	61.13	-39.52	1.0785	1.0592
-45	1.0492	11.05	-36.88	1.0569	1.0509
-90	1.0681	151.05	-32.42	1.0849	1.0630
-135	1.0813	126.44	-34.41	1.1017	1.0703
-180	1.0765	112.08	-41.98	1.0921	1.0612
135	1.0801	158.57	-41.46	1.0861	1.0620
90	1.0802	140.13	-36.99	1.0861	1.0603
45	1.0690	110.25	-37.32	1.0791	1.0541
0	1.0753	60.43	-39.79	1.0796	1.0625

Appendix F

Calibration Test Log and Results

The following procedure was carried out for each of the *K*, *C*, and *L*-band radars during the testing to determine calibration constants.

On June 16, the sequence was:

1. The *C*-band corner reflector was installed on the north-east side of the tower

2. The radars were positioned such that the average distance from the antenna apertures to the front face of the corner reflector was approximately 17.5 m

3. The following procedure was carried out for each of the *K*, *C*, and *L*-band radars:

    - The radar in question (*L*,*C*, or *K*) was pointed to maximize the power returned from the *C*-band corner reflector. The corner reflector was then adjusted to maximize the same measure.

    - The range from the aperture of the radar dish to the front face of the corner reflector was measured with a tape measure.

    - Four OVERHEAD readings were taken.

    - A ten trial partial scan was taken with the range for the partial scan determined by running the AUTOPEAK program.

4. The *C*-band corner reflector was taken off the tower and the backscatter from the tower was measured using a partial scan with a range of 17.9m. At this point the *L*-band radar was pointing as per the *L*-band radar scan on the *C*-band corner

reflector. (i.e. at the north-east side of tower)

5. The *L*-band Corner Reflector was installed on the south-west side of the tower.

6. The procedure itemized in 3) above was carried out for the *L*-band radar only.

7. The truck was moved to increase the range to approximately 22m.

8. Step 5) was repeated.

9. The *L*-band corner reflector was taken down from the tower.

10. The backscatter from the tower was measured with the radars left pointing as they had been in step 6).

11. The *C*-band corner reflector was installed on the north-east side of the tower.

12. Step 3) was repeated.

13. The truck was moved to increase the range to approximately 27m.

14. Step 3) was repeated.

15. The *C*-band corner reflector was removed.

16. The backscatter from the tower was measured with radars pointing such that the TV camera showed the space between the two ABS sections of the tower.

17. The *L*-band corner reflector was installed on the south-west side of the tower.

18. The procedure itemized in 3) above was carried out for the *L*-band radar only.

On July 11 the sequence of measurements was:

1. The *C*-band corner reflector installed on the north-east side of the tower. The south-west side of the tower was left bare.

2.

- The *K*-band radar was pointed to maximize the power returned from the *C*-band corner reflector. The corner reflector was then adjusted to maximize the same measure.

- The range from the aperture of the radar dish to the front face of the corner reflector was measured with a tape measure.

- Four OVERHEAD readings were taken.

- A ten trial partial scan was taken with the range for the partial scan determined by running the AUTOPEAK program.

3. The *C*-band corner reflector was removed, and the tower backscatter measured with the radars pointing as per 2)

4. The *C*-band reflector was re-installed.

5. The steps itemized in 2) were carried out using the *C*-band radar.

6. Step 4) was repeated.

7. The *L*-band corner reflector installed on the south-west side of the tower. The north-east side of the tower was left bare.

8. The steps itemized in 2) were carried out using the *L*-band radar.

9. The *L*-band corner reflector was removed, and the tower backscatter was measured with the radars pointing as per 8)

10. The *L*-band reflector was re-installed.

11. Step 2) was repeated.

12. The *L*-band corner reflector was removed, and the tower backscatter measured with the radars pointing as per 11)

13. The *L*-band corner reflector was re-installed.

14. Step 2) was repeated for the *C*-band radar.

15. The *L*-band corner reflector was removed, and the tower backscatter measured with the radars pointing as per 14).

Table F-1: *C*-Band Calibration Test Results

Test Date (1987)	July 11	July 11	June 16	June 16	June 16
Trial Number	1	1	1	1	1
Center Freq. (GHz.)	5.150	5.150	5.167	5.130	5.127
Size of Corner Reflector (m)	0.714	1.117	0.714	0.714	0.714
Sigma of Corner Reflector (m*m)	80.204	480.411	80.734	79.582	79.489
Tx Power (v)	1.013	1.010	0.996	0.998	0.993
Measured Range (m)	17.340	28.740	17.540	21.980	26.850
Range Offset (m)	0.180	0.180	0.180	0.180	0.180
True Range (m)	17.520	28.920	17.720	22.160	27.030
Indicated Range (m)	17.800	30.900	18.100	23.050	28.850
Rx HH Voltage (v)	-0.482	-0.383	-0.386	-0.277	-0.194
Rx VV voltage (v)	-0.451	-0.396	-0.439	-0.278	-0.185
Rx H Background Voltage (v)	-0.006	-0.007	-0.007	-0.007	-0.007
Rx V Background Voltage (v)	-0.006	-0.006	-0.007	-0.007	-0.007
Kh (max)	276.2	219.3	189.4	244.9	273.2
Kh (min)	262.8	203.8	176.1	221.3	236.5
Kv (max)	242.2	233.0	243.9	246.6	249.3
Kv (min)	229.6	219.3	228.8	223.0	214.3
Average Kh	230.3				
Average Kv	233.0				
Average Khv or Kvh	231.7				

Table F-2: *L*-band Calibration Test Results

Test Date	(1987)	July 11	June 16	June 16	June 16
Trial Number		1	1	1	1
Center Frequency	(GHz)	1.570	1.570	1.572	1.575
Size of Corner Reflector	(m)	1.117	0.714	1.117	1.117
Sigma of Corner Reflector	(m*m)	44.648	7.454	44.761	44.932
Tx Power	(v)	1.771	1.682	1.690	1.657
Measured Range	(m)	17.440	17.500	17.390	21.850
Range Offset	(m)	0.263	0.263	0.263	0.263
True Range	(m)	17.703	17.763	17.653	22.113
Indicated Range	(m)	18.000	17.900	18.000	22.850
Rx HH Voltage	(v)	-2.530	-1.053	-2.380	-1.629
Rx VV Voltage	(v)	-3.046	-1.401	-3.009	-2.007
Rx H Background Voltage	(v)	-0.054	-0.044	-0.045	-0.052
Rx V Background Voltage	(v)	-0.030	-0.040	-0.045	-0.086
Kh (max)		8293.8	9556.0	7549.3	9074.9
Kh (min)		7742.8	8146.7	7136.9	8253.0
Kv (max)		11752.9	16488.8	11973.5	14068.5
Kv (min)		11298.8	14708.8	11278.2	11851.2

Test Date	(1987)	June 16	June 16	June 16
Trial Number		1	1	1
Center Frequency	(GHz)	1.566	1.577	1.570
Size of Corner Reflector	(m)	0.714	0.714	1.117
Sigma of Corner Reflector	(m*m)	7.416	7.520	44.648
Tx Power	(v)	1.652	1.605	1.635
Measured Range	(m)	21.920	26.870	26.740
Range Offset	(m)	0.263	0.263	0.263
True Range	(m)	22.183	27.133	27.003
Indicated Range	(m)	22.800	28.800	28.700
Rx HH Voltage	(v)	-0.807	-0.522	-1.104
Rx VV Voltage	(v)	-0.796	-0.593	-1.347
Rx H Background Voltage	(v)	-0.045	-0.045	-0.045
Rx V Background Voltage	(v)	-0.045	-0.045	-0.045
Kh (max)		14347.9	14435.8	9615.5
Kh (min)		11476.7	10216.7	8168.2
Kv (max)		13979.8	13277.4	14112.7
Kv (min)		11147.8	13484.5	12346.8
Average Kh		9530.0		
Average Kv		13340.7		
Average Khv or Kvh		11435.4		

Appendix G

Computer Simulation Listings

```
10 REM PROGRAM TO CALCULATE RATIOS OF RANDOM SPECTRA
15 PRINT "PROGRAM RUNNING..."
20 PI=4*ATN(1)
25 RATIOMAX=0:RATIOMIN=100
30 WA=2*PI*250*86:WB=2*PI*250*87:WC=2*PI*250*88:WD=2*PI*250*89:WE=2*PI*250*90
32 H1=.562:H2=.832:H3=1:H4=.832:H5=.575
34 V1=.646:V2=.891:V3=1:V4=.813:V5=.549
36 C1=.549:C2=.912:C4=1.072:C5=.741
38 D1=.531:D2=.912:D4=1.072:D5=.741
40 PRINT "ANGLE H C RATIO PWRRATIO RATIO2 RATIOMAX RATIOMIN"
50 REM FOR I=2*PI/36 TO 2*PI STEP 2*PI/8
55 I=0
65 FOR HE=.8 TO 0 STEP -.2
66 FOR HD=1 TO 0 STEP -.2
67 FOR HC=1 TO 0 STEP -.2
70 FOR HB=1 TO 0 STEP -.2
71 FOR HA=1 TO 0 STEP -.2
72 REM HA=.6:HB=.2:HC=0:HD=0:HE=.9
80 PHA=2*PI*293/360:PHB=2*PI*325/360:PHC=2*PI*358/360:PHD=2*PI*390/360
:PHE=2*PI*420/360
90 PCA=2*PI*228/360:PCB=2*PI*300/360:PCC=2*PI*355/360:PCD=2*PI*410/360
:PCE=2*PI*476/360
95 K=.016/2.6
100 SUMH=0:SUMC=0:SUMH1=0:SUMC1=0
110 FOR T=0 TO .0026 STEP .000016
120 HT1=HA*SIN(WA*T+PHA+I):HT2=HB*SIN(WB*T+PHB+I)
:HT3=HC*SIN(WC*T+PHC+I)
122 HT4=HD*SIN(WD*T+PHD+I):HT5=HE*SIN(WE*T+PHE+I)
124 H=HT1*H1+HT2*H2+HT3+HT4*H4+HT5*H5
130 CT1=HA*SIN(WA*T+PCA+I):CT2=HB*SIN(WB*T+PCB+I)
:CT3=HC*SIN(WC*T+PCC+I)
132 CT4=HD*SIN(WD*T+PCD+I):CT5=HE*SIN(WE*T+PCE+I)
134 C=CT1*C1+CT2*C2+CT3+CT4*C4+CT5*C5
160 H=ABS(H)
170 C=ABS(C)
```

```
180 SUMH=SUMH+H:SUMC=SUMC+C
185 SUMH1=SUMH1+H*H:SUMC1=SUMC1+C*C
190 NEXT T
200 RATIO=(SUMC^2/SUMH^2)
201 IF RATIO > RATIOMAX THEN RATIOMAX=RATIO
202 PRAT=(SUMC1/SUMH1)
203 RATIO2=PRAT/RATIO
204 IF RATIO < RATIOMIN THEN RATIOMIN=RATIO
205 H=SUMH*K:C=SUMC*K
210 PRINT USING " #.#";HA;HB;HC;HD;HE;
:PRINT USING "    #.###";H;C;RATIO;PRAT;RATIO2;RATIOMAX;RATIOMIN
212 REM LPRINT USING " #.###";RATIO;PRAT;RATIO2
215 NEXT HA:NEXT HB:NEXT HC:NEXT HD:NEXT HE
220 REM NEXT I
230 END
240 STOP
```

```
10 REM PROGRAM TO CALCULATE RATIOS OF RANDOM SPECTRA
15 PRINT "PROGRAM RUNNING..."
18 PRINT "HA    HB    HC    HD    HE    RATIO  RATIOL  RATIOH  I"
20 PI=4*ATN(1):RATIOH=0:RATIOL=1000
30 WA=2*PI*250*86:WB=2*PI*250*87:WC=2*PI*250*88:WD=2*PI*250*89:WE=2*PI*250*90
60 FOR HE=.2 TO 1 STEP .2:FOR HD=0 TO 1 STEP .2:FOR HC=0 TO 1 STEP .2:
70 FOR HB=0 TO 1 STEP .2:FOR HA=0 TO 1 STEP .2
80 I=0
100 SUMH=0:SUMH1=0
110 FOR T=0 TO .0026 STEP .000005
120 HT1=HA*SIN(WA*T+I):HT2=HB*SIN(WB*T+I):HT3=HC*SIN(WC*T+I)
122 HT4=HD*SIN(WD*T+I):HT5=HE*SIN(WE*T+I)
124 H=HT1+HT2+HT3+HT4+HT5
160 H=ABS(H)
180 SUMH=SUMH+H
185 SUMH1=SUMH1+H*H
190 NEXT T
194 SUMH=SUMH*.000005/.0026
196 SUMH1=SUMH1*.000005/.0026
200 RATIO=(SUMH1/SUMH^2)
204 IF RATIO>RATIOH THEN RATIOH=RATIO
206 IF RATIO<RATIOL THEN RATIOL=RATIO
212 PRINT USING " #.#  ";HA;HB;HC;HD;HE;
213 PRINT USING "  #.###";RATIO;RATIOL;RATIOH;
214 PRINT USING " ###";I*180/PI
225 NEXT HA:NEXT HB:NEXT HC:NEXT HD:NEXT HE
230 END
240 STOP
```